

# Preloading of a lumpy clay fill

A study into the closure of the interlump voids of a mechanically dredged stiff clay fill

A.M.L. Dortland

Technische Universiteit Delft



---

Cover figure: backhoe dredger Magnor taken at Hull United Kingdom by Boskalis

# Preloading of a lumpy clay fill

A study into the closure of the interlump voids of a mechanically dredged stiff clay fill

by

A.M.L. Dortland

to obtain the degree of Master of Science  
at the Delft University of Technology,  
to be defended publicly on September 4, 2019 at 3:30 PM.

Student number: 4237145  
Project duration: November 12, 2018 – September 4, 2019  
Thesis committee: Prof. dr. ir. C. Jommi, TU Delft, chair  
Dr. ir. H.A. Abels, TU Delft  
Dr. ir. A.A.M. Dieudonné, TU Delft  
Dr. ir. R.L.J. Helmons, TU Delft  
Ir. S.R.K. Vos, Boskalis, company supervisor

An electronic version of this thesis is available at <http://repository.tudelft.nl/>.



# Acknowledgements

This MSc thesis marks the end of an extremely educative period to which I look back with great joy. The support and guidance of several people were invaluable during this study, and I would like to thank some people in specific.

First of all, I would like to thank Prof. Jommi for being an outstanding professor and supervisor. Her passion for the discipline, enthusiasm and kindness were extremely helpful and supportive. Despite her busy schedule, she always took the time to answer my questions and steer me in the right direction.

Secondly, I would like to thank Mario Martinelli for his help with the MPM model. He guided me exceptionally well through the model. Owing to his help, I learned a lot about the model and certainly enjoyed using it. Mario has an exceptional knowledge of MPM, and I would like to express my gratitude for his patience and clear explanations.

I would also like to thank Dr. Anne-Catherine Dieudonné for her insights into the microstructure and diffusion process. Furthermore, she let me think critically and mentioned the missing links. I would also like to take this opportunity to thank Dr. Hemmo Abels for his help to improve my scientific writing and to discuss the geological background. I also want to express my appreciation to Dr. Rudy Helmons for the support in the model options. The experimental work in this study would not have been possible without the support of the Boskalis Environmental team and Wim Verwaal, who were extremely supportive.

A special thanks to my company supervisor, Ir. Bas Vos. I enjoyed my time at Boskalis and would like to thank him for this opportunity. He helped me in finding and keeping direction during my thesis, which was extremely helpful as I sometimes got lost in details.

Lastly, I would like to thank my family for their love and support during my studies. My time in Delft would not have been so enjoyable without my friends. They took care of the well-deserved distraction via numerous coffee breaks and pleasant times outside the faculty.



# Summary

Mechanical dredging of a stiff clay results in clay lumps. Those clay lumps can be reused for the construction of land reclamation projects, and hereby economic and environmental value is generated. Placement of the clay lumps in water result in a matrix of clay lumps and an interlump void space. The collapse of the interlump void space will cause large settlements and needs to be overcome before the site can be used for construction. Preloading is an effective method to close the interlump voids. Stiff clays soften over time due to unloading and swelling. As a result, the strength and stiffness of the clay lumps decrease over time. The presence of discontinuities accelerates the softening process. It was proposed by Leung et al. (2001) that the interlump void space closes under a reduced preload of 25 kPa. The interlump void space closes under a reduced preload because the lumps soften over time. The question rises if closure occurs within a normal construction timespan, i.e., 1 - 2 years, under this reduced preload.

In this study, a combined experimental and numerical approach is applied to determine the influence of soil characteristics, softening and the presence of discontinuities on interlump void closure. The influence of softening due to chemical and hydro-mechanical swelling is tested by experimental swell-load tests on stiff overconsolidated Boom clay samples. Additionally, the presence of discontinuities is studied by CT images, and a miniature clay fill test is performed to study the softening time and the rearrangement effect. Furthermore, a numerical study is performed in which the influence of specific soil characteristics on void closure was researched by a sensitivity analysis.

By the experimental tests, it is shown that a pore water chemistry change alters the degree of swelling and its compressibility. Furthermore, fissures were identified in the sample material by CT images. The smallest micro-fissures could not be identified due to the resolution of the images. Consequently, it is impossible to estimate the effect of fissures on the hydraulic conductivity. Therefore, literature data was used to estimate the hydraulic conductivity and this was used as the input in the calculations. In the numerical study, it was shown that MPM could model the softening behaviour over time. The sensitivity analysis showed that the MPM model responds consistently to parameter sensitivity analyses. This leads to the conclusion that MPM can be used as a investigation tool to increase the understanding of the influence of parameter variability on the final interlump void closure problem.

The resulting strains of the numerical model comply with the theoretically calculated strains. It was expected that the numerical strains were smaller than the experimentally determined strains, due to the presence of interlump voids in the numerical model. But, the numerical strains are larger than the experimental strains. In the sensitivity analysis, it was found that the final strains and closure time are highly dependant on the soil characteristics. It is likely that the input of the MPM model differs compared to the true sample material and thus different strains result.

The time until the interlump void space closes was determined by a simplified geometry in MPM under a preload of 25 kPa. For an unfissured Boom clay, interlump closure takes place after approximately 16 years while for a fissured Boom clay it only takes 2 months. Thus, closure of the highly simplified geometry takes place within a normal construction timespan for a fissured Boom clay. It must be kept in mind that the results are highly dependant on the geometry, lump size and soil characteristics. Therefore, these results can not be generalized into an estimate of the interlump void closure time for any stiff lumpy clay fill.

In conclusion, the feasibility of MPM was explored and it turned out to be a promising method to model the interlump void closure problem. Further studies are required to check if the model gives plausible results for more advanced constitutive soil models and geometries. If the results are positive, MPM can be used as a investigation tool to increase the understanding of the interlump void closure time for more refined geometries.



# Contents

|   |            |
|---|------------|
| <b>Acknowledgements</b>                                 | <b>i</b>   |
| <b>Summary</b>  | <b>iii</b> |
| <b>List of Figures</b>                                  | <b>vii</b> |
| <b>List of Tables</b>                                   | <b>ix</b>  |
| <b>Nomenclature</b>                                     | <b>xii</b> |
| <b>1 Introduction</b>                                   | <b>1</b>   |
| 1.1 Background . . . . .                                | 2          |
| 1.2 Research question . . . . .                         | 2          |
| 1.3 Scope of work . . . . .                             | 3          |
| <b>I Literature review</b>                              | <b>5</b>   |
| <b>2 Description clay characteristics</b>               | <b>7</b>   |
| 2.1 General clay characteristics . . . . .              | 7          |
| 2.1.1 The definition of stiff clay . . . . .            | 7          |
| 2.1.2 Overconsolidation . . . . .                       | 8          |
| 2.1.3 Double structure . . . . .                        | 8          |
| 2.1.4 Degree of saturation . . . . .                    | 10         |
| 2.1.5 Aging . . . . .                                   | 10         |
| 2.1.6 Swelling . . . . .                                | 12         |
| 2.2 Boom clay . . . . .                                 | 15         |
| 2.2.1 Geological background . . . . .                   | 15         |
| 2.2.2 Geotechnical properties . . . . .                 | 19         |
| <b>3 Lumpy fill</b>                                     | <b>23</b>  |
| 3.1 Dredging technique . . . . .                        | 23         |
| 3.2 Lump size distribution and bulking . . . . .        | 23         |
| 3.3 Settlements . . . . .                               | 24         |
| 3.3.1 Closure of interlump void space . . . . .         | 24         |
| 3.3.2 Consolidation and Creep . . . . .                 | 26         |
| <b>II Methodology</b>                                   | <b>29</b>  |
| <b>4 Methodology</b>                                    | <b>31</b>  |
| 4.1 Experimental testing . . . . .                      | 31         |
| 4.1.1 Sample material . . . . .                         | 31         |
| 4.1.2 Fissure identification tests . . . . .            | 32         |
| 4.1.3 Miniature clay fill test . . . . .                | 32         |
| 4.1.4 Determination consolidation coefficient . . . . . | 33         |
| 4.1.5 Swell and consolidation test . . . . .            | 33         |
| 4.2 Numerical modelling . . . . .                       | 36         |
| 4.2.1 Numerical model . . . . .                         | 36         |
| 4.2.2 Model set-up . . . . .                            | 39         |
| 4.2.3 Sensitivity analysis . . . . .                    | 43         |

|            |  |           |
|------------|--|-----------|
| <b>III</b> | <b>Results and discussion</b>  | <b>47</b> |
| <b>5</b>   | <b>Results and discussion</b>  | <b>49</b> |
| 5.1        | Experimental tests . . . . .   | 49        |
| 5.1.1      | Sample material: index tests and degree of saturation . . . . .      | 49        |
| 5.1.2      | Fissure identification tests . . . . .                               | 50        |
| 5.1.3      | Miniature clay fill test . . . . .                                   | 51        |
| 5.1.4      | Determination consolidation coefficient . . . . .                    | 51        |
| 5.1.5      | Swell-load test . . . . .  | 52        |
| 5.1.6      | Summary experimental results. . . . .                                | 55        |
| 5.2        | MPM . . . . .  | 56        |
| 5.2.1      | Results of sensitivity analysis . . . . .                            | 56        |
| 5.2.2      | Summary numerical results . . . . .                                  | 66        |
| 5.2.3      | Model issues in MPM. . . . .   | 66        |
| 5.3        | Comparison experimental, numerical and theoretical strains . . . . . | 68        |
| <b>IV</b>  | <b>Conclusions and recommendations</b>                               | <b>71</b> |
| <b>6</b>   | <b>Conclusions</b>   | <b>73</b> |
| <b>7</b>   | <b>Recommendations</b>   | <b>75</b> |
| 7.1        | Recommendations on experimental methodology . . . . .                | 75        |
| 7.2        | Recommendations on numerical methodology . . . . .                   | 76        |
|            | <b>Bibliography</b>  | <b>77</b> |
| <b>V</b>   | <b>Appendices</b>  | <b>83</b> |
| <b>A</b>   | <b>Geotechnical vocabulary</b>                                       | <b>85</b> |
| <b>B</b>   | <b>Index tests</b>   | <b>87</b> |
| <b>C</b>   | <b>Diffusion script</b>  | <b>93</b> |
| <b>D</b>   | <b>Fehmarn Project</b>   | <b>95</b> |
| D.1        | Project overview . . . . .   | 95        |
| D.2        | Geology . . . . .  | 96        |

# List of Figures

|      |  |    |
|------|--|----|
| 1.1  | Schematic profile of a reclamation fill formed by stiff clays directly after placement . . . . . | 1  |
| 1.2  | Profile before preloading . . . . .  | 2  |
| 1.3  | Profile after preloading . . . . .   | 2  |
| 1.4  | Reader's guide . . . . .   | 3  |
| 2.1  | USDA soil texture identification triangle . . . . .  | 7  |
| 2.2  | Stiff clay limits . . . . .  | 7  |
| 2.3  | Graphical representation of the failure envelope of OC and NC clays . . . . .                    | 8  |
| 2.4  | Double structure clay . . . . .  | 9  |
| 2.5  | Diffusive double layer . . . . .   | 9  |
| 2.6  | Influence of water content and compaction density on microstructure . . . . .                    | 9  |
| 2.7  | Three fracture types . . . . .   | 11 |
| 2.8  | Orientation of various fractures . . . . .   | 11 |
| 2.9  | Suction in Singapore marine clay . . . . .   | 13 |
| 2.10 | Range of water content in clay sample . . . . .  | 13 |
| 2.11 | Compression of Champlain clay . . . . .  | 13 |
| 2.12 | Wetting and drying cycles clay . . . . .   | 13 |
| 2.13 | Clay structure: T-O and T-O-T . . . . .  | 14 |
| 2.14 | Expanding clay minerals . . . . .  | 14 |
| 2.15 | Micro-stratigraphical lithology of Boom clay . . . . .   | 16 |
| 2.16 | Location of the Boom clay formation . . . . .  | 17 |
| 2.17 | Reconstruction of the eroded part of the Boom formation . . . . .                                | 17 |
| 2.18 | Undrained shear strength as a function of depth . . . . .  | 21 |
| 3.1  | Mechanical dredger: Backhoe . . . . .  | 23 |
| 3.2  | Mechanical-Hydraulic dredger: Trailing suction hopper . . . . .                                  | 23 |
| 3.3  | Bulking coefficient on the transport barge . . . . .   | 24 |
| 3.4  | Surface settlements over time for sequential loading steps . . . . .                             | 26 |
| 3.5  | Loading of clay cake and clay lumps structure . . . . .  | 26 |
| 3.6  | Excess pore pressure isochores inside clay lumps . . . . .                                       | 27 |
| 4.1  | Geographical location of the quarry . . . . .  | 32 |
| 4.2  | Micro CT scanner . . . . .   | 33 |
| 4.3  | Drainage and loading conditions for Rowe cell . . . . .  | 33 |
| 4.4  | Pore size density function of Boom clay . . . . .  | 35 |
| 4.5  | Cumulative void ratio intrusion of Boom clay . . . . .   | 35 |
| 4.6  | Eulerian vs Lagrangian description . . . . .   | 37 |
| 4.7  | Space discretisation of MPM . . . . .  | 37 |
| 4.8  | Computation scheme of MPM . . . . .  | 38 |
| 4.9  | Suction visualized in $p - \tau$ plane . . . . .   | 40 |
| 4.10 | Input geometry MPM model . . . . .   | 41 |
| 4.11 | Boundary conditions model . . . . .  | 41 |
| 4.12 | Dilatancy angle for MC model . . . . .   | 41 |
| 4.13 | Mesh refinements . . . . .   | 44 |
| 4.14 | Minimum, max bulk modulus and average bulk modulus upon wetting . . . . .                        | 45 |
| 4.15 | Model with altered inner geometry but similar boundary conditions. . . . .                       | 46 |
| 5.1  | CT scan: section 1. . . . .  | 50 |
| 5.2  | CT scan: section 2. . . . .  | 50 |

|      |   |    |
|------|---|----|
| 5.3  | CT scan: section 3. . . . .   | 51 |
| 5.4  | CT scan by micro CT scanner . . . . .   | 51 |
| 5.5  | Diffusion in mesopores . . . . .  | 52 |
| 5.6  | Diffusion in micropores . . . . .   | 52 |
| 5.7  | Results swell tests on sample block 1 . . . . .   | 53 |
| 5.8  | Results swell tests on sample 2 . . . . .   | 53 |
| 5.9  | Result swell test on sample block 2 . . . . .   | 53 |
| 5.10 | Results load tests on sample block 2 . . . . .  | 53 |
| 5.11 | Result of loading test . . . . .  | 54 |
| 5.12 | Result load test on sample block 2: void ratio versus vertical effective stress. . . . .                          | 54 |
| 5.13 | Total strain versus normalized time for five mesh refinements . . . . .   | 57 |
| 5.14 | Total void space versus normalized time for five mesh refinements . . . . .                                       | 57 |
| 5.15 | Deviatoric strains in the clay balls at timestep $T_v = 5 * 10^{-4}$ for the different mesh refinements . . . . . | 57 |
| 5.16 | Volumetric strains in the clay balls at several timesteps for mesh refinement 4 . . . . .                         | 58 |
| 5.17 | Porosity over time for mesh refinement 4. . . . .   | 58 |
| 5.18 | Result of sensitivity analysis for the hydraulic conductivity for mesh refinement 4 . . . . .                     | 59 |
| 5.19 | Result of sensitivity analysis hydraulic conductivity . . . . .   | 59 |
| 5.20 | Visualization of the deviatoric strains for the different hydraulic conductivities . . . . .                      | 60 |
| 5.21 | Visualization of the pore pressure . . . . .  | 60 |
| 5.22 | Result of sensitivity analysis for stiffness: strain versus normalized time . . . . .                             | 61 |
| 5.23 | Theoretical case: swelling for stiff and a less stiff material with a constant preconsolidation stress . . . . .  | 61 |
| 5.24 | Stiffness = 2503 kpa. Pore pressure at certain timesteps inside the clay balls for mesh refinement 4 . . . . .    | 62 |
| 5.25 | Stiffness = 1073 kpa. Pore pressure at certain timesteps inside the clay balls for mesh refinement 4. . . . .     | 62 |
| 5.26 | Result of sensitivity analysis for suction: total strain versus normalized time . . . . .                         | 62 |
| 5.27 | Result of sensitivity analysis for preload: total strain versus normalized time . . . . .                         | 63 |
| 5.28 | Moment of load application . . . . .  | 64 |
| 5.29 | Result of sensitivity analysis for application preload: strain versus normalized time . . . . .                   | 64 |
| 5.30 | Failure inside clay balls . . . . .   | 65 |
| 5.31 | Deviatoric strains for cohesive clay balls . . . . .  | 65 |
| 5.32 | Mean effective stress for non-cohesive clay ball . . . . .  | 65 |
| 5.33 | Mean effective stress for cohesive clay ball . . . . .  | 65 |
| 5.34 | Mean effective stress during softening for different geometries . . . . .   | 66 |
| 5.35 | Mesh refinement 4: vertical effective stresses . . . . .  | 68 |
| 5.36 | Results of MPM model 9. (comparable model to swell test.). . . . .  | 69 |
|      |   |    |
| A.1  | PI Classification . . . . .   | 85 |
| A.2  | Swell potential . . . . .   | 86 |
|      |   |    |
| B.1  | Plot of the Casagrande test . . . . .   | 87 |
| B.2  | Check of Casagrande test data . . . . .   | 87 |
| B.3  | Grain size distribution curve . . . . .   | 90 |
| B.4  | Typical range of adsorption values . . . . .  | 91 |
| B.5  | Activity index classes . . . . .  | 91 |
| B.6  | Results of methylene blue tests on filter paper. . . . .  | 91 |
|      |   |    |
| D.1  | Location of the Fehmarnbelt . . . . .   | 95 |
| D.2  | Planned tunnel trajectory . . . . .   | 95 |
| D.3  | Conceptual impression of the reclaimed land . . . . .   | 96 |
| D.4  | Overview of the geology in the longitudinal direction . . . . .   | 97 |
| D.5  | Glacier movements during Pleistocene . . . . .  | 98 |
| D.6  | Glacial till lumps on the barge . . . . .   | 99 |
| D.7  | Glacial till after re-handling . . . . .  | 99 |
| D.8  | Clay mineralogy of 120 samples from different Palaeogene deposits . . . . .                                       | 99 |

# List of Tables

|     |  |    |
|-----|--|----|
| 2.1 | Literature classification data of Boom clay . . . . .  | 20 |
| 2.2 | Classification of the upper three geotechnical formations of the Boom clay formation . . . . . | 20 |
| 2.3 | Mineralogy of the Boom clay . . . . .  | 20 |
| 2.4 | Cross section of the Boom clay . . . . .   | 20 |
| 4.1 | Overview of input sensitivity analysis . . . . .   | 43 |
| 5.1 | Overview of index test results on a Boom clay sample . . . . .                                 | 49 |
| 5.2 | Unloading and loading consolidation coefficients . . . . .                                     | 53 |
| B.1 | In situ water content results . . . . .  | 87 |
| B.2 | Liquid limit results . . . . .   | 88 |
| B.3 | Results of plastic limit test . . . . .  | 88 |
| B.4 | Undrained shear strength data of Boom clay sample. . . . .                                     | 88 |
| B.5 | Specific gravity test results . . . . .  | 89 |



# Nomenclature

|       |                                  |             |
|-------|----------------------------------|-------------|
| $A$   | Activity index                   | (–)         |
| $c$   | Cohesion                         | ( $kPa$ )   |
| $D$   | Collective diffusion coefficient | (–)         |
| $E$   | Stiffness                        | ( $kPa$ )   |
| $e$   | Void ratio                       | (–)         |
| $g$   | Gravitational constant           | ( $m/s^2$ ) |
| $G_s$ | Specific gravity                 | (–)         |
| $I_p$ | Plasticity index                 | (–)         |
| $K$   | Bulk modulus                     | ( $kPa$ )   |
| $k$   | Hydraulic conductivity           | ( $m/s$ )   |
| $K_0$ | Lateral stress coefficient       | (–)         |
| $N_c$ | Bearing capacity factor          | (–)         |
| $p$   | Pressure                         | ( $kPa$ )   |
| $q$   | Deviatoric stress                | ( $kPa$ )   |
| $R$   | Radius                           | ( $m$ )     |
| $S$   | Saturation state                 | (–)         |
| $s$   | Suction                          | ( $kPa$ )   |
| $S_u$ | Undrained shear strength         | ( $kPa$ )   |
| $t$   | Time                             | ( $s$ )     |
| $v$   | Velocity                         | ( $m/s$ )   |
| $w$   | Water content                    | (–)         |
| $W_L$ | Liquid limit                     | (–)         |
| $W_L$ | Plastic limit                    | (–)         |

## Greek letters

|            |              |              |
|------------|--------------|--------------|
| $\epsilon$ | Strain       | (–)          |
| $\eta$     | Porosity     | (–)          |
| $\gamma$   | Unit weight  | ( $kN/m^3$ ) |
| $\kappa$   | Permeability | ( $m^2$ )    |

---

|           |                  |           |
|-----------|------------------|-----------|
| $\nu$     | Poissons ratio   | (-)       |
| $\phi$    | Friction angle   | °         |
| $\rho$    | Density          | $kg/m^3$  |
| $\sigma'$ | Effective stress | ( $kPa$ ) |
| $\tau$    | Turtuosity       | (-)       |

**Abbreviations**

*MBA* Methylene blue adsorption

*MP* Material point

*MPM* Material point method

*NC* Normally consolidated

*OC* Overconsolidated

*OCR* Overconsolidation ratio

—

# 1

## Introduction

Dredging is the removal of clay, sand, or rock from the bottom of water bodies and disposal at another location. Sedimentation causes a gradual fill in waterways. Accordingly, routine removal by dredging is a necessity to maintain open waterways. Another reason for dredging is capital dredging, that is the activity of creating new civil works such as a tunnel or a harbour. Dredged soil is often seen as an unwanted product and is disposed at rare dump sites. Reusing the dredged material solves the problem of scarce disposal ground and decreases the costs of building materials.

Research over the last 15 years has shown that dredged material can be reused as resource material. Accordingly, this results in broad environmental, societal, and financial benefits. The dredged material can be used for engineering, and environmental uses. Some examples of engineering adoption are construction projects, flood and coastal protection, and land improvement. Possible environmental projects in which dredged material can be reused are habitat creation, sustainable relocation, and water quality improvement (Dacus, 2009).

The growing population in land-scarce areas like Singapore, together with the shortage of sandy construction materials results in a significant interest in land reclamation by dredged clays. Dredging works conducted by Boskalis, such as the proposed Fehmarnbelt project and Pulau Tekong project, generate enormous volumes of dredged clay. These clays can be reused for land reclamation, with this creating economic and environmental value.

The reuse of coarse dredged material for several engineering purposes is common practice, although this is not the case for clays. Certain clay characteristics such as particle size, structure, and water holding capacity cause ambiguities. Consequently, resulting in many uncertainties of the behaviour of clay after dredging. A distinction is made between soft and stiff clays given the different engineering nature of the materials. The dredging technique, i.e. mechanical or hydraulic, also has a significant effect on the resulting building material. This study will focus specifically on the reuse of **stiff mechanically dredged clays** for land reclamation projects.

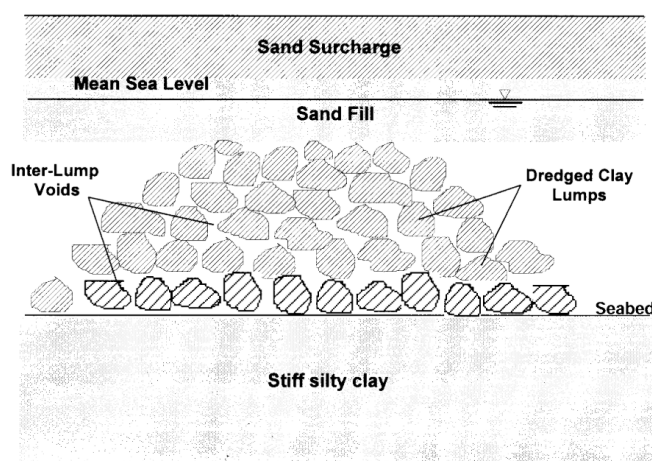


Figure 1.1: Schematic profile of a reclamation fill formed by stiff clays directly after placement (Leung et al., 2001). The reclamation fill is formed by a thick layer of stiff lumpy clay lumps and the interlump void space is initially filled by water. The sand layer on top acts as a preload and flattens the top surface.

## 1.1. Background

Mechanical dredging of stiff clay forms clay lumps, and these lumps can be reused on a reclamation fill. A matrix of clay lumps and interlump void space result after placement (fig: 1.1 and fig: 1.2). Loading of this lumpy structure will result in large settlements by the collapse of the interlump void space. Those large settlements can be in the order of 40% of the total fill height (Kostkanová et al., 2014).

Those large settlements need to be overcome before a construction can be built upon. Hence, the contractor needs to preload the lumpy clay fill before the reclamation fill is handed over to the client. It is proposed that closure of the interlump voids already occurs by a reduced preload. This is because the clay lumps soften over time and thereby reduce stiffness and strength (Karthikeyan et al., 2004).

Softening of the clay lumps occur due to two different processes: (i) unloading of the material (ii) hydro-mechanical (Karthikeyan et al., 2004) and chemical swelling. The strength and stiffness are also largely influenced by the presence of discontinuities. The strength and stiffness decreases due to following three reasons (Skempton et al., 1969): (i) increase of softening of clay along discontinuity surface (ii) decrease in overall strength due to surfaces of weakness (iii) progressive failure by local concentrations of shear stress that exceed the peak strength. Internal tensile stresses are formed by the variation in softening inside a lump. As a consequence, cracks form and the outer part of the lump falls off while the inner part stays intact (Alapakam, 2006). This process is called aggravation of the outer part.

Preloading by a reduced load results in closure of the interlump voids due to the aggravation of the outer part. A matrix of stiff and soft parts (fig: 1.3) forms after closure of the interlumps void space. The stiff parts are formed by the unaltered inner parts of lumps, while the softer parts are formed by the deformed outer shells of the lumps (Karthikeyan et al., 2004).

Leung et al. (2001) concluded that the interlump void space of a stiff lumpy clay fill closes under a reduced preload of 25 kPa. This conclusion was purely based on a smallscale experimental test. They stated that interlump closure is not the main issue in a lumpy stiff clay fill as the period before loading is long, i.e. 4-5 years. Such that, full dissipation of suction can take place. Nowadays projects generally have a shorter timespan, i.e. 1-2 years, before handover to the client. The question rises if the interlump void space still closes within this timespan under a relatively small preload.



Figure 1.2: Schematic profile of clay lumps before preloading: a matrix of stiff lumps and interlump void space filled by water.



Figure 1.3: Schematic profile of clay lumps after preloading: a matrix of stiff and soft zones.

## 1.2. Research question

The objective of this report is to gain more insight in the closure of the interlump voids on a reclamation fill formed by mechanically dredged stiff clay lumps. The required preload is closely related to the time of interlump void closure. The following research question is formulated for the investigation:

*Will the interlump void space of a stiff lumpy clay fill close under a preload of 25 kPa within 1-2 years?*

Before the research can be answered it is important to understand the governing processes. Furthermore, a modelling tool is required to answer the research question. Accordingly, the following sub questions are defined:

1. *What are the governing mechanisms in interlump void closure and which process is dominant?*
2. *Does the chemistry of water have an influence on softening?*
3. *Can the problem be analysed by means of the available MPM code?*

### 1.3. Scope of work

Several processes influence the final behaviour of a lumpy clay fill. Interlump closure is closely related to the initial soil characteristics, swelling and the presence of discontinuities, as described in the literature review. An experimental and numerical approach is used to increase the understanding of the interlump void closure problem. The experimental study looks into the presence of discontinuities and the influence of softening. Besides, a miniature clay fill test similar to the test of Leung et al. (2001) will be performed. In the numerical study the influence of initial soil characteristics is studied by the sensitivity analysis.

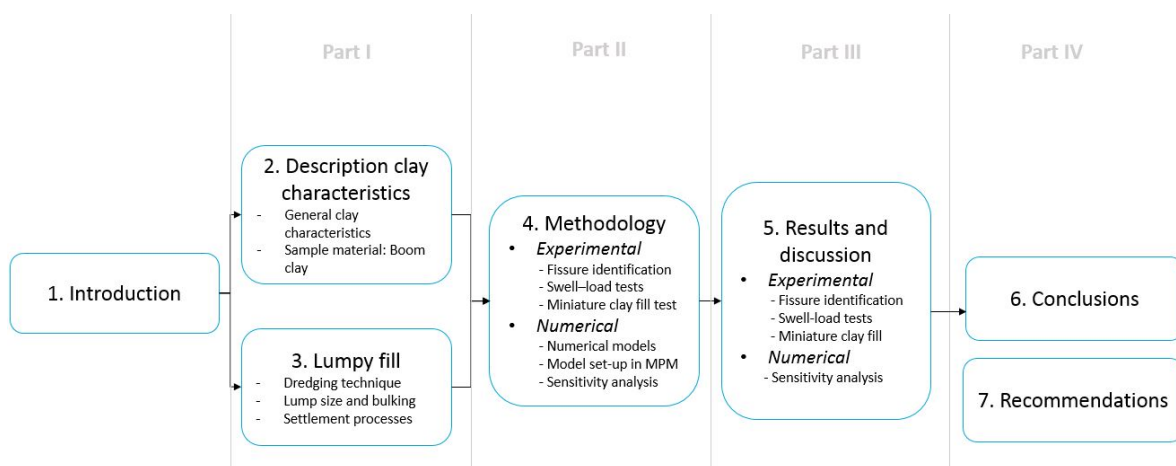


Figure 1.4: Reader's guide. The research consists of an experimental and numerical approach.



# I

## Literature review



# 2

## Description clay characteristics

This chapter is subdivided into two different sections. The general clay characteristics are described in the first section (2.1). Several clay characteristics differentiate from other clastic minerals and thereby influence the engineering behaviour. These properties are platy crystals, extremely small size, surface and internal chemistry, capacity to absorb water, and their capacity for cation exchange (Moon, 1972). This study focuses on the Boom clay, accordingly the geological background and soil characteristics of the Boom clay are discussed in section 2.2.

### 2.1. General clay characteristics

#### 2.1.1. The definition of stiff clay

Clay is a natural sedimentation material that is composed primarily of fine-grained phyllosilicate minerals. Soil scientists identify particles smaller than  $2 \mu\text{m}$  as a clay particle, while sedimentologists use a definition of  $<4 \mu\text{m}$  (Guggenheim et al., 1995). The soil texture triangle, figure 2.1, defined by the USDA is a straightforward method to classify the soil. Distinction between soft and stiff clays has to be made because of their different engineering behaviour. A material that is hard to indent by a thumb is a stiff clay according to the BS 5930 standard (Norbury, n.d.). The liquidity index and undrained shear strength can also be used to classify the clay. Deposits in their natural state with a liquidity index (LI) below 0.5 are considered stiff clays. An explanation of the liquidity and plasticity index is given in appendix A. The definition of a stiff clay based on the liquidity index is a water content limit. Below this water content limit, the clay is defined stiff as shown in figure 2.2. Another commonly used definition for stiff clays is an undrained shear strength which exceeds 75 kPa (Lancelotta, 2009). In this report, the following definition of clay will be used: **A fine-grained, low permeable material with plastic properties.** The clay is identified as stiff in case: **the liquidity index  $<0.5$  and the undrained shear strength  $>75$  kPa.**

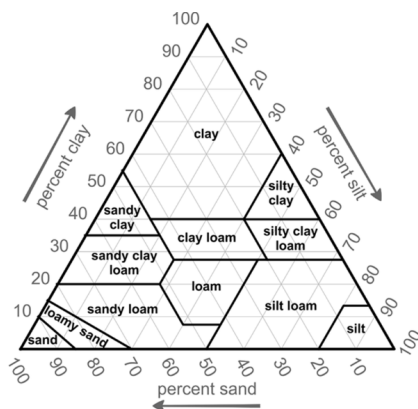


Figure 2.1: USDA soil texture identification triangle (Groenendyk et al., 2015).

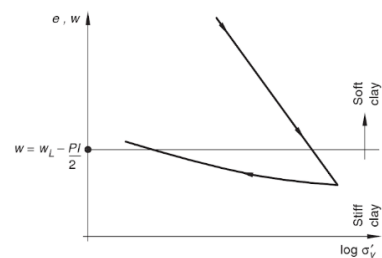


Figure 2.2: Distinction between soft and stiff clays based on water content and overburden pressure (Lancelotta, 2009).

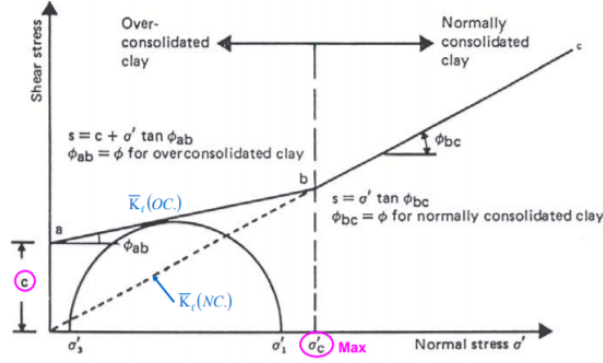


Figure 2.3: Graphical representation of the failure envelope of OC and NC clays. OC clay have an apparent cohesion term while this is not present for NC clays (Lambe, 1958).

### 2.1.2. Overconsolidation

Stiff clays are often overconsolidated, which means that the material has experienced higher stresses in the past than its current overburden stress. The rate of overconsolidation is expressed by the overconsolidation ratio: the ratio of the maximum past pressure over the current overburden pressure.

$$OCR = \frac{\sigma'_{vmax}}{\sigma'_{v0}} \quad (2.1)$$

Figure 2.2 shows that a stiff clay can have a different degree of overconsolidation. A normally consolidated clay at great depths can even be defined as a stiff clay (Lancelotta, 2009). In practice, dredging of clays will occur at shallow depths, hence dredged stiff clays have experienced larger stresses in the past than its current overburden stress. Consequently, they are in an overconsolidated state.

Lancelotta (2009) proposed that a given behaviour of stiff clay cannot only be associated with the overconsolidation ratio. Therefore, a more general principle is to describe the behaviour by the difference between the initial state conditions and the corresponding state. For some clays the factual pre-consolidation stress ( $\sigma'_{v,max}$ ) is smaller than the apparent one ( $\sigma'_{v,pc}$ ). Accordingly, it is not realistic to correlate the soil properties to OCR. This difference is presumably caused by the memory loss of earlier preloads due to swelling, fissuring and/or debonding (Krogsbøll et al., 2012). An overconsolidated clay 'memorizes' the preload history and, this is translated into the apparent cohesion, see figure 2.3. Overconsolidated clays are cohesive, while normally consolidated clays are not. The origin of the apparent cohesion is not fully understood, but it is probably formed by altered mineral bonds (Rogers, n.d.).

#### Processes causing overconsolidation

Overconsolidation can be present due to several natural and manmade processes. Natural large scale processes are melting of past glaciers, erosion of overburden (Coduto et al., 2011), and uplift as a result of tectonics (Mertens et al., 2003). Smaller-scale natural processes are groundwater changes and alteration of the soil by chemical processes. Man-made processes resulting in an overconsolidated clay are an excavation and temporary loading (Coduto et al., 2011).

### 2.1.3. Double structure

A natural clay deposit includes a microstructure and a mesostructure, this is illustrated in figure 2.4. Individual particle elements are formed by clay minerals in a flocculated or dispersed configuration. The configuration depends on the depositional environment as well as the level of compaction. The elements join together and form an aggregate, the porosity inside the aggregate is called the microporosity. Clay aggregates together with silt and sand particles form the mesostructure of the deposit and the porosity in between the particles is called the mesoporosity (Wang and Wei, 2015).

#### Microstructure

The microstructure of the clay is formed by several platy clay minerals with negatively charged faces and positively charged edges. A net negative charge typically is present due to isomorphous substitution (Armstrong, 2014). Clay minerals have a very specific structure and are consequently charged. The cation-exchange-capacity (CEC) and

diffuse double layer (DDL) are two important aspects that needs to be understood as they have a large influence on clay behaviour.

Water is held in the soil by capillary and adsorption forces (Lambooy, 1984). The degree of adsorption depends on the cation exchange capacity (CEC). It is the capacity of a soil to hold exchangeable cations expressed in adsorbed milli-equivalents per gram of soil. The negatively charged clay and organic matter particles hold the cations by electrostatic forces (Ketterings et al., 2007). The CEC can be used as a measure of the total surface charge of a clay (Paassen et al., 2004).

The charge distribution in the pore fluid (diffusive layer) plus the charged particle surface (Stern surface) is called the diffusive double layer (DDL) as visualized in figure 2.5. Exchangeable dissolved cations are present in the DDL, and the thickness of the DDL is a measure for the decrease of surface potential with distance from the clay particle surface (Paassen et al., 2004).

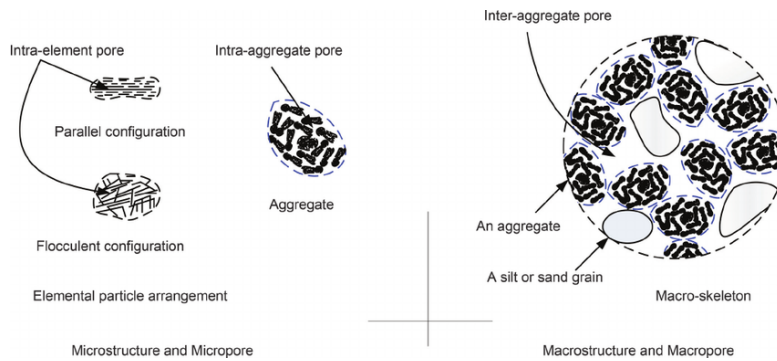


Figure 2.4: Double structure clay, including micro- and mesoporosity (Wang and Wei, 2015). In this report the mesoporosity refers to the porosity in between the grains and aggregates. In this figure the mesoporosity is called the macroporosity, but this term is not used later in the report.

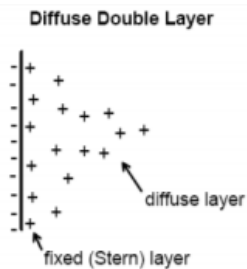


Figure 2.5: Diffusive double layer (Eastern Mediterranean University, 2013).

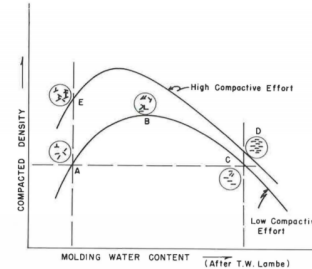


Figure 2.6: Influence of water content and compaction density on microstructure (Lambe, 1958).

### Flocculated or dispersed

Flocculation usually occurs if clays are deposited in a high salt content regime. The exact flocculation concentration depends on pH, clay mineral type, and type of dissolved salt (Mitchell, 2001). Lambe (1958) discovered that a soil compacted dry of optimum tends to flocculate, while soil tends to disperse when compacted at a water content wet of optimum. This can be explained by a high concentration of electrolytes in the case of low water content, resulting in a flocculated structure (Tate, n.d.). A flocculated structure has a higher hydraulic conductivity, larger strength and stiffness although more brittle (Kruse, 1985). The compressibility and sensitivity are high in flocculated structure due to its 'open' structure. Contrarily, in a dispersed structure the compressibility and sensitivity are low. For this reason, soil properties in a dispersed soil are more related to the mesostructure while for a flocculated fabric the soil properties are closely connected to the microstructure. Heavily overconsolidated clays demonstrate a high degree of near horizontal orientation. Consequently, the compressibility and sensitivity are low for heavily overconsolidated clays (Attewell and Farmer, 1976). This fact implies that the original fabric is disturbed by overburden pressures, resulting in a more dispersed structure. Intersection between the diffusive double layer is likely to be present in a dispersed fabric. Consequently, resulting in more swell compared to a flocculated structure.

### 2.1.4. Degree of saturation

In situ stiff clay deposits are compacted. As a result, they are in an initial unsaturated state (Alonso et al., 1999). The reason for its initial unsaturated state is compaction followed by rebound: (i) compaction of the clay results in a decrease of pore space and water content (ii) when the stress is removed the soil will rebound and regain some volume, resulting in a three-phase medium. As the permeability of an overconsolidated clay is very small, it can take extremely long until the clay has become fully saturated by surface water. The relation between hydraulic conductivity and the time since its initial unsaturated state gives an indication for the degree of saturation of the in situ material. Another cause for the initial unsaturated state is the water content at compaction: in case an unsaturated clay is compacted, the mesopores may not be fully saturated. The micropores are always saturated (Carman, 1953), but the degree of saturation in the mesopores depends on the water content at compaction.

Weathering during the recent past (e.g. late quaternary) is another cause of unsaturated clays, although they are located below groundwater or sea level. The degree of saturation will influence the behaviour of the clay, for this reason the behaviour is characterized as either 'dry' or 'wet' of the optimum moisture content. A material is characterized as 'wet' if occluded air voids are present and continuous air voids characterize a 'dry' soil. In a 'wet clay' occluded air is attached to the skeleton and is unlikely to travel as bubbles within the porewater (Barden, 1974). Very small air pockets will always be present in a saturated overconsolidated clay. This is because air pockets smaller than the air entry value will not be reached by the pore fluid.

### 2.1.5. Aging

Several modifications of structure occur between sedimentation and the present state. Significant changes of mechanical and physical properties are associated with aging phenomena (Ltifi et al., 2014). Some processes harden the soil while other processes weaken the bindings (I. Vanicek and M. Vanicek, 2008). Overconsolidation by loading has a major influence as earlier described in section 2.1.1. Other effects that harden or soften the material with time are: cementation, weathering, wash-out, drying, and discontinuities.

#### Cementation

Precipitation of mineral materials in the pore space leads to the hardening of sediments, referred to as cementation. The precipitated minerals form a 'cement' in between the grains. Consequently, porosity and permeability decrease by cementation as the cement forms an essential part of the soil (The editors of Encyclopaedia Britannica, n.d.[a]). Calcite ( $CaCO_3$ ), silica ( $SiO_2$ ), iron oxides ( $Fe_xO_x$ ), and clay minerals are common cementing minerals (Editors of the geological society, n.d.)

#### Weathering

Climatic influences can cause permanent changes in the state and geotechnical properties of a material, referred to as weathering. Physical and chemical processes cause an alteration of the original state of the material (The Editors of Encyclopaedia Britannica, n.d.[b]). Physical weathering can be induced by temperature changes (e.g. frost wedging, shrinkage/expansion) and pressure changes (e.g. plant activities and erosion). Chemical weathering is induced by rainwater, which reacts with the minerals and forms stable minerals (Nelson, 2014). Weathering changes the mechanical behaviour of a material, for clays this can be traced back to structural changes of the microstructure. The result is mechanical decay and a corresponding decrease in sensitivity (Cafaro and Cotecchia, 2001). Accordingly, strength and stiffness decrease due to weathering.

#### Wash-out

Leaching of the original salty pore water by rain, i.e. a decrease in salt concentration, can cause a major decrease in strength. The microstructure changes from a flocculated structure to a dispersed, thereby largely reducing the strength (Skempton and Northey, 1952). Section 2.1.6 describes the effect of pore fluid chemistry in more detail. If the microstructure in the clay has changed due to wash-out it is called quick clay. The well known Rissa landslide occurred due to the presence of quick clay.

#### Drying-out

Drying of soil takes only place close to the surface. The soil surface layer will shrink by drying, correspondingly leading to a local increase of strength and stiffness. On the contrary, the overall strength will decrease due to the formation of tensile cracks (I. Vanicek and M. Vanicek, 2008)

### Discontinuities

Discontinuities play an important role in the stability and strength properties of stiff clays, namely the strength decreases compared to the intact clay. Minor structural features, i.e. fissures, are common for overconsolidated clays. Therefore, a deep understanding of the effect of discontinuities is required. Figure 2.7 and figure 2.8 visualizes the three fracture types and the orientation in respect to the principal stresses. Two other discontinuity surfaces, i.e. bedding plane and secondary variation, are also discussed in this section.

- Bedding plane: the surface that separates one layer from another, e.g the surface between a clay and a silty clay layer (Vandenberghe et al., 1997).
- Faults and shear zones: faults and shear zones are formed by compressional or tensional forces (Lancelotta, 2009). Tectonic events give rise to compressional or tensional forces, causing relative displacements along the slip zone.
- Joints: brittle fracture surfaces along which almost no displacement occurred. The principal cause of jointing is crustal movement. Minor irregular jointing patterns can also be caused by contraction upon consolidation and crystallization. Or by expansion and/or contraction due to a hot igneous intrusion (The Editors of Encyclopaedia Britannica, n.d.[a]).
- Fissures: extension fractures filled with air or gas. In case they are filled with minerals, they are called veins (Khattak, n.d.). Fissured clays can be formed by tectonism (Picarelli et al., 2006), or by stress release combined with chemical and physical weathering (Skempton et al., 1969). The concentration of fissures formed by stress release and weathering increases towards the surface, while their mean size decreases. In clays the term fissure is generally used for randomly oriented small scale discontinuities (Standing, 2018). The peak shear strength of a fissured sample is lower than for a continuous sample. There are three different reasons for the decrease in the overall strength of a fissured clay (Skempton et al., 1969):
  - softening of clay along fissures
  - fissures and joints cause local concentrations of shear stress, which exceed the peak strength of the clay, leading to progressive failure
  - fissures and joints are both surfaces of weakness. Consequently, the overall strength is smaller than for an intact material
- Secondary variation: Secondary variation in the soil structure arises due to the dissolution and precipitation of minerals. An example of secondary variation is septaria surface. A shear failure plane is another example of a secondary variation surface that forms by dissolution processes (Santamarina and Shin, 2009). Most shear failure planes are a result of tectonics and are correspondingly not a secondary variation discontinuity surface.

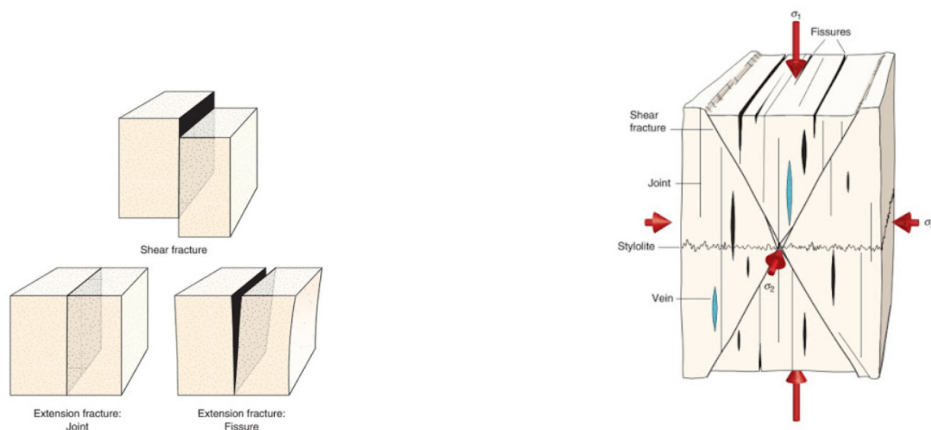


Figure 2.7: Three types of fractures: Shear fracture, joint and fissure (Khattak, n.d.).

Figure 2.8: The orientation of various fracture types in respect to the principal stresses (Khattak, n.d.).

Terzaghi (1936) was the first who quantified the influence of joints and fissures on the strength. He showed that the overall strength can decrease by one fifth to one tenth for highly fissured clays of the intact strength of a small clay sample. Larger samples are more likely to contain joints and fissures, such that larger samples generally have a lower strength. Nishimura (2005) called this the sample-size effect. Skempton (1977) found that the **strength of an over-consolidated (OC) fissured clay is governed by the fissure strength**, corresponding to the fully softened strength. The fully softened strength of an OC soil is equal to the shear strength of the reconstituted normally consolidated soil. This value is smaller than the peak strength of the OC clay but greater than the residual strength (Sorensen and Okkels, 2013). The operative strength of fissured clays is smaller than the strength of a small intact sample. In consequence, discontinuities are of major importance in engineering works, especially for overconsolidated clays. It is extremely important to identify the presence of discontinuities in overconsolidated clays, although this is not an easy task. Their presence could be identified by a large number of cores. But the best method to identify the large discontinuities, although costly, is by excavation pit. Small fissures can only be determined by a micro CT scanner (section 4.1.2).

### 2.1.6. Swelling

Clays can show expansive behaviour, although this will not be the case for all clays. Bolt (1956) subdivided the swelling processes into (i) mechanical and (ii) chemical. Mechanical processes such as dissipation of suction occur in the inter aggregate (mesovoids) spaces, whereas the intra-aggregate (microvoids) void space is governed by chemical swelling (Taylor and Smith, 1986). As a result of swelling the undrained shear strength and stiffness decrease. The activity index, see appendix A, signifies the expected volume change of the material. Discontinuities have a major effect on the swelling, see section 2.1.5, so the activity index alone is not sufficient to define the expected swell.

#### Mechanical swelling

Relaxation of the mean stress sets a negative pressure in the porewater, referred to as suction (Taylor and Smith, 1986). The magnitude will be comparable to the initial mean effective stress before excavation (Karthikeyan et al., 2004), as described in equation 2.2. This negative pore pressure dissipates when clay is dumped in water, that is to say the reverse process of consolidation resulting in swell. This process is called an elastic quick swelling response, which can also be referred to as rebound. Unloading induces a progressive deterioration of the soil properties. Accordingly, loss of cementation and breakdown of diagenetic bonds results in a decrease of strength and stiffness (Calabresi and Scarpelli, 1985).

$$u_s = p' = \frac{1}{3}(\sigma'_v + 2\sigma'_h) \quad (2.2)$$

Robinson et al. (2004) performed swelling tests (figure 2.9 and 2.10), on a kaolinite (LI=0.57) and a Singapore marine clay (LI=0.45). It is important to mention that this test was performed on reconstituted samples. As a consequence, the clay will soften faster than an in situ sample. An increase of suction during 3-dimensional swelling can be explained by the Cryer-Mandel effect, afterwards followed by a decrease in suction. The Cryer-Mandel effect describes the non-monotonic pore pressure evolution. The dissipation of suction takes longer for larger samples, owing to an increase in drainage path. No clear relationship is known between the rate of swell and the size of the lump (Ott, 2017). The water content closer to the edge is higher compared to that in the center after full dissipation of suction (figure 2.10). Robinson et al. (2004) modelled the dissipation of suction by non-linear models for free swelling lumps by a finite element method (FEM). The FEM and experimental results corresponded reasonably well, although the final stage of dissipation was a lot faster in the experimental results. A probable reason is microcracking of the clay lumps, leading to an increase in permeability. The microcracks are formed by internal tensile stresses formed by the variation of softening and swelling within the sample (Alapakam, 2006).

Cui et al. (2002) assumed that the degree of mechanical swell in extremely dense compacted clay can be neglected, since the mesopores are closed such that suction is prevented. Figure 2.11 shows the pore closure due to different compressing stresses on a Champlain clay (Delage and Lefebvre, 1984), from this figure it results that all inter-aggregate pores, i.e. mesopores, are closed by an experienced pressure of 1452 kPa.

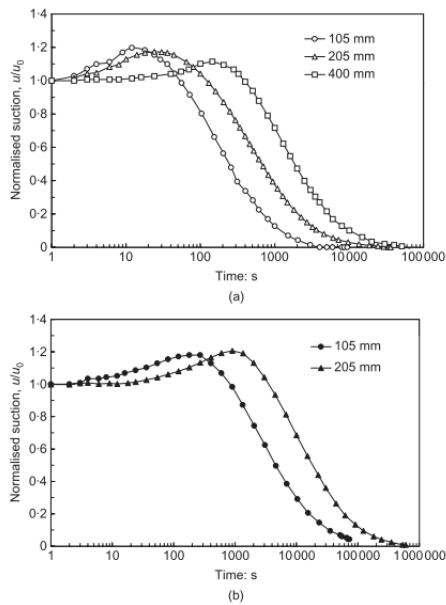


Figure 2.9: Suction normalized to the initial suction for Kaolinite and Singapore marine clay (Robinson et al., 2004). Increase in suction is present due to the Cryer-Mandel effect.

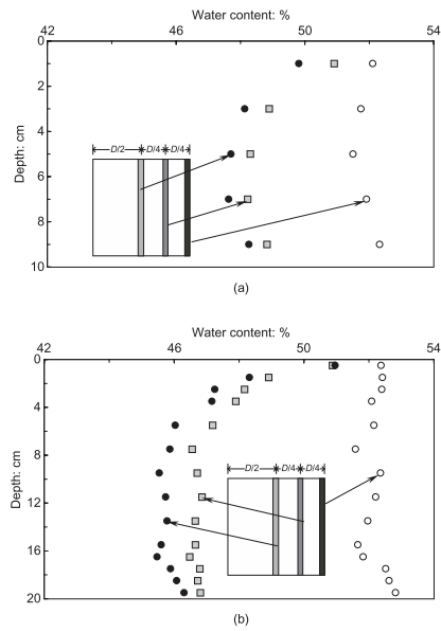


Figure 2.10: Range of water content in sample: higher water content closer to edge of the sample (Robinson et al., 2004).

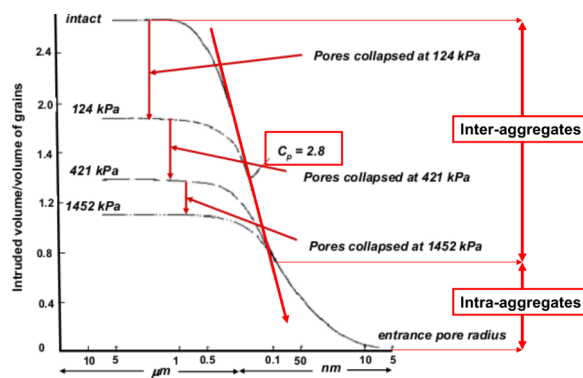


Figure 2.11: Progressive collapse of finer pores by increasing compression of a Champlain clay (Delage and Lefebvre, 1984).



Figure 2.12: Lump submerged in water (top); lump exposed to 4 wetting-drying cycles (bottom) (Kostkanová et al., 2014).

Disintegration due to oscillations of suction

Kostkanová et al. (2014) stressed the importance of wetting/drying cycles on the structure of a single unconfined lump. A simple experimental submersion test was performed: one lump was submerged in water for the whole testing

period while the other lump went through four wetting-drying cycles. The disintegration as a result of the suction oscillations is clearly visible in figure 2.12. Disintegration by wetting and drying cycles can be ignored for highly plastic clays transported by barge as the drying time is relatively short. Contrarily, this is of major importance for lower plasticity clay, especially because they may lose their intact structure during the transportation and rehandling process.

### Chemical swelling

Two types of chemical swelling exist: (i) crystalline swelling occurs at inter-layer separations of 10-22 Å (ii) diffuse double layer swelling takes place at inter-layer separations of >22 Å. Diffuse double layer swelling is also called osmotic swelling (Rao, 2013). Hydration of clay is associated with chemical swelling, however not all clays swell chemically. Clay minerals that are part of the T-O-T group can show chemical expansive behaviour, because there is no hydrogen bond at the interlayer. T-O-T is a combination of tetrahedral and octahedral sheets that together form a mineral (figure 2.13). Nevertheless, not all T-O-T minerals show chemical expansive behaviour (Cotecchia, 2018). Clay composition and swelling are related by the concept of cation dissociation, i.e. dissociation of the cations located between the structural sheets, this results in negatively charged particles which tend to repel (Foster, 1954). The interaction between the clay mineral double layers is the main reason of the repulsive pressure (Taylor and Smith, 1986) and depend on:

- Cation type present,  $Na^+$  is a monovalent cation and cause more expansion than divalent  $Ca^{2+}$
- Concentration of ions in solution
- Amount of water present in the soil

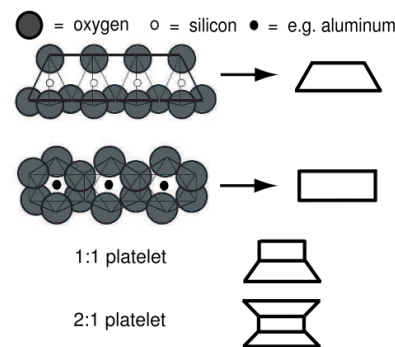


Figure 2.13: Clay structure: T-O and T-O-T (Bader, 2005).

| Clay        | Average free-swell (%) | Range (%) |
|-------------|------------------------|-----------|
| Na-smectite | 1500                   | 1400–1600 |
| Ca-smectite | 102                    | 65–145    |
| Illite      | 89                     | 60–120    |
| Kaolinite   | 28                     | 5–60      |

Figure 2.14: Clay mineral expansion (Taylor and Smith, 1986).

Table 2.14 shows the different types of minerals and their average percentage of swell. Illites have a relative low degree of swelling caused by neutralization of the charges by potassium. In case of low levels of potassium, illites are prone to swell (Foster, 1954). Chemical swelling is especially an issue for unsaturated clays in which the micropores are not (completely) hydrated, like clays undergoing wetting and drying cycles. Heavily overconsolidated clays generally have completely saturated micropores (Alonso et al., 1999), accordingly chemical swell can only occur by pore water changes.

### Pore water chemistry change

Elmashad (2017) reported that saline water decreases the swelling characteristics of clay. The extent depends on

the clay mineralogy and the liquid limit of the clay. Therefore, this effect can be ignored for clays with a low liquid limit. Saline water is slightly basic while freshwater is slightly acid, thus a higher concentration of  $H^+$  is present in fresh water. Consequently, a higher degree of swell will occur if initial saline pore water is substituted by freshwater. Pore water chemistry changes of the micropores will influence the chemical bonds, these chemistry changes occur only due to changes of water salinity between the depositional environment and the current water salinity. Diffusion is the governing process for pore water chemistry change, as stiff clays have a small permeability this is an extremely slow process. The well-known landslide at Rissa, Norway, occurred due to a change in porewater chemistry. The clay was deposited in a salt water regime and precipitation of rainwater caused an increase in the  $H^+$  concentration resulting in a decrease of strength.

The swelling characteristics can only be determined correctly if the sample is tested in water with the same salinity as present at the location of construction. A remoulded sample can not correctly estimate the swelling characteristics due to two reasons: (i) the original pore water is not present anymore, this is only important if the depositional environment differs from the current environment (ii) effect of fissures and discontinuities is not taken into account.

## 2.2. Boom clay

As part of a joint venture, Boskalis will conduct the planned dredging and reclamation works for the Fehmarnbelt project. Glacial clay tills and Palaeogene clay are present at the project location, further background information on the project and geology is given in appendix D. Another large scale expected dredging work to be conducted by Boskalis is Pulau Tekong in Singapore. At this location, soft as well as stiff clays are part of the proposed dredging work. In this study, experimental tests will be performed to increase the understanding of the required preload to close the interlump voids and its correlation to mechanical and chemical swell. The experimental tests in this study are conducted on Boom clay samples. It is chosen to perform the tests on the Boom clay as it is a Palaeogene stiff clay, relatively easily accessible and extensively studied clay. Chapter 2.2 gives an overview of the local geology and a geotechnical description of the engineering properties of the material.

### 2.2.1. Geological background

The Boom clay formation has been extensively studied for different geotechnical purposes and for clay mining. The formation was studied for several construction projects in the area around Antwerp and the world-class underground testing laboratory for radioactive waste disposal. Outcrops are located at some locations in Belgium, Germany and Province Zeeland (Mertens et al., 2003). Since the 13th century, the clay is exploited along the Rupel and Scheldt rivers for brick making. Nowadays the clay is mined in quarries south of Antwerp. Figure 2.16 presents the location of the top of the formation, claypits, and outcrop areas.

#### Lithology

The Boom clay is a formation deposited in the southern part of the North Sea basin during the Lower Oligocene. It is a continuous, high plasticity, layered clay layer of several tens of meters which consists of alternating silty clay and stiff clay layers of several tens of centimeters. Additionally, some organic rich black horizons are identified in the upper part of the Boom clay formation (Mertens et al., 2003) and several pale grey carbonate-rich horizons are also observed within the deposit. Those carbonate-rich horizons are formed by early diagenesis of marly zones resulting in calcite-concretions (septaria) (Dehandschutter et al., 2005). Besides the calcite-concretions the Boom clay also includes pyrite concretions (nodules). Bacteria produced hydrogen sulfide which forms the basis together with bivalent iron for the formation of pyrite nodules (Vandenberghé et al., 1997). Layered pyrite is identified at some outcrop locations as well as pyrite nodules in the different formations (Vandenberghé et al., 2014).

Figure 2.15 visualizes the microstratigraphic lithology of the Boom clay. A summary of the most important features in the units is given in this paragraph. The Boom clay is located in between two sand layers in which the top of the Ruisbroek sand formation forms the base of the Boom clay formation. The Belsele-Waas member is the lowest unit of the Boom formation and can be identified by two unusual thick silt layers. The Terhagen member is located above the Belsele-Waas unit and is characterized by grey clay with only a few black stained layers. Three septaria horizons are present and additionally red/brownish layers are present in the Terhagen member. A sudden systemic presence of black terrestrial organic layers is the identification for the base of the Putte member. Another striking feature in the Putte member is a coarse-grained silty double band (DB) that is thicker compared to the other silty layers. The top of the Boom clay formation is bounded by the Voort Sand formation, which overlies the Putte member (Vandenberghé et al., 2014). Distinct layers can be marked as horizons. The key horizons are: S=Septaria, R=Red/brown layer, DB=double band and the boundary between the grey and black clay layer (Vandenberghé et al., 2014).

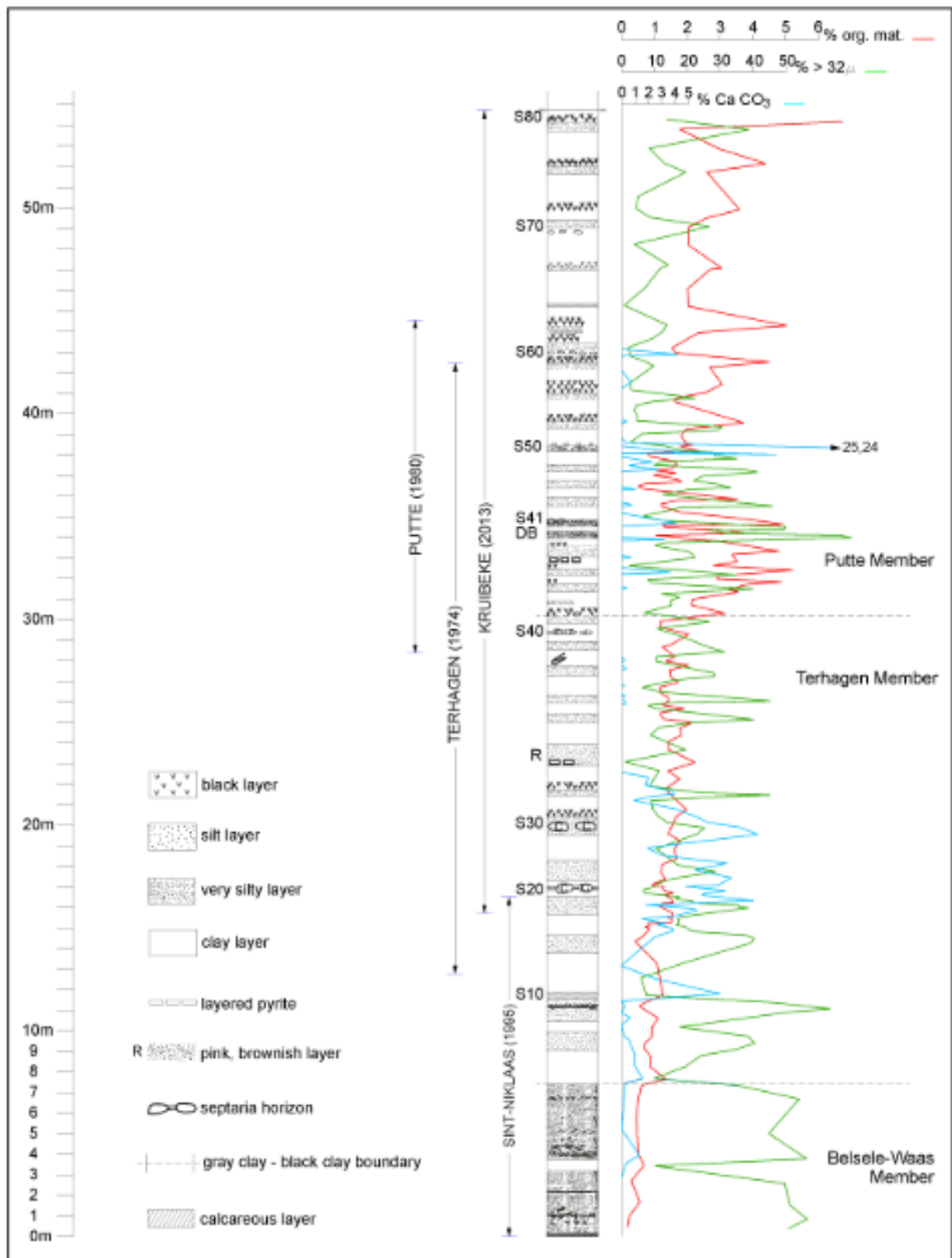


Figure 2.15: Micro-stratigraphical lithology of Boom clay at several outcrops. This figure shows the maximum exposed section ever observed. On the left of the stratigraphic column the exposed sections at some clay pits are indicated. The year stands for the year maximum exposure was present at the specific clay pit. The key horizons are indicated by S=Septaria, R=red/brown layer, DB=double band (Vandenberghe et al., 2014).

**Paleotectonical, paleoclimatic and paleogeographical setting**

Burial and uplift history of the Boom clay at the Antwerp area resulted in an overconsolidated clay. The clays in the north of Belgium were overconsolidated in the past but are nowadays buried at their deepest level ever experienced (Mertens et al., 2003). The maximum thickness of the Boom clay formation is 165 m, but the thickness varies per location due to erosion and uplift processes. The thickness of the Boom formation varies between 80 m at the Antwerp area (Vandenberghe et al., 2014) and 165 m in Mol. The difference in thickness can be explained by differential vertical tectonics during the late Rupelian, subsequently followed by erosion of the Boom formation at the Antwerp area (Demoulin, 2018). The sea-level drop during late Rupelian - early Chattian caused erosion of the Antwerp area with a rate of at least 6 mm / 100 yr. Figure 2.17 shows a schematic reconstruction of the eroded part of the Boom clay formation. Due to this erosion, the Boom clay exhibits a brittle stress strain behaviour as is typical for overconsolidated clay (Van Impe and Flores, 2007).

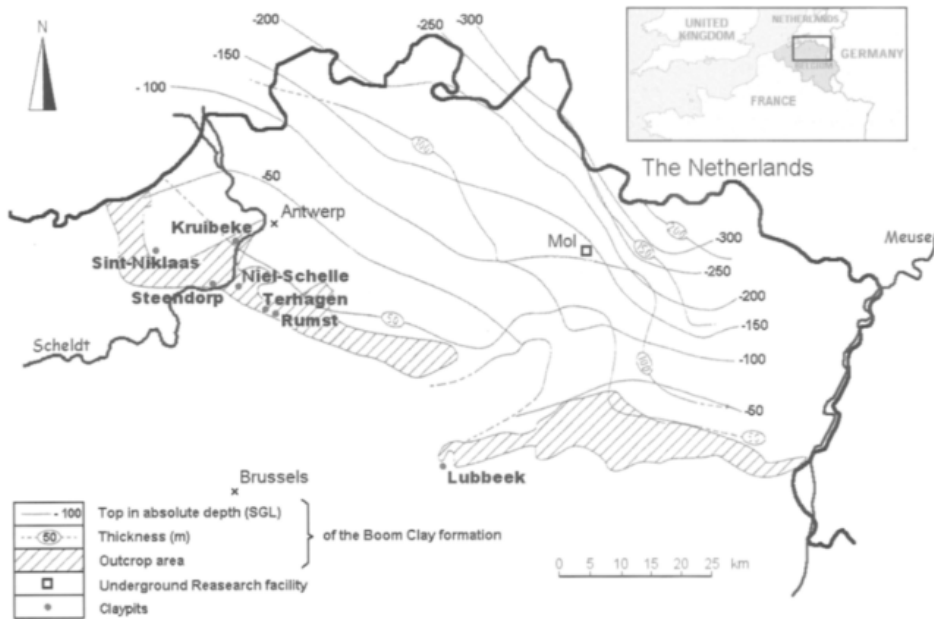


Figure 2.16: Geographic location of the Boom clay formation (Mertens et al., 2003).

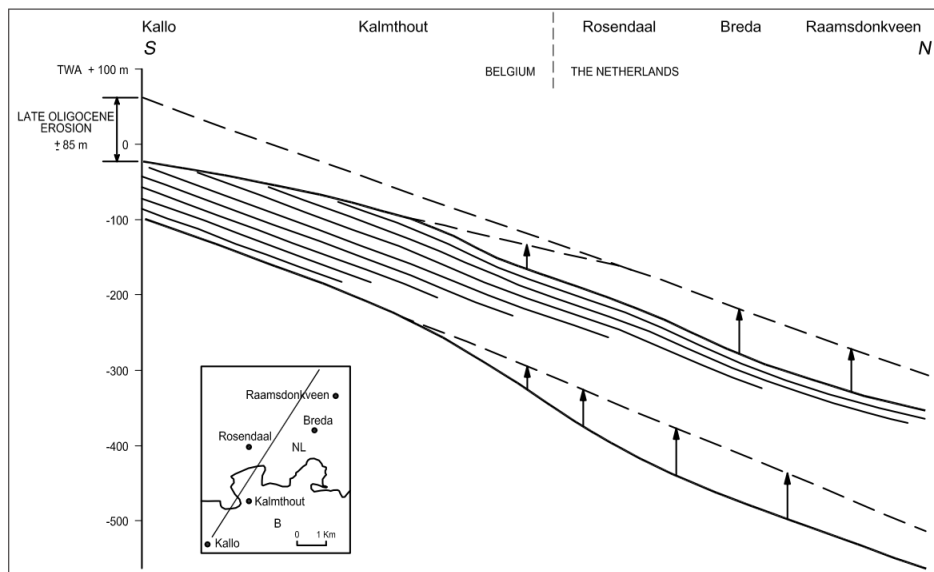


Figure 2.17: Reconstruction of the eroded part of the Boom formation: approximately 85 m of the top of the formation is eroded south of Antwerp (Vandenberghe et al., 2014).

Preserved macro and micro-fossils and the mineral glauconite indicate a marine depositional environment. Clays in the Black Caspian-Sea and Aral Lake have a similar lithology and macrofossil content as the Boom clay, hence this is an indication for an epicontinental sea. Deposition in the North Sea basin took place at varying water depths between 50 and 100 m. Accordingly, the depositional characteristics changed periodically, resulting in sub-horizontal layering (Mertens et al., 2003) of silty clay and clay layers. Eustatic sea-level changes and tectonics are two possible causes of cyclic water depth changes forming cyclic sub-horizontal layering. As the layers are continuous and a great cyclic regularity is present, it is more probable that the layers are formed by eustatic sea-level changes. This is confirmed by spectral analysis of the resistivity log data in which a relationship between the layering and the Milankovitch cycles was obtained (Vandenberghé et al., 2014). From this relationship, it follows that the alternating silty clays and stiff clays form the main cyclicity with a timespan of 41 ka (Abels et al., 2007).

Oxygen isotopes of biogenic carbonates indicate that a sudden cooling took place at the start of the Oligocene. Sea level decreases as a result of the quick build up of large ice caps over parts of Antarctica. The Boom clay is identified as a transgressive formation. Thus, it was deposited in relative deep water. The climatic conditions do not match with the observed transgressive formation. For this reason, it can be concluded that the Rupelian transgression is attributed to regional subsidence. The evolution of the Alpines induced regional subsidence of the North sea basin (Vandenberghé et al., 2014).

### Discontinuities

Several discontinuities are present within the Boom clay formation. The most important discontinuity surfaces are the sub-vertical joints and the smaller irregular dipping joints. Other discontinuity surfaces such as faults, diapiric structures, conchoidal fractures, and open bedding planes are identified at some locations but are not systematically present in the clay.

- Sub-vertical joint pattern: The most outstanding macro-discontinuity visible in the outcrop locations of the Boom clay is the sub-vertical joint pattern (Vandenberghé et al., 2014). The joints are spaced between 0.5 and a few meters and the jointing density is constant along the depth. No displacements or slickensided surfaces are present along the joints. Slickensided is a term for smooth striations along the joint slip surface (The editors of Encyclopaedia Britannica, n.d.[b]). These slickensided surfaces are formed by clay minerals which have undergone small displacements (  $10 \mu\text{m}$  ). Subsequently, this results in oriented clay minerals along the displacement surface. The small displacements are probably caused by volume changes of the compacting clay (N. Vandenberghé (personal communication, February 25, 2019)).

Striations are absent as is the throw along the fault. Thus, it can be concluded that these joints have a tensional origin. The tensional origin can not be explained by regional tectonic history nor by burial/uplift. Shrinkage due to small pore fluid losses is the most probable origin of the joints. It is unknown what the origin is of pore fluid losses, as the clay layer is relatively thick (Mertens et al., 2003). The joints are only present in the top 40-50 m of the Antwerp area, which can be explained by the cohesion and vertical stress relation determined by Mertens et al. (2003).

- Smaller, irregular dipping joints: Smaller, more irregular dipping joints, with more curved and uneven surfaces are related to the development of the vertical joint pattern. In literature the smaller irregular dipping joints are often referred to as fissures. This term will also be used later in this report. The smaller irregular joints are closely spaced and are a spacing of cm is typical. The smaller joints commonly have a plumose structure and are often slickensided (Mertens et al., 2003). The plumose structure is an intricate pattern resembling a 'feather' shape. Intensity changes of the stress field causes such a pattern during the growth of a joint (Pluijn and Marshak, n.d.).
- Faults: The Antwerp area has only undergone moderate vertical movements since the Oligocene, while from the Neogene to the present the stress field remained constant (Mertens et al., 2003). Faults are only identified at the Kruikebe clay pit where a normal meter-scale fault zone is present. The fault zone is related to differential regional tectonic tilting during the late Oligocene (Vandenberghé et al., 2014).
- Diapiric structures: Diapiric structures are only present under the current location of the Scheldt river and were detected by high-resolution seismics. Their existence can be explained by river valley erosion which diminished the vertical stress. As a result, the clay was squeezed upwards by the horizontal stresses formed by the deep burial (Mertens et al., 2003).

- Conchoidal fractures: In the very clay-rich parts of the Boom clay conchoidal fractures can form (Vandenbergh et al., 2014). Fine-grained materials can form a smooth curved fractures surface, called a conchoidal fracture (Editors of Sandatlas, n.d.).
- Bedding planes: Clear bedding planes are visible between the alternating silty clay and clay layers. But no discontinuity planes are identified at the bedding planes in situ. Fine bedding fissility is only observed in outcrops along black Boom clay layers. The black Boom clay layers have a high detrital organic matter content due to weathering (Vandenbergh et al., 2014).
- Septaria horizons: Three septaria horizons are present in the Terhagen member. They originate from early diagenesis of marly zones that resulted in calcite concretions (Dehandschutter et al., 2005).

The most important discontinuities of the shallow (40-50 m) Boom clay formation at the Antwerp area are the sub vertical joints and the smaller, irregular joints. Those discontinuities are systematically present in the upper part of the Boom clay formation. The geotechnical properties are largely influenced by discontinuities as explained in section 2.1.5. Therefore, it is extremely important to have a deep understanding of their occurrence. The smaller, irregular joints can also be referred to as fissures, such that the Boom clay is described as a medium to highly fissured clay in which many of the fissures have a slickensided appearance (Piriyakul and Haegeman, 2009).

### 2.2.2. Geotechnical properties

This section describes the geotechnical properties of the Boom clay based on literature. Several of those literature values are used as an input for the MPM model.

#### Geotechnical literature description

The Boom clay is described as a stiff clay with an undrained shear strength between 75-160 kPa (Mertens et al., 2003). De Beer (1967) performed several unconfined compression tests as well as unconsolidated undrained triaxial tests and visualized the results in figure 2.18. The scatter in the results is related to the fissured state of the clay. It is a moderately swelling clay with illite and kaolinite as the dominant minerals (Bernier et al., 1997). Other characteristic properties are summarized in table 2.1 and the mineralogy in table 2.3.

The Boom clay has been subdivided into 4 main geotechnical formations, BK1 to BK4. The geotechnical formations do not correspond directly to the lithological formations as mentioned in section 2.2.1. A weathered top layer, BK0, with varying thickness from a few decimeters to 4 m is identified at the surface (Schittekat, 2001). Figure 2.4 visualizes the location of the geotechnical formations in a cross-section along the trajectory. BK1 is a banded sequence that consists mainly of silty horizons and some clayey horizons. The geomechanical properties are well known as this unit has been intensively investigated for different civil works north of Antwerp. The underlying BK2 formation is more clayey with reference to BK1 and corresponds partly to the black clay observed at the clay pit of Kruibekke. The following formation, BK3, consists of silty and clayey horizons. BK3 outcrops south of Antwerp and is also intensively investigated. The horizon from grey to black clay is located within formation BK3. A transitional sequence of silty to clayey fine sands which progresses into the underlying sand formation characterizes BK4 (Schittekat, 2001). An overview of the index properties of the three formations is summarized in table 2.2. It is a natural material with variable properties per location. Accordingly, those values can only be used as a first indication.

|                                       |                             |
|---------------------------------------|-----------------------------|
| Mean percentage of particles $< 2\mu$ | 49%                         |
| Liquid limit                          | $81.25 \pm 8.25\%$          |
| Plastic limit                         | $29.05 \pm 3.35\%$          |
| Plasticity index                      | 52.20                       |
| Activity                              | 1.07                        |
| Presence of montmorillonite           | no                          |
| Presence of pyrites                   | yes                         |
| Presence of septaria                  | in nearly horizontal layers |
| Classification of Casagrande          | C H                         |
| Natural water content                 | 25–32%                      |
| Mean bulk density                     | 1.9 t/m <sup>3</sup>        |

Table 2.1: Literature classification data of Boom clay (De Beer, 1967).

|   | Units             | BK1  | BK2  | BK3  |
|---|-------------------|------|------|------|
| % particles $< 20\mu$                         | %                 | 80   | 80   | 80   |
| % particles $< 2\mu$                          | %                 | 50   | 57   | 54   |
| Natural water content w                       | %                 | 27   | 29   | 30   |
| Liquid limit LL                               | %                 | 66   | 73   | 60   |
| Plasticity index IP                           |                   | 40   | 44   | 35   |
| Unit weight of dry soil Y <sub>d</sub>        | kN/m <sup>3</sup> | 15.3 | 14.6 | 14.7 |
| Unit weight of soil Y                         | kN/m <sup>3</sup> | 19.4 | 19.2 | 19.3 |
| Unit weight of solid particles Y <sub>s</sub> | kN/m <sup>3</sup> | 26.5 | 26.5 | 26.5 |

Table 2.2: Classification of the upper three geotechnical formations of the Boom clay formation (Schittekat, 2001)

| Mineralogy (wt.%)       |       |
|-------------------------|-------|
| Clay minerals           | 60    |
| illite                  | 20–30 |
| smectite                | 10–20 |
| chlorite                | 5–20  |
| kaolinite               | 20–30 |
| mixed illite/smectite   | 5–10  |
| mixed chlorite/smectite | 5–10  |
| Quartz                  | 20    |
| Feldspars               | 5–10  |
| Carbonates              | 1–5   |
| Pyrite                  | 1–5   |
| Organic carbon          | 1–5   |

Table 2.3: Mineralogy of the Boom clay (Bernier et al., 1997).

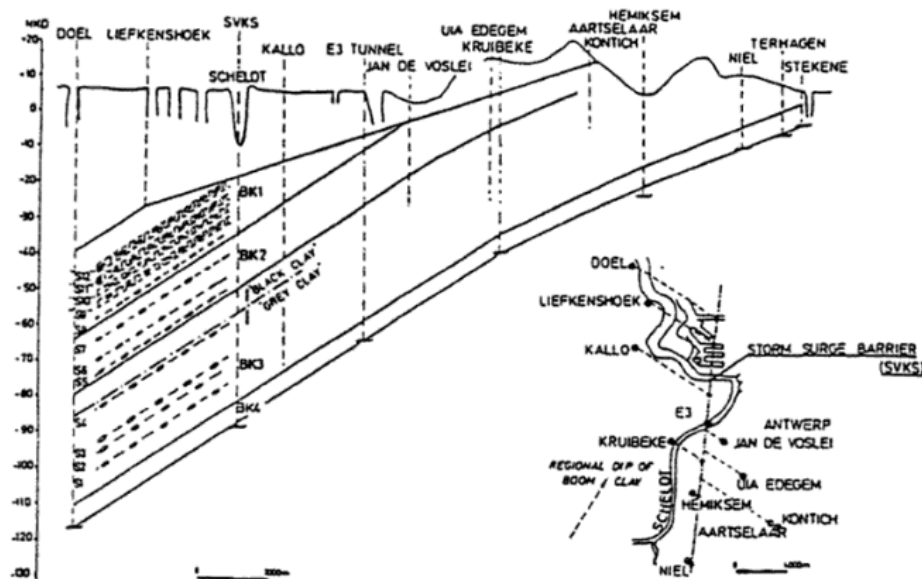


Table 2.4: Cross section of the Boom clay presenting the different geotechnical formations (Schittekat, 2001).

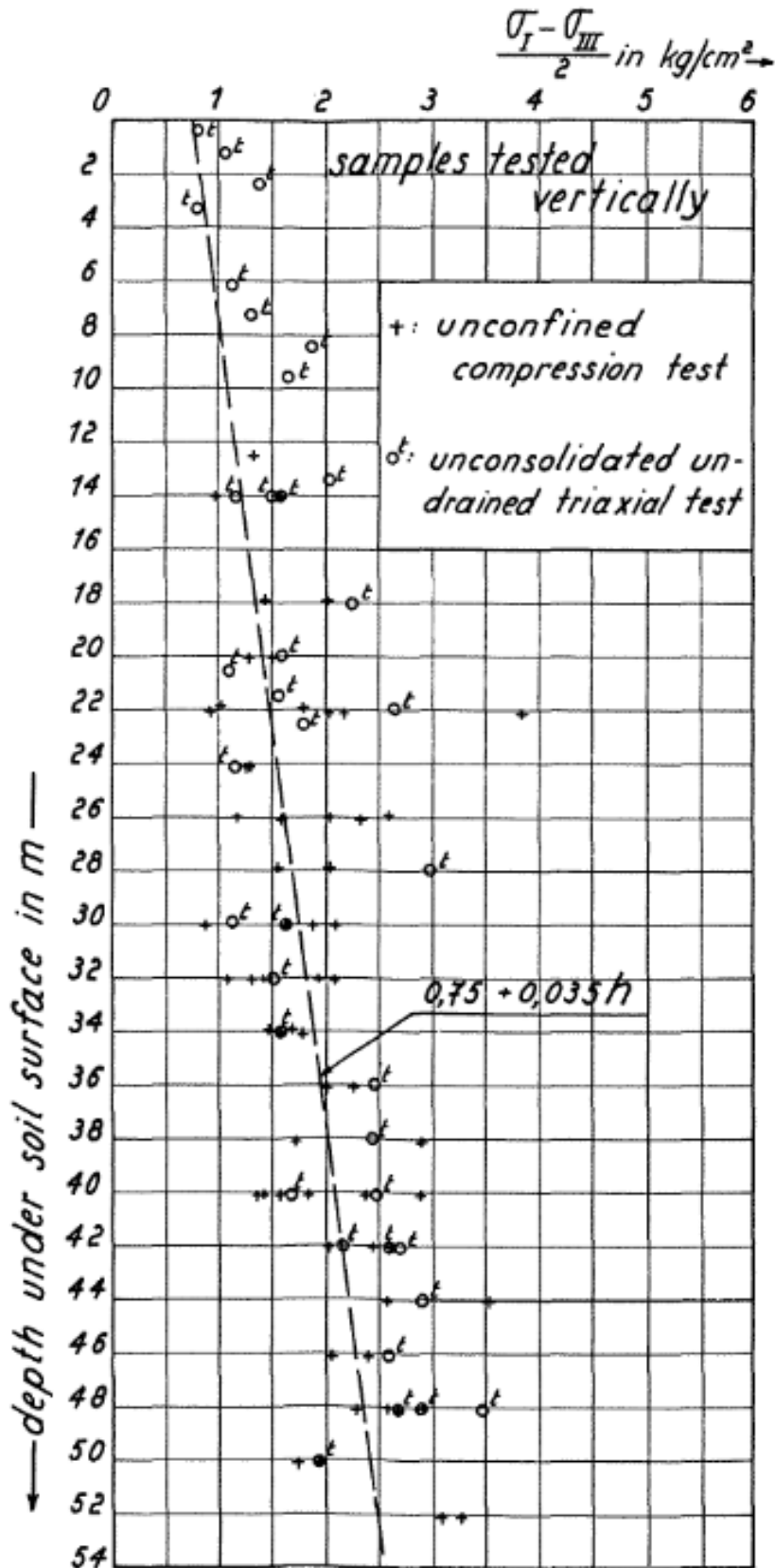


Figure 2.18: Undrained shear strength as a function of depth for the Boom clay. The presence of scattering is related to the fissured state (De Beer, 1967).



# 3

## Lumpy fill

This chapter describes how a lumpy fill is formed. Section 3.1 describes the different dredging techniques and their resulting products. This study focuses on mechanical dredging and this is described in more detail. Section 3.2 elaborates on the resulting lump size distribution and bulking factor of the mechanically dredged lumps. Three different settlement processes take place after placement, elaboration on this is presented in section 3.3. This report focuses on the first settlement process, i.e. closure of the interlump void space as stated in section 3.3.1.

### 3.1. Dredging technique

Stiff clays can be mechanically dredged or by a combined mechanical-hydraulic method (IADC, n.d.). Mechanical dredging is a technique that removes sediments through direct application of mechanical forces while adding very little process water (PIANC, 2014). The resulting products of a mechanical dredging method are clay lumps. Combined mechanical-hydraulic dredging is a dredging technique which combines mechanical forces with water suction forces. A combination of slurry and smaller clay balls result as the end product of a mechanical-hydraulic dredging method. The preferred dredging technique depends on local conditions such as soil characteristics, water depth and climate. Stiff clays are most commonly dredged mechanically, by reason of obtaining the largest total fill volume. Another advantage of mechanical dredging is the minimal loss of fines and thereby the preservation of surrounding ecological environments. Accordingly, there is chosen to focus on **mechanical dredging** in this study.



Figure 3.1: Mechanical dredger: Backhoe. A backhoe dredges the material by a single dredging bucket. (IADC, 2014a).



Figure 3.2: Mechanical-Hydraulic dredger: Trailing Suction Hopper. Hydraulic suction and mechanical are combined in this method. (IADC, 2014b).

### 3.2. Lump size distribution and bulking

Mechanical dredging will result in clay lumps ranging up to several meters (Karthikeyan et al., 2004). An advantage of lumpy fill material is its high strength and reduced compressibility provided by the large intact stiff lumps (Manivannan et al., 2000). Contrarily, this is also the reason of large initial settlements due to lump closure and long-term consolidation. The outer shell of the lump will be altered due to the cutting and transportation process, which causes the formation of fissures. Dumping of the lumps on the transportation barge and on the reclamation fill have a considerable impact and results in fissuring and breakage of the lumps.

The lump size distribution has a major influence on the bulking factor: clay lumps of equal size will form a larger volume than a well-graded lump size distribution. The size of the dredger (bucket size and available cutting power), the intact clay characteristics (plasticity and undrained shear strength) and degree of fissures and discontinuities all influence the lump size. Mechanical dredging will result in large clay lumps up to several meters (Karthikeyan et al., 2004). The exact size depends on the soil characteristics, the dredging equipment, as well as the transportation and placement process. Highly plastic clays can be prone to swelling as explained in section 2.1.6. Consequently, this also influences the lump size. The presence of fissures and discontinuities will decrease the lump size, owing to the sample-size effect (Nishimura, 2005), as stated in section 2.1.5. Dykstra (2013) reported that an unweathered highly plastic stiff clay without discontinuities can form lumps up to several cubic meters at the fill. Clays often contain discontinuities, and therefore the lumps are generally smaller in size. The experience of the dredging process at the Island of Punggol Timor in Singapore resulted in an approximate size of  $8 \text{ m}^3$  directly after dredging; the transportation and placement process reduced the lump size to  $0.5\text{-}2 \text{ m}^3$ . At Halmstad Harbor, Sweden, stiff silty clay lumps were dumped by bottom-open barge and had an approximate volume  $1 \text{ m}^3$  (Karthikeyan et al., 2004).

Bulking is the change of soil volume in a containment area to the initial in-situ volume (PIANC, 2014). The lump size distribution has a major influence on the bulking factor. The shape of the lumps also influences the bulking factor: the density of a matrix formed by spheres will be larger than for cubical or irregular shaped lumps (Leung et al., 2001). The bulking factor changes over time; in dredging works the initial bulking factor direct after placement is the most important one. The total scheduled disposal volume is based on the bulking factor directly after placement. The in-situ characteristics of the soil along with the excavation, transport and deposition process influences bulking. The bulking factor can only be truly known by simulating the dredging and deposition process. Figure 3.3 gives an overview of the bulking factor at the transport barge for different soil types. Depending on the deposition conditions and the soil specific characteristics, the final bulking factor can be estimated. Generally, this factor on the fill will be smaller than at the transport barge due to rehandling.

|                        |      |
|------------------------|------|
| Gravel                 | 1.10 |
| Mud                    | 1.10 |
| Peat                   | 1.35 |
| Soft clay              | 1.20 |
| Su < 50 kPa            |      |
| Clay                   | 1.35 |
| 50 kPa < Su < 100 kPa  |      |
| Hard clay              | 1.45 |
| 100 kPa < Su < 200 kPa |      |
| Pieces of rock < 10 cm | 1.45 |
| 10 to 20 cm            | 1.70 |
| 20 to 60 cm            | 2.00 |

Figure 3.3: Bulking coefficient in the transport barge for different materials (VOUB, 2010).

### 3.3. Settlements

Three different ranges of settlements are expected, all occurring due to different 'consolidation' processes. The three different processes are: (i) large settlements by closure of the inter-lump voids, (ii) primary consolidation and (iii) fuzing of clay in inter-lump and intra-lump, which is a creep process. Closure of the inter-lump void space is a quick process, resulting in large settlements as described in subsection 3.3.1. Primary consolidation and creep are both smaller-scale consolidation processes and are closely associated as described in subsection 3.3.2.

#### 3.3.1. Closure of interlump void space

Mechanical dredging of stiff clay results in a lumpy deposit. Large interlump voids are initially present, also referred to as macroporosity. According to Kostkanová et al. (2014) an initial interlump porosity of 40% is typical for a lumpy clay deposit, but the exact initial interlump porosity depends on the lump size distribution and the stiffness of the clay (Karthikeyan et al., 2004). Closure of these interlump voids will cause major displacements, therefore preloading is a necessity to overcome these large settlements. Large immediate settlements took place after preloading at the Halmstad Harbour and Pasir Panjang Terminal.

Closure of the interlump void space is a result of two different processes: (i) rearrangement of the clay lumps and (ii) deformation and breakage of the lumps. The lump size distribution, initial stacking and plasticity have a large influence on the rearrangement of the clay lumps. Large clay lumps are less likely to rearrange than smaller lumps due to the stacking as well as the existence of shear forces between large, highly plastic, clay lumps. For stiff plastic clays it is expected that the effect of deformation and breakage is the most important one, as the clay lumps are relatively large and highly plastic.

Clay lumps will always deform if they are loaded by a surcharge larger than the bearing capacity of the clay. The bearing capacity can be determined by multiplication of the bearing capacity factor and undrained shear strength. For undrained homogeneous clays ( $\phi = 0$ ) the bearing capacity factor is given by the Prandtl solution (Griffiths and Fenton, 2001):

$$N_c = 2 + \pi = 5.14 \quad (3.1)$$

As clays soften and contain discontinuities, it is expected that the interlump voids close under a reduced surcharge. A decrease in suction is expected when clay lumps are placed in water, resulting in swell which causes a lower effective stress as explained in section 2.1.6. Internal tensile stresses are formed by the variation in swell and softening inside a lump, therefore causing cracks and aggravation of the outer part of the lump while the inner part stays intact (Alapakam, 2006). Another cause of small fissures at the outer shell is the cutting and transportation process.

Preloading by a reduced surcharge will deform the outer shell of the lumps, and the disintegrated parts of the clay lumps will fill the interlump void space (Robinson et al., 2004). It is of great importance to get a good understanding of the initial suction and degree of swelling as well as the discontinuities of the clay because the required surcharge depends on these factors. Swelling will lower the effective strength of the smaller clays lumps and the edges of the larger lumps. The edges will deform and disintegrate under a relative small preload. Furthermore, the overall strength of the lump is decreased by fissures and discontinuities as described in section 2.1.5.

The required preload for swollen clay lumps will be smaller than the load required to deform an intact, unswollen clay lump. Hence the surcharge should ideally be placed on the fill after a large part of the swelling due to the dissipation of suction has occurred. The dissipation time of suction for large stiff clay lumps may take too long within the time limits of construction. Several factors will influence the required preload to close the interlumps, but no exact relationship is known. The influencing factors are:

- soil characteristics (e.g. strength, stiffness, plasticity, OCR, discontinuities, mineralogy)
- lump size distribution
- shape of lumps
- time until preloading

After closure of the interlump voids a zonation exists in the deposit as visualized in figure 1.3. The initial interlump void space is filled with disintegrated lumps. The soil within the initial interlump void space (NC) has other properties than the parts formed by the inner, unaltered, part of the lumps (OC). The most important difference is the void ratio, which is larger in the interlump soil (Leung et al., 2001). Closure of the interlump void space under a reduced surcharge will not occur in all cases. Moreover there are two causes: (i) there was not enough time for suction to dissipate such that the preload is too small to deform the lumps, or (ii) the mesopores in extremely overconsolidated clays can be completely closed (section 2.1.6), thus mechanical swell is prevented.

From experimental and full-scale historical cases, the expectation rises that an immediate large settlement takes place under a reduced preload. Leung et al. (2001) performed an experimental study into this subject. A short summary is presented in the following paragraph.

Experimental test on stiff Singapore marine clay Leung et al. (2001) conducted several one-dimensional compression tests to evaluate the load-settlement response of a lumpy clay fill. The experiments were performed on the Singapore clay. The in situ shear strength of the used material is 100 kPa, and its preconsolidation pressure is 480 kPa. The liquid limit of the clay is 48%, and its plastic limit is 24%. The clay is not active with an activity index of 0.453.

The clay was remoulded after which it was hydraulically recompressed to 100 kPa. A cylindrical scoop was used to obtain well-rounded 50 mm diameter balls. The test sample consists of clay balls in a hexagonal packing, and the void space is filled with de-aired water. Five different loads were sequentially applied to the sample, resulting in the settlement-time results presented in figure 3.4. Preloading by 25 kPa resulted in a large immediate settlement, which mainly can be attributed to the closing of the interlump void space. The immediate surface settlement for loading under 50 kPa is significantly reduced by the preload. The subsequent surface settlement increases gradually with time, similar to more homogeneous soil consolidation.

Figure 3.5 shows the pore size reduction of a homogeneous clay cake and the clay lump system after preloading. The clay lumps are squeezed by the preload and fill the interlump voids. From these results it can be concluded that most of the interlump pores close during preloading under a load of 25 kPa. The total porosity after the closure of the interlump voids is still larger than that of a homogeneous clay cake. Crushing at the points of contact was

observed for some clay balls at the end of the preloading stage (25 kPa). Crushing occurred because a redistribution of load took place. The following load step (50 kPa) caused more deformation and crushing. Afterwards, the intact structure of the clay balls was hardly visible anymore after the second loading stage.

This experiment was performed on small clay balls. The results cannot directly be generalized because the clay balls are small, and the clay is not extremely stiff. It would also be better to use intact clay balls instead of a reconstituted clay, because remoulding changes the original structure of the clay. A remoulded sample will soften more than an intact sample due to the loss of overconsolidation pressure in a remoulded sample. Cementation and ageing effects, as well as discontinuities and the original pore water chemistry, are also lost during the remoulding process.

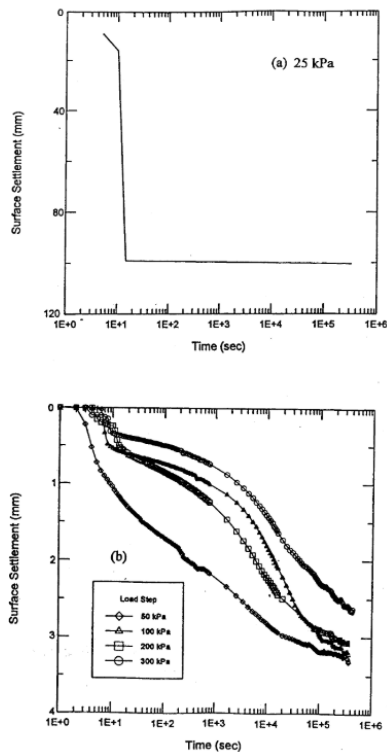


Figure 3.4: Surface settlements over time for sequential loading steps. The largest immediate settlements already occur by a preload of 25 kPa (Leung et al., 2001).

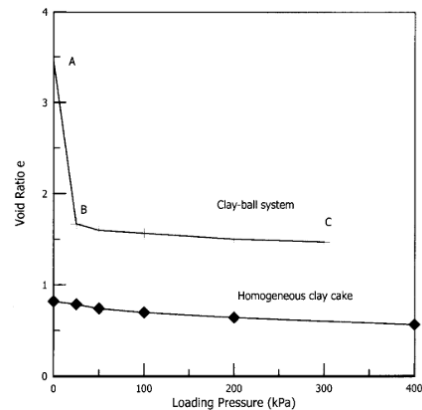


Figure 3.5: Comparison of void ratio change during loading of a homogeneous clay cake and clay lumps. A-B: Pre-loading by 25 kPa. B-C: loading up to 300 kPa. The processes are similar and correspond to a consolidation process (Leung et al., 2001).

Additionally, Leung et al. (2001) performed several centrifuge model tests to determine the effect of size, shape and undrained shear strength on the total settlements. Prototype stresses are simulated more realistically in a centrifuge and the consolidation time is expedited. The centrifuge test measures the total settlement strain over a 6-8 year prototype timespan. The conclusion of this test was that the shape, size and strength all influence the initial void ratio of the system. Larger settlements occur for tests performed on samples which induce a larger initial void ratio of the system. Increase in size and increase in strength results in a system with a higher initial void ratio due to the packing of the lumps. Spherical lumps will form a denser packing than cubical or irregular shaped lumps. Therefore, the total settlements of the system are smaller.

### 3.3.2. Consolidation and Creep

Whitman (1970) reported that the rate of consolidation depends on the matrix characteristics surrounding the clay lumps, while the compressibility of a lumpy fill results primarily from deformation of clay lumps. The consolidation can be further explained by figure 3.6, showing that the excess pore pressure is higher inside the lumps than at a fixed location. These results reveal that the interlump (macro) permeability is higher, in the order 10, than the intralump (meso) permeability (Leung et al., 2001). Therefore primary consolidation depends mainly on the characteristics

of the surrounding clay around the original unaltered lump. The rate decreases with an increased loading pressure because the voids close up. The consolidation and creep is dominated by the interlump permeability in two ways: (i) rapid pore pressure dissipation in the interlump soil (consolidation) and (ii) accelerated fluid transfer from the intralump voids to the interlump voids due to the greater pore pressure difference (creep) (Yang et al., 2002). The long term settlement can be called creep; it is the very slow process of fuzing of the lumps.

The case study at Punggol Timor in Singapore reported the presence of NC and OC zones within the clay lump fill after 12 years (Karthikeyan et al., 2004). It can be concluded that a certain homogenization of the clay fill has taken place, but there is still a distinct difference in strength and pore sizes. Complete homogenization of the fill is a long term creep process. The case study at Punggol Timor adheres to the modelling tests performed by (Yang and Tan, 2005).

Yang et al. (2002) stated the importance of self weight consolidation of a lumpy clay fill because the completion of the dredging and dumping process takes a significant amount of time, e.g. 5 years in the Pulau Tekong reclamation project. Dissipation of the pore pressure in the interlump voids is relatively rapid because the high permeability in the NC zones of the fill. As a result, almost full dissipation of the pore pressure at the interlump voids occurred in the Pulau Tekong project before placement of the surcharge. The projects Boskalis undertakes generally have a shorter timespan on account of economics. For this reason, full dissipation of pore pressures in the NC is not expected.

Sand layers can be deposited between the lumpy clay layers, and the sand will settle by gravity in between the lumps and increase the consolidation coefficient in between the lumps (Ott, 2017). Depending on the allowed long term settlements of the reclamation area, this may be an interesting method to decrease the settlements. Sand needs to be placed between every 3 m of clay to fully penetrate into the voids (Hartlen and Ingers, 1981). A major disadvantage of this technique is the large amounts of sand to fill the voids.

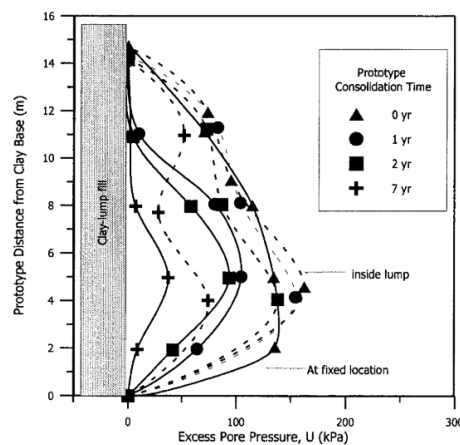


Figure 3.6: Excess pore pressure isochores inside lump (dotted line) and at fixed location (solid line) (Leung et al., 2001). The excess pore pressure decreases over time.



# II

## Methodology



# 4

## Methodology

In this study, a combined experimental and numerical approach is applied to increase the understanding in the interlump void closure problem. The experimental tests are performed on Boom clay samples, and the numerical model uses the clay characteristics of the Boom clay as input. The global arrangement of the consolidation and softening process is 1D for both the experimental and numerical method. While, the consolidation and softening process inside the material are actually in 2D. The experimental tests govern the true material behaviour, while the numerical approach is governed by the material model. The material model (constitutive model) approximates the real material behaviour. Thus, the outcome is highly dependant on the material model used.

In the literature study it was described that interlump void closure is closely related to the initial soil characteristics, softening and the presence of discontinuities. These processes are studied by the following methods:

- The presence of discontinuities result in an increase of the hydraulic conductivity. Their presence can be identified by CT-scans, and an estimate about the corresponding increase in hydraulic conductivity can be made. The estimated fissured hydraulic conductivity of the Boom clay will be used as an input in the numerical model.
- Softening of the clay lumps occurs due to two different processes: (i) unloading of the material (ii) hydro-mechanical (Karthikeyan et al., 2004) and chemical swelling. Softening due to chemical and hydro-mechanical swelling is tested in the swell-load test. Besides, the influence of hydro-mechanical swell is also tested in the numerical model.
- The research question was based on the experimental tests performed by Leung et al. (2001). A similar test is executed to increase the understanding in the softening time and the corresponding interlump void closure under a reduced preload.
- The influence of initial soil characteristics on interlump void closure is tested by a numerical model. A sensitivity analysis for a broad range of initial soil characteristics is performed.

### 4.1. Experimental testing

#### 4.1.1. Sample material

The experimental tests are performed on Boom clay samples originating from the Tuinlei-Schelle quarry south of Antwerp. The exact geographical location is shown in figure 4.1. In February 2019 four large blocks ( $0.025 \text{ m}^3$ ) were taken from the quarry. The blocks were sampled from a location of approximately 6 m below surface level. It is inevitable to disturb the blocks slightly; nonetheless this will also occur during the dredging process. The natural structure of the clay is of great importance for the tests. The clay was sampled in large blocks and stored in a climate room in airtight bags to maintain the natural structure.

The index tests are performed according to literature standards. A more extensive description of the methodology of the index tests can be found in appendix B

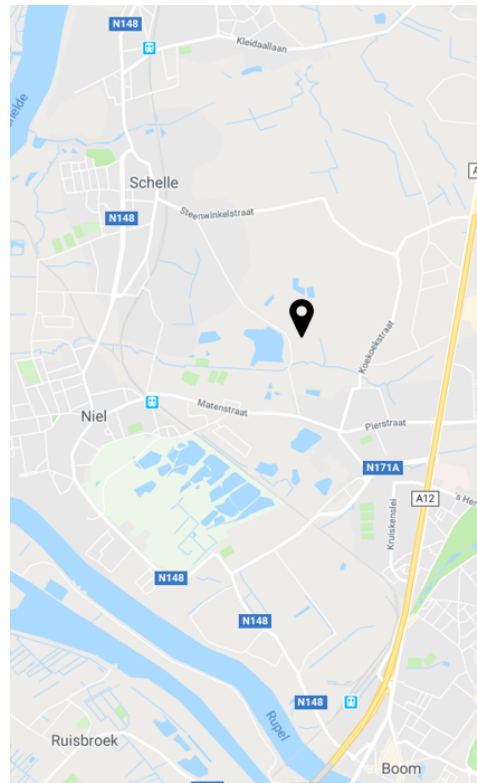


Figure 4.1: Geographical location of the quarry where the Boom samples were extracted.

#### 4.1.2. Fissure identification tests

Fissures and micro-fissures are likely to be present in the Boom clay sample originating from the Tuinlei-Schelle quarry (figure 4.1). The larger fissures can be determined by a medical CT scan apparatus. The micro-fissures are extremely small and can only be observed by a micro CT scanner.

The Boom clay is very brittle. Hence it is impossible to determine the presence of fissures in the sample by direct visual identification. Fissures are induced by the cutting process, and therefore this method is not representative for the natural fissure density. Computed tomography (CT) is a computerized x-ray imaging method that can produce 2D slices of a material such that more insight in the structure can be obtained. A sampling block ( $L \approx 40$  cm,  $H \approx 30$  cm,  $W \approx 30$  cm) was placed in the CT scanner. The presence of large fissures can be determined by this method as the resolution of the images is 0.40 mm.

The micro CT scanner (fig: 4.2) is a computer tomography scanner of Phoenix nanotom (180 kV). A very small sample with a diameter of 4 mm is prepared with care to minimize the disturbance of the initial structure. The sample is placed in a holder in the micro CT scanner and scanned for an hour. Several image slices in three directions are generated as an output. The actual resolution of the images depends on the sample size as its resolution is 1/1000 of the sample size. Accordingly, the resolution of the images is 4  $\mu\text{m}$ .

#### 4.1.3. Miniature clay fill test

Leung et al. (2001) performed a preloading test on a miniature clay fill. The clay balls were formed by a remoulded and recompressed material up to 100 kPa. He concluded that interlump closure occurs under a reduced preload of 25 kPa (section 3.3.1). Within this study, a similar test will be performed. In contrast to the experiment conducted by Leung et al. (2001), the sample material used within this study will be in its original state. Only sample material in its natural state can govern the effect of discontinuities and the overconsolidated state. The goal of this test is to verify the results of the test conducted by Leung et al. (2001) for a natural sample. The rearrangement of the clay balls and softening time is studied by this experimental test.

##### Test setup

The miniature clay fill test is performed in a Rowe cell with a diameter of 15 cm, seeing that this setup is similar to the setup used in Leung's experiment. A Rowe cell is a hydraulic consolidation cell in which the sample is subjected to

a vertical axial pressure applied by water pressures (Manual of soil laboratory testing, 1966). In this test the sample is loaded by a flexible diaphragm, i.e. free strain loading, such that a uniformly distributed pressure is applied to the clay balls (BS1377, 1990). The water can leave the test cell by two-way vertical drainage through a porous cap as in figure 4.3. The setup is prepared according to the BS1377 standards.

#### Preparation of clay balls

The rearrangement effect can only be governed realistically if the clay balls are small in comparison to the test volume. As otherwise, the influence of the stapling of the balls becomes too large. The rule of thumb is that the size should be 20 times smaller than the diameter of the setup. Ideally, round clay balls with a diameter of 0.5 cm are used in this test. But as the material is very stiff, and therefore it is hard to prepare small balls, there is chosen to perform the test on small cubes of  $1 \text{ cm}^3$ .



Figure 4.2: Micro CT scanner at Delft University of Technology.

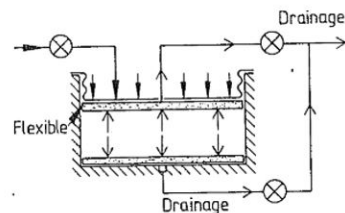


Figure 4.3: Drainage and loading conditions for Rowe cell: two-way vertical drainage with free-strain loading (BS1377, 1990).

#### 4.1.4. Determination consolidation coefficient

To increase the understanding of the softening time, a small softening test is performed. Softening of a small clay cube is a relatively fast process due to the small size. A first estimate of the softening time can be obtained by a preliminary small scale test. A simple test is performed in which a cube of  $1 \text{ cm}^3$  is placed in a cup of water. Complete softening is reached when the clay cube turns into a slurry under a very small push by a fingertip. The consolidation coefficient upon unloading can be determined by the softening time.

The unloading consolidation coefficient can be determined by this small scale test and can be compared to the loading consolidation coefficient based on literature values. Furthermore, it can be compared to the unloading and loading consolidation coefficients that result from the swell-load test as described in section 4.1.5.

#### 4.1.5. Swell and consolidation test

The Boom clay is an overconsolidated clay and is likely to swell due to the dissipation of suction and/or by a pore water chemistry change. It is important to know the in situ pore water chemistry in the micropores as the pore water chemistry influences the microstructure of the material, i.e. flocculated or dispersed. Before the swell test results can be interpreted correctly, it is necessary to know the pore water chemistry of the material at its in situ location. So, before the material is dredged. In the second part of this section, the methodology of the swell and consolidation test is described.

##### Pore water chemistry of Boom clay

The pore water chemistry of a clay deposit depends on the initial depositional environment and the current salinity of the (sea)water on top of the deposit. The pores of clay deposited in a freshwater environment might become saline by the diffusion with the saline water located on top of the deposit. As the salinity of the pore water chemistry influences the microstructure, it is important to know the pore water chemistry of the deposit truly. Especially when the clay was deposited in a freshwater environment.

In the literature review (section: 2.2.1) it was described that the Boom clay was deposited in a marine environment and overlain by saline water. Consequently, the pore water chemistry is likely to be saline. But its exact salinity is unknown as the salinity of the depositional environment is uncertain. In this section, a calculation is performed that estimates the timespan of the diffusive process between freshwater deposited clay and saline water on top as this is the most extreme case. This calculation gives insight in the timespan of the diffusive process. The Boom clay was deposited in a marine environment. Accordingly the timespan of the diffusive process will be substantially shorter than as it was deposited in a freshwater environment.

The current pore water chemistry in the meso- and micropores in the Boom clay can be determined by a simplified calculation. The concentration of the micropores will change by diffusion if the concentration differs compared to the concentration of the mesopores. The concentration of the micropores depend on the concentration of the mesopores and vice versa, thus it is a coupled process. A simplified calculation is performed to get a feeling of the timespan of the diffusive process for the Boom clay. The pore water chemistry in the micropores can be determined by the simplified calculation. Several assumptions are made for the input parameters and for the built-up of the model, these assumptions can be justified because this is a rough calculation to get a first idea about the order of time of the diffusive process.

#### Simplifying assumptions

The volume of the mesopores is relatively large compared to the micropores. Therefore, the diffusion will be mainly governed from the mesopores towards the micropores, and a simplifying assumption is made. It is assumed that diffusion only takes place from the mesopores towards the micropores and the concentration of the mesopores is not influenced by the pore chemistry of the micropores as their volume is relatively small compared to the mesopores. This means that the coupling term is ignored. As the coupling term is ignored a simple numerical diffusion model can be made to determine the diffusion time from fresh to salty water in the micropores. The first step is to run the model for the diffusion process in the mesopores. When the porewater in the mesopores changed from fresh to salty water, the diffusive process between the micropores and mesopores starts.

#### Governing equations

The diffusion equation for constant  $D$  can be expressed by equation 4.1 (Bochner, 1949), in which the density of the diffusive material is  $\phi$  [ $kg/m^3$ ] and  $D$  is the collective diffusion coefficient. The collective diffusion coefficient for a diffusive material in a soil can be obtained by the terms expressed in by equation 4.2.  $D_{sp}$  [ $m^2/s$ ] is the diffusion coefficient in the considered fluid,  $\tau$  [-] is the tortuosity and  $\eta_{connected}$  [-] is the connected porosity of the material. The change of density of the diffusive material in 1D over time can be obtained by equation 4.3 by the Euler forward method.

$$\frac{\partial \phi(\mathbf{y}, t)}{\partial t} = D \nabla^2 \phi(\mathbf{y}, t) \quad (4.1)$$

$$D = D_{sp} * (1/\tau) * (\eta_{connected} * S_w) \quad (4.2)$$

$$\frac{\partial \phi_i}{\partial t} = D \left( \frac{-(\phi_i - \phi_{i-1})}{\delta x^2} + \frac{\phi_{i+1} - \phi_i}{\delta x^2} \right) \quad (4.3)$$

#### Input diffusive process in mesopores

This script first determines the diffusion over time in the mesopores. The matlab code is presented in appendix C. The mesopores are the pores larger than 10 nm (Aylmore and Quirck, 1967) and are identified in figure 4.4. The micropores are smaller than 10 nm and are presented by the left peak.

- The connected porosity in the mesopores of stiff clay, such as the Boom clay is 33
- The tortuosity for swelling clays range from 1.5-2.2 [-] (Chertkov and Ravina, 2010), a value of 1.7 is used within this script.
- The saturation of an overconsolidated clay varies, a value of  $S_w = 0.95$  is used here.
- The diffusion coefficient of salt in water ranges from  $0.63 - 4 * 10^{-9}$  [ $m^2/s$ ] for stratified lakes to oceanic brines (Toth, 1975), a value of  $3 * 10^{-9}$  [ $m^2/s$ ] is used within this calculation.
- The density of the diffusive material, i.e. the density of salt, is  $0.5 kg/m^3$  in freshwater and  $35 kg/m^3$  in seawater (Editors of Freshwater inflows, n.d.). This density changes over time by the diffusion of salt.

Input diffusive process in micropores

The next step is to determine the timespan of diffusion in the micropores, assuming that diffusion in the mesopores has completed. The input is the same as in the mesopore problem except:

- Micropores are in general fully saturated in stiff clays, resulting in a value of  $S_w = 1$ .
- The porosity of the micropores is 5% (Lima, 2011).
- The tortuosity of the micropores can be determined by (Yong et al., 2010):

$$\left(1 - \frac{r}{r_p}\right)^2 \left[1 - 2.10 \frac{r}{r_p} + 2.09 \left(\frac{r}{r_p}\right)^3 - 0.95 \left(\frac{r}{r_p}\right)^5\right] m \tag{4.4}$$

in which  $r$  = radius of dissolved species  $((30 * 10^{-10})/2) m$  and  $r_p$  = a typical radius pore space  $((40 * 10^{-10})/2) m$ .

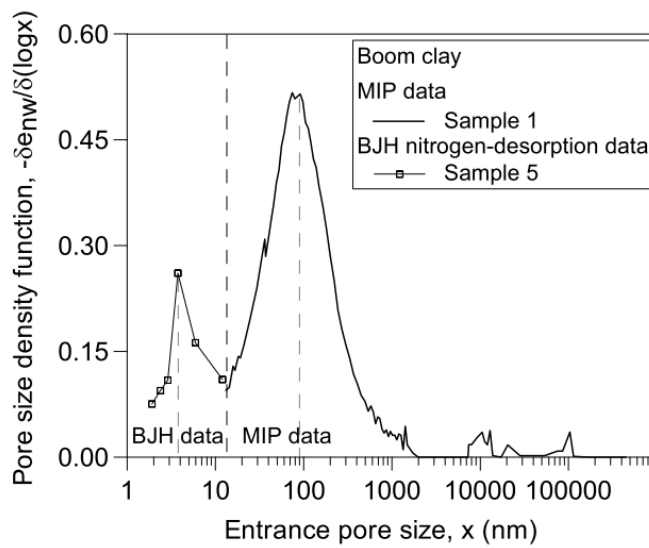


Figure 4.4: Pore size density function of Boom clay determined by BJH nitrogen desorption test and MIP. The micropores are smaller than 10 nm, and the mesopores are larger than 10 nm (Lima, 2011).

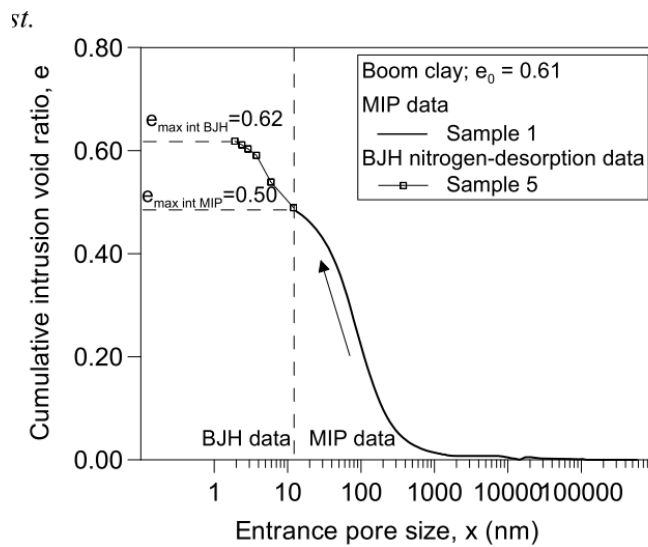


Figure 4.5: Cumulative void ratio intrusion of Boom clay. (Lima, 2011).

### **Swell-load test**

A cylindrical soil specimen with a diameter of 6.3 cm and variable heights, i.e. 20mm and 28/30 mm, is enclosed in a stainless ring. The sample is prepared with care by a ring lubricated with vaseline to decrease friction. The bottom and top are flattened by a thin iron wire to minimize the disturbance of the natural features. The top and base cap are provided by a porous stone and filter paper to allow drainage and are connected to drainage tubes (NGI, n.d.). The test is performed in a climate chamber with a temperature of 9.9°C and 88.2% humidity such that water density is kept constant.

The sample is loaded by a small seating pressure of 1.57 kPa. The load should be small to allow the clay to swell. The stress due to its self-weight is normally disregarded as it is negligible compared to the applied stress. The different samples are all loaded by the same stress. After the load is applied, the sample is wetted by saline water. Wetting of the natural clay sample results in the dissipation of suction, such that free swell will occur. Saline water is used to simulate the swelling behaviour of clays that are placed in saline water. The salty water is prepared by a solution of artificial salts of Instant Ocean and demineralized water to a density of  $1027 \text{ kg/m}^3$ , seeing that this density is comparable to seawater at 10°C. The effect of saline water on the microstructure of the clay is also tested. Therefore, the same test as described above on a 20 mm sample is performed with fresh demineralized water.

The above-described test is repeated for a different sample block, although originating from the same location. The larger ring had a height of 30 mm instead of 28 mm. After most of the swelling has taken place several loads are stepwise applied. In this research the main interest lies in the direct load response and not in the longterm effect. Therefore, every load step is only applied for approximately 24 hours. The applied loads are: 4.72 kPa, 20.45 kPa and 51.93 kPa, and they include the seating pressure.

## **4.2. Numerical modelling**

The influence of initial soil characteristics and softening is studied by a sensitivity analysis with a numerical model. It is not possible to develop a specific code, within the timeframe of this study. Thus, an available code will be used. The advantages and disadvantages of three different codes will be described in section 4.2.1. Afterwards the model set-up (section: 4.2.2) and the input for the sensitivity analysis is defined (section 4.2.3).

### **4.2.1. Numerical model**

The model should include several features to model the interlump void problem correctly. The requirements for the model are:

- work with two-phase materials as the clay is (partly) saturated
- be able to include a hydro-mechanical coupling
- the material behaviour has a dependency on suction, and this should be implemented
- include constitutive equations that can model the behaviour of a stiff clay
- ideally, be able to model large strain problems because the proper softening time can be obtained. This is because the coupled process depends on the current configuration instead of the initial one. Large strain equations can account for the softening process that changes the configuration such that the time dependent behaviour is written in the current configuration rather than in the initial configuration.

### **Twente academic code implementing DEM**

The code developed by the University of Twente solves the field equations by a Discrete Element Method (DEM). DEM captures the dual nature of granular media, which behaves like a solid and as a fluid. A DEM model is able to:

- Calculate numerically finite particle displacements and rotations
- Perform automatically contact detection for an assembly of particles

The collective interaction of all individual objects gives rise to the bulk behaviour (EDEM, n.d.). This code does not contain the constitutive equations and the proper coupled equations that are required to model the interlump void closure problem. Accordingly, it cannot be used to model the interlump void problem.

### Plaxis

Plaxis is a user-friendly numerical model based on the Finite Element Method (FEM) formulation that includes several constitutive models. Plaxis can model the coupled process, a two-phase material, and the dependency of the material behaviour on suction. Unfortunately, it is not possible to model large strain problems in Plaxis as it experiences difficulties with those large deformations. This is because of its reliance of Lagrangian finite elements on a mesh (Vardon, 2019).

The FEM formulation is not able to model large displacement problems and thus not suitable for an interlump void closure problem. Softening of clay lumps could possibly be modelled by the user-defined Barcelona Basic soil model in Plaxis. The Barcelona Basic model is an unsaturated model that includes collapse upon wetting (Plaxis, n.d.). Because it is an unsaturated model, it is definitely not an ideal model to govern softening behaviour. But its possibilities could be further researched.

### MPM

Material Point Method (MPM) is a numerical technique that is especially useful for large deformation problems such as progressive failures, flow slides and some settlement problems. MPM discretizes the media in two different frames: one frame is based on a set of material points (MPs) and the second frame is a computational mesh as visualized in figure 4.7. Each MP represents a portion of the total continuum and is allowed to move through the mesh. It is assumed that the mass of this subdomain is fixed during the calculation to ensure mass conservation. The MP moves attached with the deformations, and so do the quantities which are carried by the MPs, i.e. velocities, strain and stresses. While, the computational mesh stays in the same position (Martinelli, 2016a). Figure 4.8 visualizes the computation scheme of a typical problem setup.

MPM is a relative new method and is based on the arbitrary Lagrangian-Eulerian (ALE) formulation. The ALE formulation is a mixed method that combines the advantages of the Eulerian and Lagrangian formulation. To better understand this, it is important to truly understand the advantages and disadvantages of the Eulerian and Lagrangian formulation. Figure 4.6 shows the difference between an Eulerian and Lagrangian description. The main difference is that the governing equations for Eulerian formulations are solved on the fixed grid and the material moves through the mesh. While in Lagrangian methods, the grid is attached to the material being simulated (Nguyen, 2014). Consequently, it is unable to model large deformations. However, the Eulerian method also includes several disadvantages: (i) the material points are not tracked and therefore cause difficulties with history-dependent materials, (ii) difficulties in defining material boundaries and (iii) computationally intensive due to the convective term, whereas this term is not present in a Lagrangian formulation (Nguyen, 2014).

Unfortunately, MPM suffers from the following three disadvantages: (i) The numerical error can become fairly large due to two reasons. Firstly integration is undertaken on the MPs, which results in a large numerical error. Secondly, error accumulation can take place due to mapping forwards and backwards (Vardon, 2019). (ii) Boundary condition issues arise as a result of MPs that end up in adjacent elements, i.e. in the adjacent element across the boundary with different material properties and lastly (iii) the calculation time can blow up for small permeabilities and small elements due to the explicit integration scheme in time.

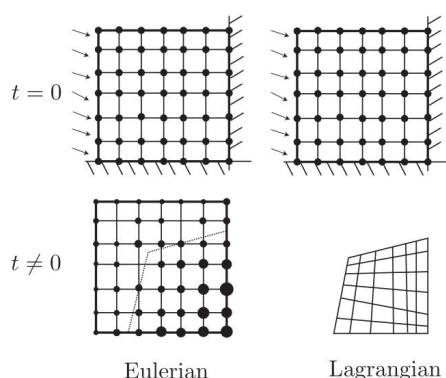


Figure 4.6: Eulerian vs Lagrangian description (Nguyen, 2014).

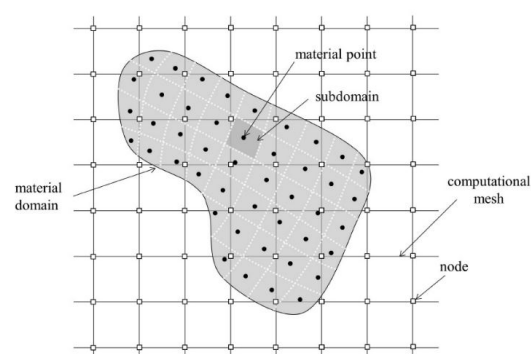


Figure 4.7: Space discretisation of MPM. The computational mesh is formed by a fixed Eulerian grid while the Lagrangian material points overly the Eulerian grid. (Martinelli, 2016a).

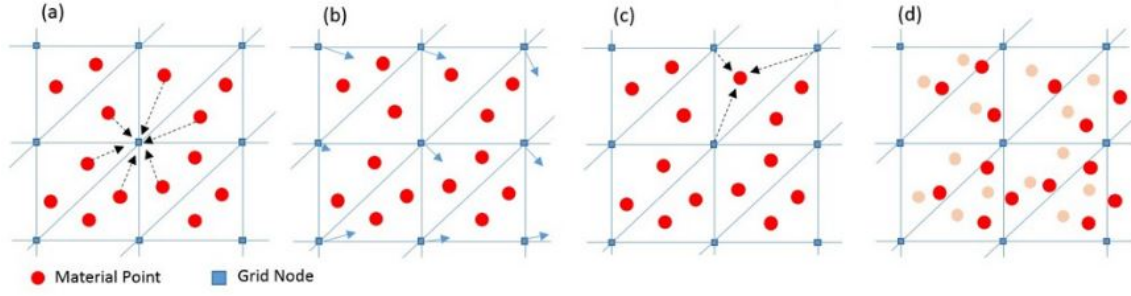


Figure 4.8: Computation scheme of MPM: Figure 4.8a: All state variables are mapped from the MPs to the nodes of the mesh by means of interpolation functions. Figure 4.8b: The governing equations of motion are solved and thereby solving the nodal accelerations. A standard FEM calculation is undertaken, the main difference is that area integration is carried out on the material points instead of on the gauss points. Figure 4.8c: The nodal values are used to update acceleration, velocity, stresses, strains and the position of the MPs. Figure 4.8d: The assignment of MPs to finite elements is updated after mesh adjustment (Martinelli, 2016a).

### Governing equations

The governing equations for a coupled dynamic two-phase problem that are implemented in the dynamic program of Deltares (*Dynamic MPM 2D DP*) are presented below. A clay ball is a two-phase material. Therefore, it is important to use a coupled two-phase formulation. The formulation by Biot (1941) formed the basis of the governing equations. The physical response of saturated soil under dynamic as well as static loading can be modelled by this formulation. The governing equations are conservation of mass and conservation of momentum of each phase and of the mixture. Finally, the equilibrium equations are solved for the accelerations of pore fluid and soil skeleton (Martinelli, 2016b). The mass conservation of the solid phase can be expressed as:

$$\frac{d}{dt}[(1-n)\rho_s] + (1-n)\rho\nabla \cdot \mathbf{v}_s = 0 \quad (4.5)$$

The conservation of mass for the liquid phase can be expressed by:

$$\frac{d(n\rho_l)}{dt} + n\rho_l\nabla \cdot \mathbf{v}_L = 0 \quad (4.6)$$

Assuming that the solid material is incompressible and disregarding spatial variations in density and porosity they can be simplified to:

$$-\frac{dn}{dt}(1-n)\rho\nabla \cdot \mathbf{v}_s = 0 \quad (4.7)$$

$$\rho_L \frac{dn}{dt} + n \frac{d\rho_l}{dt} + \rho_l \nabla \cdot \mathbf{v}_L = 0 \quad (4.8)$$

Equation 4.7 can be substituted in equation 4.8, this results in elimination of  $\frac{dn}{dt}$ .

$$(1-n)\nabla \cdot \mathbf{v}_s + \frac{n}{\rho_L} \frac{d\rho_L}{dt} + n\nabla \cdot \mathbf{v}_L = 0 \quad (4.9)$$

The liquid is considered as weakly compressible, therefore the effective volumetric strain in the liquid can be defined by:

$$\frac{d\bar{\epsilon}_L}{dt} = -\frac{1}{\rho_L} \frac{d\rho_L}{dt} \quad (4.10)$$

After substitution of equation 4.10 into equation 4.9 the conservation equation of mass of a saturated soil results, also referred to as storage equation.

$$\frac{d\bar{\epsilon}_L}{dt} = \frac{1}{n} \left[ (1-n)\nabla \cdot \mathbf{v}_s + n\nabla \cdot \mathbf{v}_L \right] \quad (4.11)$$

The conservation of momentum for the solid phase yields:

$$(1-n)\rho_s \frac{d\mathbf{v}_s}{dt} - \nabla \cdot \boldsymbol{\sigma}' - (1-n)\nabla p_L - (1-n)\rho_s \mathbf{g} - \frac{n^2 \rho_L g}{k} (\mathbf{v}_L - \mathbf{v}_s) = 0 \quad (4.12)$$

For the liquid phase:

$$n\rho_L \frac{d\mathbf{v}_L}{dt} - n\nabla p_L - n\rho_L \mathbf{g} + \frac{n^2 \rho_L g}{k} (\mathbf{v}_L - \mathbf{v}_s) = 0 \quad (4.13)$$

Adding the solid momentum equation 4.12 to the liquid momentum equation 4.13 results in the momentum equation for the mixture.

$$(1 - n)\rho_s \frac{d\mathbf{v}_L}{dt} + n\rho_L \frac{d\mathbf{v}_L}{dt} = \nabla \cdot \boldsymbol{\sigma} + \rho_{sat} \mathbf{g} \quad (4.14)$$

Overview MPM

MPM is able to model the softening behaviour of a clay lump due to the dissipation of suction. A given suction can be initialized and it dissipates over time. Thereby, reducing the mean effective stress. Section 4.2.2 describes the application of suction in the model in more detail. Chemical swelling of the lumps can not be incorporated in MPM. The presence of discontinuities can not be incorporated directly in the model because the clay balls can only be modelled as a homogeneous material. But, an indirect implementation via the permeability is possible. It is impossible to model the aggravation of the outer shell as described in section 3.3.1, because the discontinuity surfaces are not present. However, the clay ball can deform due to dissimilar decrease in strength and stiffness between the inner and outer part of the clay ball.

### 4.2.2. Model set-up

Three different numerical models were investigated. There is chosen to study the feasibility of modelling softening behaviour and interlump closure by MPM in more detail. Within this part of the study a sensitivity analysis will be conducted. The goal of this analysis is to determine the feasibility of MPM and to increase the understanding of softening and interlump void closure. The focus lies on the closure of the void space in between a regular clay ball structure in 2D. The swelling response of the material is also incorporated in this model. To model the problem in MPM, certain assumptions are made:

- Fully saturated clay balls. In section 5.1.1 it was found that the pores are fully saturated in situ. For a highly plastic clay lump it can be assumed that it stays fully saturated and no suction dissipates during the transportation process. These assumptions can be justified because the permeability of a highly plastic stiff clay is very small, and the transportation process is relatively short.
- Circular and initially homogeneous clay lumps
- All lumps have the same diameter
- Aggravation, i.e. falling apart of the outer shell, of the clay balls is impossible to model. Accordingly, the rearrangement of the clay lumps effect is ignored.

The clay balls are modelled by a Mohr-Coulomb model with an initial suction term. The Mohr-Coulomb model is a basic linear elastic perfectly-plastic soil model. The model is relatively fast as it does not include stress-dependency nor stress-path dependency nor strain dependency of stiffness. However, this is a simplifying assumption of soil behaviour. It is a reasonable assumption for stiff overconsolidated clays as the stiffness is already high and is only slightly influenced by stress and strains. But, when softening occurs due to swelling the change in stiffness is relatively large and the Mohr-Coulomb model can not model the true soil behaviour. Although the Mohr-Coulomb model can not model the non-linearity of the true soil behaviour, it can reasonably approximate the true soil behaviour for a stiff lumpy material up to failure.

The suction is equal to the mean effective stress in situ as described in section 2.1.6. Dissipation of suction results in a decrease of strength over time, which causes deformation of the lumps. Consequently, the model can be described as a reverse consolidation model. The next section describes the application of suction in the p'-q and p-q plane. The clay lumps are loaded by a preload of 25 kPa, and the load is applied by a vertical force by a rigid body. The preload is applied instantaneously after the first time step. In reality, a lumpy clay fill is loaded by a sand layer and consequently a uniform load is applied. Unfortunately, it is not possible to load the structure in MPM by a uniform load as this is not implemented yet.

#### Suction in MPM model

The model is initialized by a suction term and the initial total stress is equal to zero. An instantaneous preload is placed on top of the structure and dissipation of suction starts at the same time. The dissipation of suction results in a decrease in mean effective stress. The shear strength can be determined by:

$$\tau = M * p' + \tau_0 \quad (4.15)$$

In which  $M$  can be determined by the friction angle:

$$M = \frac{6\sin(\varphi)}{3 - \sin(\varphi)} \quad (4.16)$$

and the mean effective stress ( $p'$ ) depend on the total stress ( $p$ ) and the suction ( $s$ ) (eq: 4.17). and  $\tau_0$  measures the contribution of cohesion.

$$p' = p + s \quad (4.17)$$

The shear strength can be described by equation 4.18 in which the suction term is equal to minus the pore water pressure ( $-p_w$ ). From equation 4.18 it follows that the suction in the  $p - \tau$  plane can be expressed in an apparent  $\tau_0$  term, as visualized in figure 4.9.

$$\tau = M * (p - p_w) = M * p - M * p_w = M * p + M * s \quad (4.18)$$

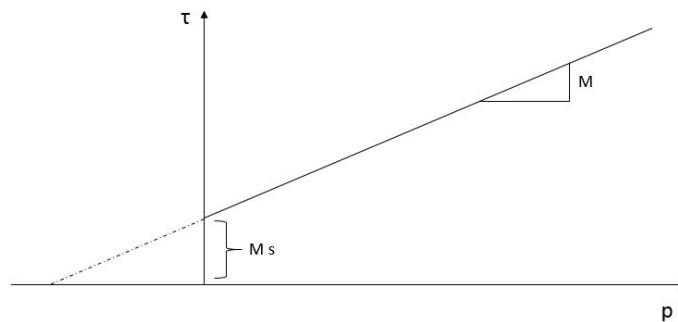


Figure 4.9: Suction visualized in  $p - \tau$  plane

### Geometry model

Figure 4.10 shows a simple arrangement of circular balls. Closure of the interlump pore space can be modelled by the grey rectangle as this is the representative volume. The dimensions of the representative volume are: width =  $0.5 * D$ , height =  $\sin(60) * D$ . The interlump void space is 9.31 in the representative volume. This geometry can be modelled in the program GID, which serves as the input for the numerical model. To model the problem correctly mesh refinement is necessary. Mesh refinement is especially important in between the clay balls, more precisely at the locations where the clay balls will merge. The geometry is adjusted slightly such that no extreme small elements arise. Adjustments in geometry lead to a final interlump pore space of 7.24%. A more detailed description of the adjustments on geometry is explained in section 4.2.3.

### Boundary conditions

Figure 4.11 presents the geometry of the clay ball model. The clay balls are laterally constrained such that only vertical displacements can take place. The load is applied by a vertical force by a rigid plate that is applied instantaneously at the first time step. In between the clay balls there is an empty space which represents the water in between the balls. The permeability of the interlump void space is infinite, such that the water can easily flow into the clay lumps. It is impossible to assign material properties of water to the surface in between the clay balls. Because a boundary condition problem will arise as the generalized boundary condition is not implemented yet in the MPM model. The water flow from the empty space in between the balls into the clay balls is governed by a pore pressure difference. Excess water pressure is assigned to the clay balls, and water flow into the clay ball results. No restriction is in place on how much water can flow in or out of the clay ball, but there is a restriction at which locations the flow can take place. The green lines in figure 4.11 represent the fixed flow boundary for water and soil, while the orange lines represent the free flow boundary for water.

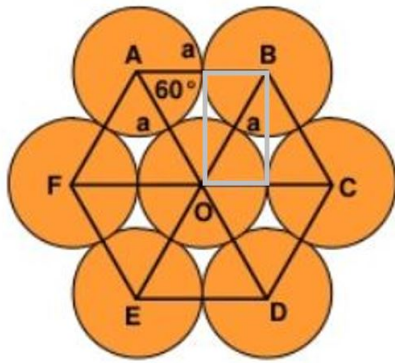


Figure 4.10: Input geometry MPM model, the width is  $0.5D$  and the height is  $\sin(60^\circ)D$ .

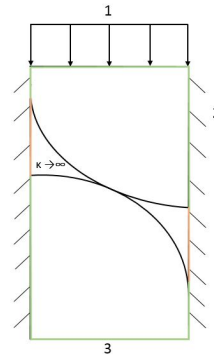


Figure 4.11: Boundary conditions model: (1) loading by vertical force by rigid plate (2) laterally constraint (3) Fixed (green) and free (orange) flow boundaries for water flow.

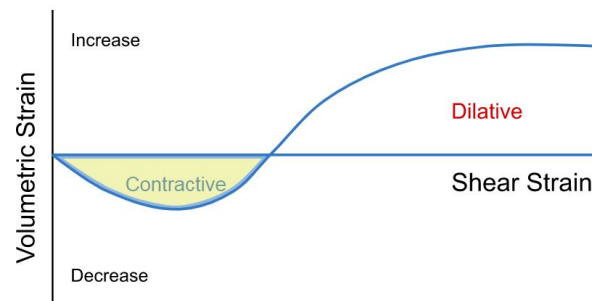


Figure 4.12: Volumetric strains versus shear strains. Shearing of an overconsolidation clay first results in compression and followed by expansion (Wikipedia, n.d.).

### Input of the model

The initial input of the model is described in this paragraph. The initial input is based on clay characteristics of the Boom clay as described in Chapter 2.2. A sensitivity analysis of certain input parameters will be conducted and is presented in section 4.2.3.

- Porosity = 0.36 (–); (Shaw, 2010)
- Density solid = 2720 ( $kg/m^3$ ); result pycnometer test and literature values
- K0-value = 1.0 (–); a isotropic stress state is assumed in the clay ball after excavation
- Hydraulic conductivity =  $1 * 10^{-5}$  ( $m/s$ ); The intrinsic permeability for the Boom clay at the surface is two orders higher than intact and unfissured clay at Mol. For this reason a hydraulic conductivity of  $1 * 10^{-10}$  ( $m/s$ ) is realistic. But as calculation time will blow up due to the explicit time stepping scheme a larger hydraulic conductivity is used.
- Youngs modulus = 1800 ( $kPa$ ); Average youngs modulus at 10m below seabottom. A more extensive explanation is given in the paragraph below.
- Poissons ratio = 0.2 (–)
- Cohesion = 0.1 ( $kPa$ ); The MPM model is not working properly without a cohesion term. Therefore, a very small cohesion is applied.
- Friction angle = 23 ( $^\circ$ ); (Li, 2013)

- Dilatancy angle = 0 (°); An OC clay shows dilatancy (fig: 4.12) while a NC clay does not. The clay is initially in an OC state, but changes towards a NC state over time by softening. Accordingly, the clay lumps are modelled without dilatancy.
- Tensile strength = 0.01 (kPa); A very small tensile strength is applied to overcome dynamic effects
- Density liquid = 1027 (kg/m<sup>3</sup>); density sea water at 10 °C;
- Bulk modulus liquid = 20000 (kPa); A realistic bulk modulus of water is 2 GPa, but a smaller value is used to decrease the calculation time. No differences in outcome are expected for this smaller bulk.
- Dynamic viscosity water = 1 \* 10<sup>-6</sup> (kPa/s);
- Excess pore pressure = 140 (kPa); Based on the expected suction for clay balls dredged from 10m below seabottom, see paragraph youngs modulus and initial suction for the calculation.

Calculation: youngs modulus and initial suction

The youngs modulus can be determined by the poissons ratio and the bulk modulus

$$E = 3(1 - 2\nu)K \quad (4.19)$$

$$K = \frac{\Delta p}{\Delta \epsilon_v} \quad (4.20)$$

In which:

$$\Delta \epsilon_v = \frac{\Delta e}{1 + e_0} = -\frac{\lambda}{1 + e_0} \ln\left(\frac{p'}{p'_0}\right) \quad (4.21)$$

Such that:

$$K = \frac{p'_0 - p'}{\frac{\lambda}{1 + e_0} * \ln\left(\frac{p'}{p'_0}\right) [kPa]} \quad (4.22)$$

The bulk modulus depends on the change in effective stress and therefore on the change in suction ( $\Delta p'$ ). In this calculation a suction that corresponds to 10m below seabed is used. The suction is governed by the in situ mean effective stress. The K0 value at its in situ location is 1.6, based on a OCR in the range of 5-10 for the Boom clay (Rijkers et al., 1998).

$$u_s = p0' = \frac{1}{3}(\sigma'_v + 2\sigma'_h) = \frac{1}{3}(10 + K0 * 2.0 * 10) * dredgingdepth = \frac{1}{3}(10 + 1.6 * 2.0 * 10) * 10 = 140 \text{ kPa} \quad (4.23)$$

Suction dissipates over time towards the final mean effective stress. In this calculation it is assumed that the final mean effective stress is equal to the applied load of 25 kPa. In reality the mean effective stress will be slightly lower than the applied load. Horizontal stresses will be slightly smaller than the vertical stresses due to arching and redistribution effects and consequently the mean effective stress is slightly smaller than the applied load.

The change in volumetric strain falls within a range depending on the loading and unloading curve:  $\lambda = 0.175$  and  $\kappa = 0.075$  (Della Vecchia et al., 2011). Correspondingly the bulk modulus is governed by a lower and upper limit.

$$K_{min} = \frac{140 - 25}{\frac{0.175}{1 + 0.5625} * \ln\left(\frac{25}{140}\right)} = 596 \text{ kPa} \quad (4.24)$$

$$K_{max} = \frac{140 - 25}{\frac{0.075}{1 + 0.5625} * \ln\left(\frac{25}{140}\right)} = 1391 \text{ kPa} \quad (4.25)$$

The youngs modulus can be found by  $E = 1.8 * K$  such that  $E_{min} = 1073 \text{ kPa}$  and  $E_{max} = 2503 \text{ kPa}$ . The unloading curve for clays upon wetting lies in between the normal loading and unloading curve. Its exact location is uncertain and therefore an average youngs modulus of 1800 kPa is used in the initial model.

### Practical usage of the model

The input variables, geometry, and mesh are defined in a pre-processing program for numerical geometries, called GID. A file with a .gom extension is generated by GID which serves, together with a .cps file, as the input for the dynamic MPM model. The file with a .cps extension is a notepad file in which information can be defined about: the initial conditions, loads, boundary conditions, contact algorithm, smoothing options and MPM calculation options. Running of the dynamic MPM model is possible via the command window. Several output files are automatically generated which can be visualized in the program Paraview.

| Variable input                     |   |                             |                           |
|------------------------------------|---|-----------------------------|---------------------------|
| Variable                           |   | Mesh Size                   |                           |
| <b>1</b>                           | 1 | Most coarse                 |                           |
|                                    | 2 | --                          |                           |
|                                    | 3 | --                          |                           |
|                                    | 4 | --                          |                           |
|                                    | 5 | --                          |                           |
|                                    | 6 | Finest                      |                           |
| <b>Hydraulic conductivity</b>      |   |                             |                           |
| <b>2</b>                           | 1 | 1.007*10 <sup>-5</sup>      |                           |
|                                    | 2 | 5.037*10 <sup>-6</sup>      |                           |
|                                    | 3 | 1.007*10 <sup>-4</sup>      |                           |
| <b>Stiffness (kPa)</b>             |   |                             |                           |
| <b>3</b>                           | 1 | 1073                        |                           |
|                                    | 2 | 1800                        |                           |
|                                    | 3 | 2503                        |                           |
|                                    |   | <b>Suction (kPa)</b>        | <b>Stiffness (kPa)</b>    |
| <b>4</b>                           | 1 | 70                          | 1180                      |
|                                    | 2 | 140                         | 1800                      |
|                                    | 3 | 280                         | 2843                      |
| <b>Preload (kPa)</b>               |   |                             |                           |
| <b>5</b>                           | 1 | 10                          |                           |
|                                    | 2 | 25                          |                           |
|                                    | 3 | 50                          |                           |
|                                    | 4 | 75                          |                           |
|                                    | 5 | 100                         |                           |
| <b>Moment of application (s)</b>   |   |                             |                           |
| <b>6</b>                           | 1 | 2                           |                           |
|                                    | 2 | 1                           |                           |
|                                    | 3 | Linearly from start         |                           |
|                                    | 4 | Instantaneous from start    |                           |
|                                    |   | <b>Cohesion (kPa)</b>       | <b>Friction angle (°)</b> |
| <b>7</b>                           | 1 | 0.1                         | 23                        |
|                                    | 2 | 10                          | 18                        |
| <b>Geometry</b>                    |   |                             |                           |
| <b>8</b>                           | 1 | Larger interlump void space |                           |
| <b>Comparable model swell test</b> |   |                             |                           |
| <b>9</b>                           | 1 | Suction (kPa)               | 84                        |
|                                    |   | Preload (kPa)               | 1.57                      |
|                                    |   | Stiffness (kPa)             | 1315                      |

Table 4.1: Overview of input sensitivity analysis. The bold numbers in the column on the left are used later in the report in the headers to appoint the variable input models.

### 4.2.3. Sensitivity analysis

A sensitivity analysis of several input properties, mesh refinements and loading schemes will be conducted. The goal is to increase the understanding of the softening and interlump void closure behaviour. It was found in the literature review that the initial soil characteristics have a large influence. Their influence is tested by the sensitivity analysis. This section describes the input that is varied in the sensitivity analysis. All other input parameters are kept similar to the ones mentioned earlier in section 4.2.2. An overview of the sensitivity analysis that will be conducted is given in table 4.1. The bold numbers in the left column are used later in the report to appoint the variable input models.

#### 1. Mesh refinement

The mesh refinement has a large influence on the reliability of the results and the calculation time. The results will be more realistic for smaller elements as the numerical error decreases. Contrarily the calculation time is governed by the smallest element. For this reason, it is important to make sure that the elements are not too small. The geometry of the circular clay balls was slightly adjusted in the corners and at the contact point between the balls to increase the element size at those specific locations. Consequently, the interlump void space changed from 9.31% for perfectly round balls to 7.24%.

Because the generalized boundary contact for a random geometry is not yet implemented in MPM a boundary problem evolves. If two materials approach each other the two different material properties of the material points

will reach the same element and cannot merge due to missing implementation of the boundary contact. It follows that the larger the element is, the larger the apparent gap is in between the clay balls. Consequently, the elements should be small at the interlump void space and at the boundaries of the clay balls. A setback of the decrease in element size is the increase in calculation time.

A sensitivity analysis of five different mesh refinements (fig. 4.13) is conducted: ranging from very coarse (number 1) to very fine (number 5). The mesh refinement is different in three zones: (i) inner part of the lump (ii) outer part of the lump (iii) contact zone. Because the mesh refinement was performed manually per zone, there does not exist a linear relationship between the mesh refinement and the number of elements. The goal of the sensitivity analysis is to find the optimum mesh. The optimum mesh has an acceptable calculation time but also realistic clay ball deformations without mesh distortion. Another influencing factor is the number of MPs per element. More realistic results will be obtained if the number of MPs per element is larger. In this model there is chosen to use six MPs per element, as three MPs per element turned out to be too rough to get reasonable results.

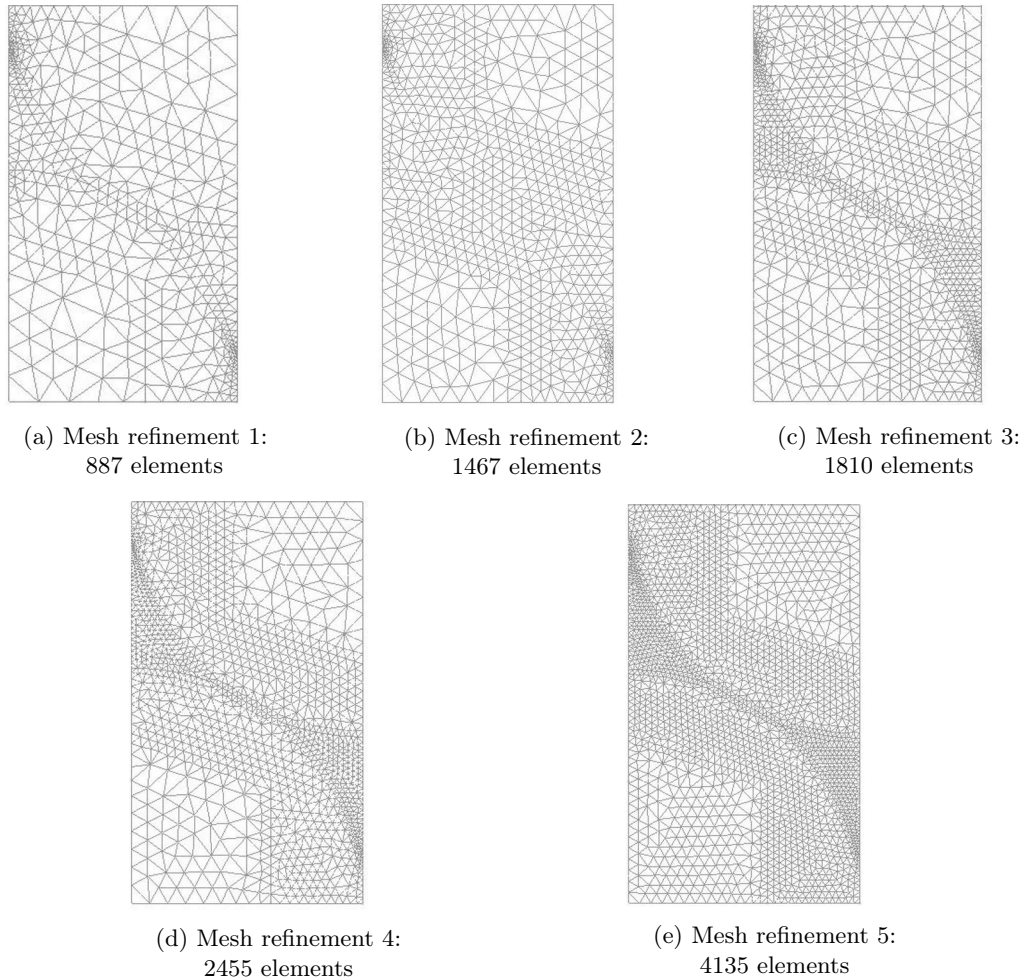


Figure 4.13: Mesh refinements: (1) course, (2) –, (3) –, (4) –, (5) finest. A non-linear relation exist between the mesh refinements as it a customized mesh. The interlump void space is 7.24% for all mesh refinements.

## 2. Hydraulic conductivity

The hydraulic conductivity is governed by several factors, including discontinuities and fissures. In section 2.1.5 it was described that discontinuities and small fissures are common for overconsolidated clays. Fissures and discontinuities can be identified, but it is difficult to quantify the influence on the permeability and hydraulic conductivity. Therefore, a sensitivity analysis will be conducted.

A small timestep is required for an explicit time-stepping scheme as it is not unconditionally stable. Accordingly, the calculation time will blow up for a very small hydraulic conductivity due to the explicit time-stepping scheme. For this reason, larger hydraulic conductivityies are used in the model. The sensitivity analysis is conducted for three different hydraulic conductivityies:  $K_1 = 1.007 * 10^{-5}$  m/s,  $K_2 = 5.037 * 10^{-5}$  m/s and  $K_3 = 1.007 * 10^{-4}$  m/s.

### 3. Stiffness

The unloading curve for clays upon wetting is uncertain. The curve will be located in between the normal loading and unloading curve (fig 4.14). An average value of 1800 kPa is used in the initial model, as this value is in between the minimum and maximum Young's modulus. A sensitivity analysis of the stiffness, i.e. youngs modulus, is conducted as uncertainty exists in its value upon wetting. Therefore, an analysis will be conducted for  $E_{min} = 1073$  kPa,  $E_{average} = 1800$  kPa and  $E_{max} = 2503$  kPa.

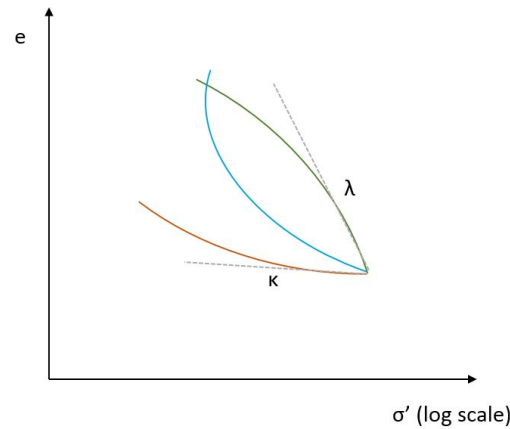


Figure 4.14: The location of unloading curve upon wetting (blue) is located in between the loading (green) and unloading (orange) curve, but its exact location is uncertain.

### 4. Suction

The initial suction in the clay balls is highly variable and depends on the initial in situ depth of the clay and the degree of overconsolidation. The suction increases linearly over the dredging depth below seabed (equation 4.23). A sensitivity analysis is conducted for three different dredging depths and their corresponding initial suctions. The stiffness depend highly on the initial suction and is therefore also altered.

- Depth - 5 m, Suction = 70 kPa and  $E = 1180$  kPa.
- Depth - 10 m, Suction = 140 kPa and  $E = 1800$  kPa.
- Depth - 20 m, Suction = 280 kPa and  $E = 2843$  kPa.

### 5. Preload and 6. Moment of load Application

Closure of the interlump voids is highly dependant on the applied preload. Therefore, the model is tested for five preloads: 10 kPa, 25 kPa, 50 kPa, 75 kPa and 100 kPa. All loads are applied instantaneously at the start.

The moment of loading in time will also be tested in the sensitivity analysis. In the original model, the load (25 kPa) is applied instantaneously at the start as described in section 4.2.2. In reality, a lumpy clay fill is dumped, and the preload will be placed several months later in time. The effect of the moment of load application is researched by this sensitivity analysis. The load is applied at 33.3% of the total softening and interlump void closure time in case 1 and at 16.7% for case 2. Furthermore, the load is applied linearly during the first 16.7% of the total time.

- 1. Load applied at 33.3%
- 2. Load applied at 16.7%
- 3. Load is applied linearly during the first 16.7%
- 4. Instantaneous load from the start (the original model)

In case the preload is not applied directly from the start, i.e. loading case 1 and 2, it is important to use the flag 'prevent separation'. This flag is a necessity because otherwise, disconnection between the loading structure and clay ball model will take place. Disconnection takes place as there is no downwards force on the loading structure.

### 7. Cohesion

In the initial setup of the model, there is chosen to model the Boom clay at critical state. Accordingly, the friction angle is  $23^\circ$  and the cohesion is 0.1 kPa. Overconsolidated clays are cohesive while normally consolidated clays are non-cohesive as described in section 2.1.1. The clay balls are initially overconsolidated and thus it would be realistic to model them with a cohesion term. But, as the clay balls soften over time, they become normally consolidated and thus non-cohesive. It is impossible to include the transition from cohesive to non-cohesive in the model. Therefore, one cohesive and one non-cohesive model are tested.

Small failure surfaces inside the clay balls might occur because the clay balls are modelled as a non-cohesive material in the initial setup. In section 5.2.1, the small scale failure surfaces are indeed identified. For this reason, the influence of cohesion will be tested. The clay balls are modelled by a friction angle of  $18^\circ$  and a cohesion of 10 kPa; those values are representative for the Boom clay formation (Mertens et al., 2003). An extra outer layer is modelled at the boundary of the clay balls with a friction angle of  $23^\circ$  and a cohesion of 0.1 kPa. This extra outer layer is required because it is unrealistic to apply cohesive forces at the contact between the clay balls. Otherwise, the clay balls are modelled as if the clay balls were cemented against each other.

### 8. Geometry

An alternative geometry of clay balls with a larger interlump porosity is tested, but all other parameters are kept constant. The goal is to check if the inner geometry of the model can be changed without changing the outer geometry, boundary conditions and loading structure. The mesh density is similar as in mesh refinement 4, but small differences may arise due to the alternative geometry of the surfaces. The geometry of the surfaces and the mesh are shown in figure 4.15.

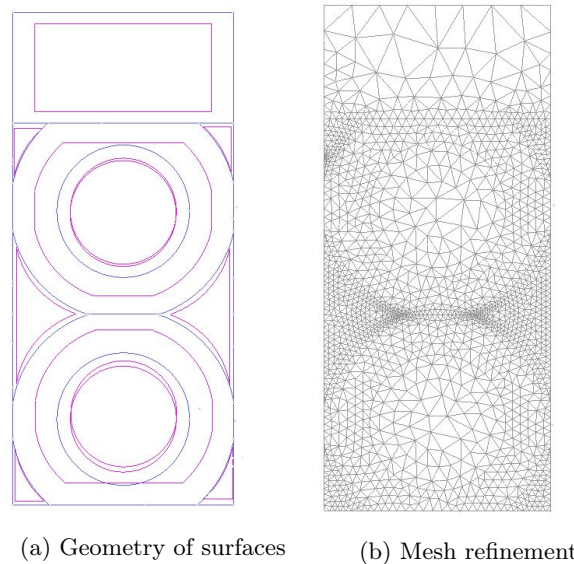


Figure 4.15: Model with altered inner geometry but similar boundary conditions.

### 9. Comparable model to experimental swell test

The result of the swell test can be compared to the strain in the MPM model. To compare the results a MPM model with a similar input to the swell test is modelled. The sample material originates from an in situ depth of approximately 6 m and thus an initial suction of approximately 84 kPa, see equation 4.23, is present in the sample. Furthermore, a seating pressure of 1.57 kPa is applied in the swell test. To compare the results an initial suction of 84 kPa and a load of 1.57 kPa is instantaneously applied in the MPM model. The stiffness is also altered in the MPM model to 1315 kPa as it is closely related to the suction (section 4.2.2). All other parameters are kept similar (section 4.2.2).

# III

## Results and discussion



# 5

## Results and discussion

The results and discussion of the experimental tests can be found in section 5.1 and the numerical results and discussion in section 5.2. Besides, the comparison of the experimental, numerical and theoretical strains is given in section 5.3.

### 5.1. Experimental tests

In section 5.1.1 the results of the index tests are presented. A simplified calculation is also provided to estimate the degree of saturation of the in situ material. The results of the fissure identification tests by the CT and micro-CT scanner are also presented (section: 5.1.2). Furthermore, the miniature clay fill test is discussed (section: 5.1.3) and the unloading consolidation coefficient is determined by a small scale softening test (section: 5.1.3). Last but not least, the results of pore water chemistry diffusion calculation and the swell and load tests are presented (section: 5.1.5).

#### 5.1.1. Sample material: index tests and degree of saturation

An overview of the index properties of the Boom clay sample is presented in table 5.1. From these results, it can be concluded that the sample blocks are indeed highly plastic stiff clays. Appendix B presents all measurements and discussion of the results.

| Overview of index properties of test sample |                      |
|---|----------------------|
| Water content (%)                           | 28.4                 |
| Plastic limit (-)                           | 27.6                 |
| Liquid limit (-)                            | 79.0                 |
| Plasticity index (-)                        | 51.3                 |
| Su (kPa)                                    | 110                  |
| Clay content (%)                            | 61.4                 |
| Specific gravity (-)                        | 2.724                |
| Activity (-)                                | normally ac-<br>tive |

Table 5.1: Overview of index test results on a Boom clay sample that originates from the Tuinlei-Schelle quarry

#### Degree of saturation

During the Rupelian (30 M year ago) the Boom clay was uplifted (Mertens et al., 2003). At that time, it was likely that it was in an initial unsaturated state as explained in section 2.1.4. A rough calculation is performed in this paragraph to determine the current degree of saturation. The current degree of saturation is of interest as it is used as an input value in the numerical model. Furthermore, it is also important to know the degree of saturation as it influences swelling.

Almost no data is available about the hydraulic conductivity at shallow depths (0-40 m), but it can be estimated as two orders larger than the hydraulic conductivity at 240 m depth (N. Vandenberghe (Personal communication,

March 25, 2019)). Fissures and faults which are present at shallower depths are the reason for the estimated increase of hydraulic conductivity. The average hydraulic conductivity of the Boom clay at depth (190-290 m) is extensively measured and has an average value of  $7.0 * 10^{-12} \text{ m/s}$  (Huysmans and Dassargues, 2006). Therefore, the hydraulic conductivity at shallow depths is approximately  $7.0 * 10^{-10} \text{ m/s}$ . If the **top** of the Boom clay formation was saturated since the Rupelian, the saturation depth can be estimated by:

$$D = (30 * 10^6) * (3600 * 24 * 365) * 7.0 * 10^{-10} = 66 \text{ km} \quad (5.1)$$

By this it can be concluded that the Boom clay is fully saturated, except for the weathered top layer.

### 5.1.2. Fissure identification tests

#### CT scan

Three sections of the Boom clay sample are presented in figure 5.1, 5.2 and 5.3. Pyrite layers and nodules are present in the Boom clay as earlier described in 2.2.1. It is likely that the bright white parts in the CT scan are pyrite. The largest pyrite nodule identified in this block of clay has a diameter of 10mm. Most of the pyrite nodules are small, but they can be up to cm size (Vandenberghe et al., 2014) and form 3% of the bulk volume of the clay (De Craen et al., 1998). This corresponds to the pyrite density in the CT scans.

Small fissures without a preferred orientation are identified on the CT scans. This corresponds to the description by Mertens et al. (2003) in section 2.2.1. The resolution of the images is 0.4 mm, some micro fissures can not be identified due to the resolution. The presence of fissures results in a decrease of strength of the material and an increase of the hydraulic conductivity and permeability as described in section 2.1.5. The increase in permeability and hydraulic conductivity is hard to quantify as it varies per location due to the presence of fissures. In case the fissure density is very high, and the fissures are connected, a large increase in permeability and hydraulic conductivity is expected.

#### micro CT scan

The result of the micro CT scan is presented in figure 5.4. Very small fissures can be identified and are indicated by the arrows. The micro fissures that are identified are not connected. But, as the resolution of the image is  $4 \mu\text{m}$  it is likely that the sample contains more micro fissures than identified and might be connected. A smaller sample size results in a higher resolution such that smaller micro fissures can be identified. Unfortunately, it was not possible to prepare a smaller sample of the material.

It is not possible to estimate the fissured hydraulic conductivity of these CT images, as the resolution is not high enough to identify the smallest fissures. Therefore, the estimate of a hydraulic conductivity in the order of  $10^{-10} \text{ m/s}$  for the fissured Boom clay is used in this study (N. Vandenberghe (personal communication, March 25, 2019)).

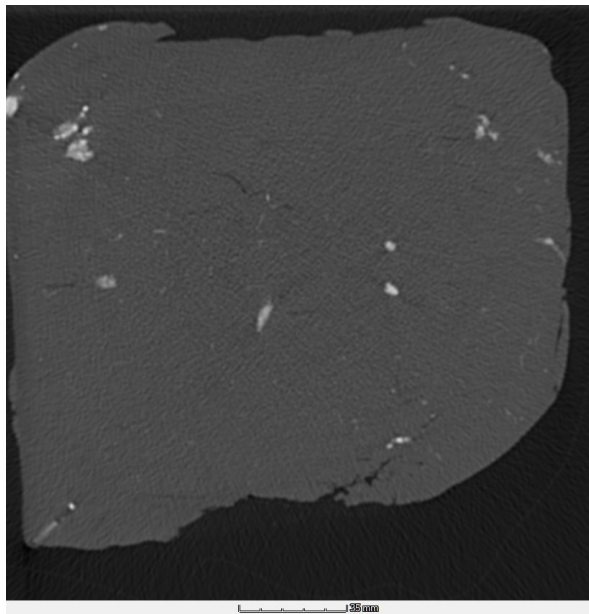


Figure 5.1: CT scan: section 1. Resolution is 0.4 mm.

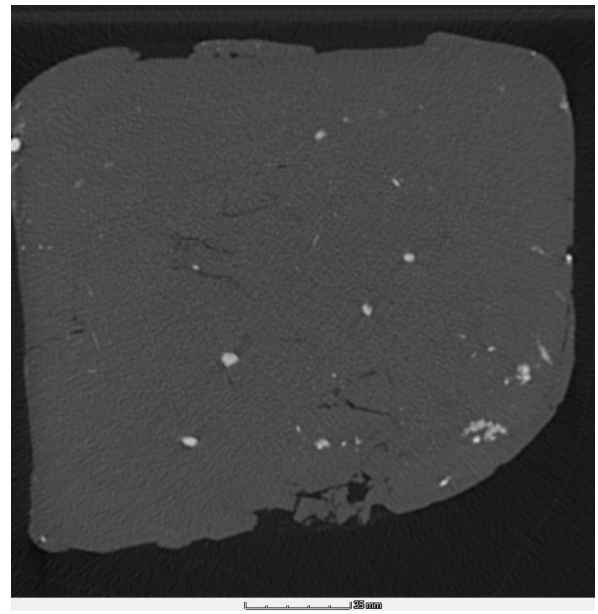


Figure 5.2: CT scan: section 2. Resolution is 0.4 mm. Nodules and fissures are present in the section, around the nodules small fissures are present.

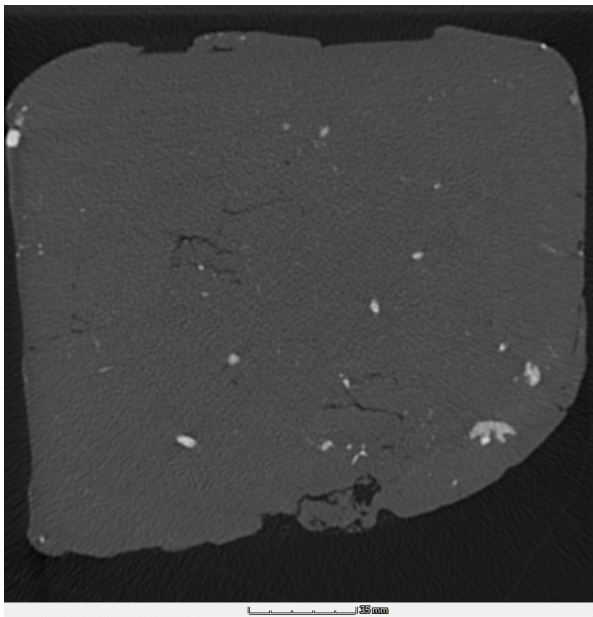


Figure 5.3: CT scan: section 3. Resolution is 0.4 mm.

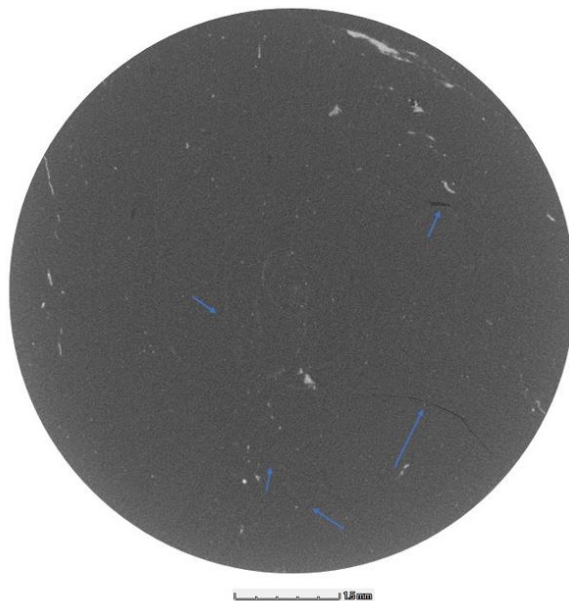


Figure 5.4: CT scan by micro CT scanner with a resolution of 4  $\mu\text{m}$ . The blue arrows indicate the micro fissures. It is likely that sample contains more micro fissures but they are smaller than the resolution.

### 5.1.3. Miniature clay fill test

The water outflow of the water in the interlump void space in the Rowe cell is slower than the softening time of the small clay cube. Consequently, the time effect of interlump closure could not be measured as the clay balls turned into a slurry before meaningful results could be obtained. It is not possible to increase the size of the clay balls as the influence of the stapling becomes too large as explained in section 4.1.3. It can be concluded that the Rowe cell with a diameter of 15 cm is not a suitable test set-up to perform a miniature clay fill test.

### 5.1.4. Determination consolidation coefficient

By the miniature clay ball test it was found that the softening time is fairly quick. To increase the understanding of the softening time, a small softening test was performed. After **15 minutes** the cube started to fall apart and turned into a slurry under a very small push by a fingertip. From this, it can be concluded that the softening process is fairly quick for small samples.

The consolidation coefficient ( $c_v$ ) can be determined by the analytical consolidation for an elastic sphere. This is an approximation as the test was performed on a cube and not on a sphere. The excess pore pressure can be disregarded for a non dimensional time of  $(c_v * t)/(r^2) = 1$  (Verruijt, 2013). Such that the unloading consolidation coefficient can be approximated (eq: 5.2), in which  $r = 0.005$  is half of the length of the sample and  $t = 15 * 60$  s the softening time.

$$\text{unloading } c_v = \frac{r^2}{t} = \frac{0.005^2}{15 * 60} = 2.80 * 10^{-8} \text{ m}^2/\text{s} \quad (5.2)$$

$$\text{loading } c_v = \frac{k}{(1/E_{oed}) * \gamma_w} = \frac{10^{-10}}{(1/1998) * 9.807} = 2.04 * 10^{-8} \text{ m}^2/\text{s} \quad (5.3)$$

The result of the small-scale softening test can be verified by the consolidation coefficient upon loading (eq: 5.3). It is determined by the theoretical hydraulic conductivity, stiffness and unit weight of water as stated in section 4.2.2. The theoretical consolidation coefficient upon loading is in the same order as the unloading consolidation coefficient that is determined by the small scale test. The unloading consolidation coefficient is larger than the loading consolidation coefficient, which is logical because the oedometer stiffness differs.

### 5.1.5. Swell-load test

To interpret the influence of pore water chemistry change correctly, it is important to know the initial pore water chemistry of the in situ deposit. Those results are described in the first section, and the swell-load test results are presented afterwards.

#### Initial pore water chemistry

Figure 5.5 presents the results of the diffusion script in the mesopores after 80000 years. It can be seen that after 80000 years the concentration in the mesopores is almost completely saline over an interval of 30 m. The concentration of the mesopores after 80000 years is saline, while the micropores still contain fresh pore water. Diffusion will take place from the mesopores to the micropores. Consequently, the input of the micropores model needs to be used as described in section 4.1.5. Figure 5.6 shows the concentration after 2 hours over an interval of 0.5 cm. It can be concluded that the diffusion process from the mesopores to the micropores does not take long as the distance between the meso and micropores is small.

This model is a simplified model with several assumptions. The coupling term is ignored and therefore this model underestimates the timespan. From this simplified model, a timespan in the order of 80000 years results. In other words, the pore water in the micropores up to 30m depth changed from fresh to saline after 80000 years. The time span of 80000 years is relatively short on the geological time scale. Therefore, the porewater in the micropores is likely to be at approximately the same salinity as present at the top of the deposit.

The Boom clay was deposited in a saline environment, but the exact salinity is uncertain. The diffusion process will be substantially quicker in case the concentration difference between the pore water and seawater is smaller compared to the fresh-saline case. Hence, it can be concluded that the salinity in the pores is equal to the salinity of the seawater.

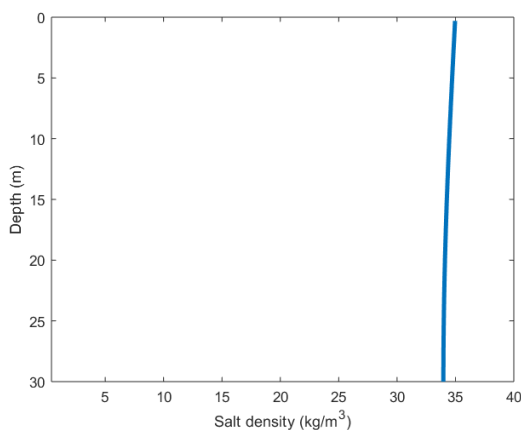


Figure 5.5: Diffusion of salty water in mesopores after 80000 years. The salinity at 30 m depth is almost similar to the salinity of the seawater on top, from which it can be concluded that the diffusive process came to an end.

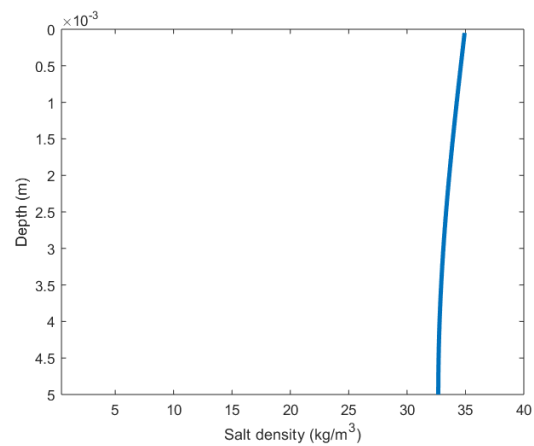


Figure 5.6: Diffusion of salty water in micropores after 2 hours. The micropores that are located  $5 \cdot 10^{-3} \text{ m}$  away from the mesopores contain a similar pore water chemistry.

#### Swell-load test results

*Please note the annotation of positive and negative strains in this report. Positive strains refer to expansive strains, while contractive strains are referred to as negative strains.*

The results of the swell tests on sample block 1 (fig: 5.7) and sample block 2 (fig: 5.9) are presented. The results between sample block 1 and 2 show the same trend, although the strains are smaller for sample block 2. Soil heterogeneity is likely to be the reason of the difference in strains.

The strains are significantly larger for the test performed with freshwater than with saline water for both sample blocks. The test performed with freshwater results in a change of pore water chemistry from saline to fresh. Consequently, the  $\text{H}^+$  concentration increases and chemical swell results (section: 2.1.6). The microstructure is altered from a flocculated structure to a dispersed structure (section 2.1.3). Intersection between the diffusive double layer is likely to be present in a dispersed structure. Therefore, a dispersed microstructure results in more swell than a flocculated structure.

It can be observed that the strains for the saline sample with a sample height of 28/30 mm are smaller compared to the saline sample of 20 mm. It is probable that the 28/30 mm sample was too large to swell completely during the time period and smaller strains result. Additionally, there is also the influence of wall friction, although a lubricate is applied.

According to the consolidation equation, it is expected that the total swelling time is quadratic related to the height of the sample. Such that an increase of 50% in sample height results in a softening process that is  $(1.5)^2 = 2.25$  times slower. However, no difference in softening time can be observed in the results. A possible explanation could be that the larger sample contains more fissures and discontinuities. This effect was described as the sample-size effect by Nishimura (2005). Consequently, the swelling path decreases and thereby the time. A larger sample is more likely to contain fissures.

| Unloading consolidation coefficients ( $m^2/s$ ) |                      |                      |
|--|----------------------|----------------------|
|  | Sample block 1       | Sample block 2       |
| Fresh 20 mm                                      | $3.28 \cdot 10^{-9}$ | $2.81 \cdot 10^{-9}$ |
| Saline 20 mm                                     | $5.32 \cdot 10^{-9}$ | $1.72 \cdot 10^{-9}$ |
| Saline 28/30 mm                                  | $1.61 \cdot 10^{-8}$ | $3.82 \cdot 10^{-9}$ |
| Loading consolidation coefficients ( $m^2/s$ )   |                      |                      |
|  | Sample block 1       | Sample block 2       |
| Fresh 20 mm                                      | -                    | $2.63 \cdot 10^{-8}$ |
| Saline 20 mm                                     | -                    | $3.94 \cdot 10^{-8}$ |
| Saline 30 mm                                     | -                    | $2.25 \cdot 10^{-8}$ |

Table 5.2: Unloading and loading consolidation coefficients obtained by the Casagrande construction method.

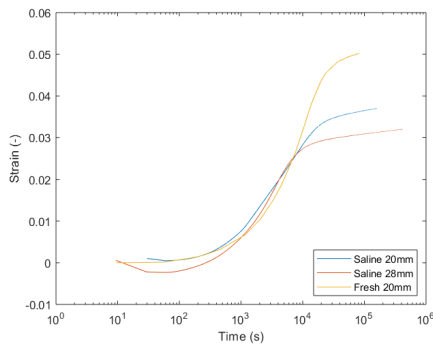


Figure 5.7: Results swell tests on sample block 1: strain versus time. A substantial larger strain results for the sample flushed by freshwater.

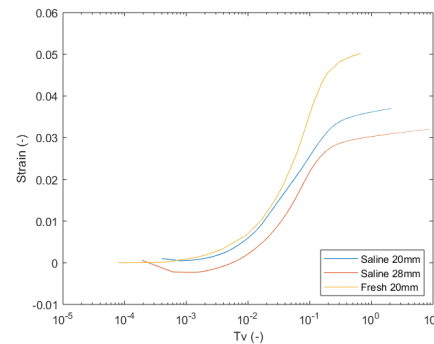


Figure 5.8: Results swell tests on sample block 1: strain versus dimensionless time. A substantial larger strain results for the sample flushed by freshwater.

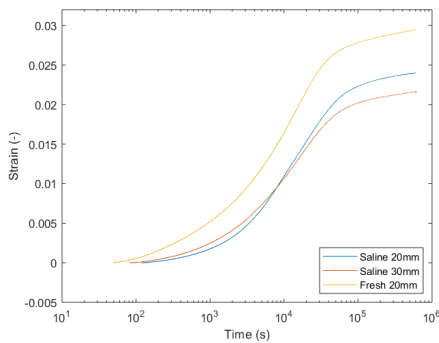


Figure 5.9: Results swell tests on sample block 2: strain versus time. A substantial larger strain results for the sample flushed by freshwater.

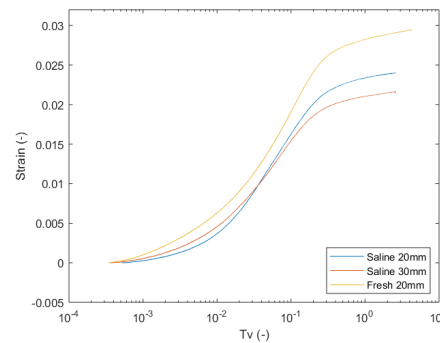


Figure 5.10: Results swell tests on sample block 2: strain versus dimensionless time. A substantial larger strain results for the sample flushed by freshwater.

Figure 5.8 and figure 5.10 show the same measurements but for the normalized time in stead of the real time. The normalized time ( $T_v$ ) is determined by  $T_v = (c_v * t)/(H^2)$  in which  $c_v$  is the unloading consolidation coefficient and H is the initial height of the sample. The unloading consolidation coefficient is obtained by the Casagrande construction method for every sample (Table 5.2). The unloading consolidation coefficients are slightly smaller compared to the coefficient found in equation 5.2.

Figure 5.11 presents the strains versus time for the three load steps. The saline sample of 20 mm shows larger negative strains compared to the 20 mm fresh sample. This difference can be explained by the flocculated and dispersed microstructure. The microstructure in the freshwater sample is likely to be dispersed, while in the saline sample a flocculated microstructure exists. The flocculated structure is more 'open' and therefore more compressible (section 2.1.3). The saline sample of 30 mm shows less negative strains compared to the 20 mm saline sample. It is probable that the 30 mm sample did not have enough time to swell completely and thus compresses less than the 20 mm saline sample. The consolidation coefficients upon loading are determined by the Casagrande construction method (tab: 5.2). The loading consolidation coefficients are in the same order as the theoretical loading coefficient (eq: 5.3).

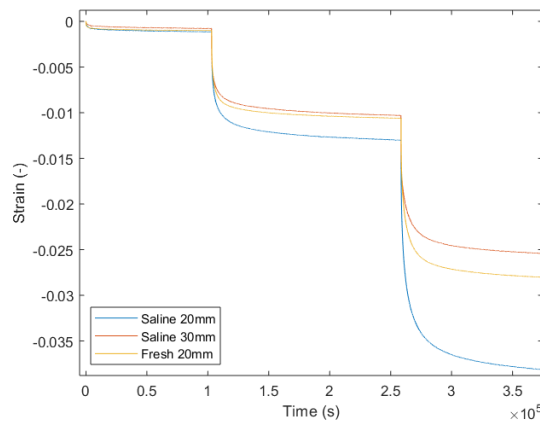


Figure 5.11: Results of loading test on sample block 2: strain versus time. Application of a load step results in a quick contractive response.

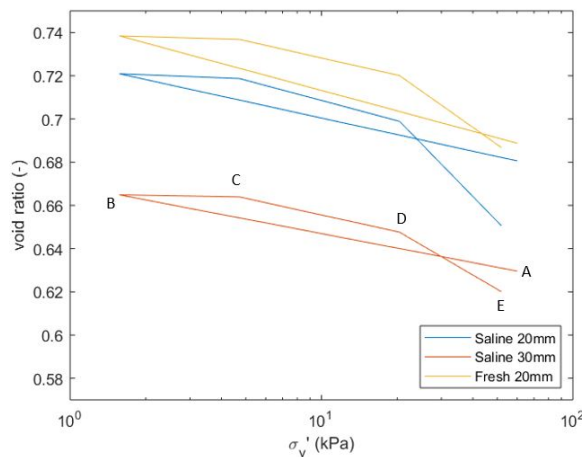


Figure 5.12: Result load test on sample block 2: void ratio versus vertical effective stress. A - B: unloading, B - C: application of first loadstep, C-D: second loadstep, D-E: third loadstep application.

The sample experiences a vertical effective stress before the test starts that is equal to the suction (60 kPa) for an isotropic stress state ( $K_0 = 1.0$ ) at its initial void ratio (Point A). The effective stress decreases towards the seating pressure during swelling and the void ratio increases until the final swelling condition is reached (Point B). The void ratio decreases over time under the applied loadsteps (B-C-D-E). It decreases quickly under the applied load of 52 kPa, especially for the 20 mm saline sample.

The swell-load results can also be plotted in terms of the void ratio versus the vertical effective stress (fig: 5.12). The unloading and loading stiffness seem to differ, although the difference is not large. The void ratio changes quicker for the third load step (D - E) compared to the first two load steps (B-C-D), especially for the 20 mm saline sample. This might imply that the original pre-consolidation stress is lost during the softening process. Unfortunately, there are no compression tests performed on Boom clay samples that originate from the surface. The compression tests that originate from a deeper part of the formation, i.e. Mol, can not be used as the material has an initial smaller void ratio. Therefore, it is uncertain if the load path is comparable to the virgin compression line or that the structure is altered by the softening process. No direct conclusions on the stiffness can be based upon figure 5.12 as the results cannot be compared to virgin compression test results. Therefore, it is uncertain if the unloading and loading stiffness truly differ or that the apparent differences are mainly an effect of measuring inaccuracies.

### 5.1.6. Summary experimental results

Interlump void closure is closely related to the initial soil characteristics, softening and the presence of discontinuities. Softening and the presence of discontinuities were studied in the experimental part of this study on Boom clay samples. The sample material was identified as a highly plastic clay by the classification tests.

It was described in literature that the Boom clay is a highly fissured clay. The hydraulic conductivity of the clay increases in case the fissures are connected. Fissures were indeed identified on the CT scans, but the smallest micro-fissures could not be identified because the resolution of the results was too low. Thus, it was not possible to estimate the fissured hydraulic conductivity as it is uncertain if the fissures are connected.

No meaningful results could be obtained by the miniature clay fill test as the softening time of the clay balls was quicker than the water outflow of the Rowe cell. To get an idea about the softening time, a small scale softening test was performed on a clay cube. The softening time was measured such the unloading consolidation coefficient could be calculated.

A swell-load test was performed in an oedometer. It was found that the pore water chemistry influences the microstructure of the material: substitution of saline pore water by freshwater results in more swell and smaller compressibility. Furthermore, the unloading and loading consolidation coefficients were obtained by the swell-load results. The unloading consolidation coefficients were an order smaller than the unloading consolidation coefficient that was found in the softening test on the clay cube.

The influence of specific soil characteristics such as the stiffness, hydraulic conductivity, suction etc. is difficult to test experimentally. Therefore, a sensitivity analysis of the soil characteristics by numerical modelling will be conducted in the next part of this study.

## 5.2. MPM

### 5.2.1. Results of sensitivity analysis

#### 1. Mesh refinement

The optimum mesh can be determined based on the displacements and calculation times. The total strains ( $\frac{\Delta H_{tot}}{H_{0\ tot}}$ ) versus normalized time ( $T_v = \frac{c_v^* t}{R^2}$ ) for five different meshes are plotted in figure 5.13. The strains govern the change of top of the clay ball structure. Initial negative strains can be identified, but shortly followed by positive strains. Positive strains take place because the upward force caused by softening is larger than the downward force by the applied preload of 25 kPa. Small negative strains can be identified after most of the softening took place, especially for the finer mesh refinements.

Larger final strains result for a courser mesh refinement due to two reasons: (i) The interlump void space does not close completely as a result of the missing boundary contact in MPM. Therefore, one element of the interlump void space will always be present in between the lumps. The larger the element is, the larger the global strains will be. (ii) It is better possible to follow the local strain gradients for a finer mesh refinement because the mesh is more flexible. Consequently, smaller global strains result for smaller elements.

The deviatoric strains at  $T_v = 5 * 10^{-4}$  are plotted for all mesh refinements (fig: 5.15). This figure shows that the local strains can be better followed for the finer mesh refinements. Accordingly, the most realistic mesh refinement is the finest mesh, i.e. number 5. For mesh refinement 5 the interlump void space is almost completely closed, and the local strains are best modelled. But as the calculation time of the finest mesh is very low, there is chosen to continue in the rest of this study with **mesh refinement number 4**. The displacements of mesh refinement 4 differ not substantially from the results for mesh refinement 5.

The total initial void ratio is governed by the void ratio inside the clay balls ( $e_a = 0.5625$ ) and the interlump void space ( $e_m = 0.0724$ ). Accordingly, the total initial void ratio is 0.6349. The change in the total void ratio over time is plotted in figure 5.14. Softening results in an increase of the void ratio inside the clay balls, while the interlump void space diminishes over time. Unfortunately, it is only possible to determine the total void ratio over time and it is not possible to determine  $e_a$  and  $e_m$  separately. To increase the understanding of the softening process over time several snapshots are taken of the process for mesh refinement 4 (fig: 5.16). The results show that softening results in positive local strains inside the clay balls. The local positive strains in the clay balls result in an expansion of the clay ball and thereby in positive total strains. The interlump void space closes over time due to the expansion and deformation of the clay lumps that results from softening.

The porosity is not automatically updated in the output due to an error in the code. The change in porosity can be determined if the updated porosity is included in the code by an extra 'update porosity flag'. Mesh refinement 4 was run another time with the updated porosity flag. The change of porosity over time as a result of softening can now be studied (fig: 5.17). The initial porosity at timestep 0 is 36% as defined in the input and over time the porosity increases locally up to 45%.

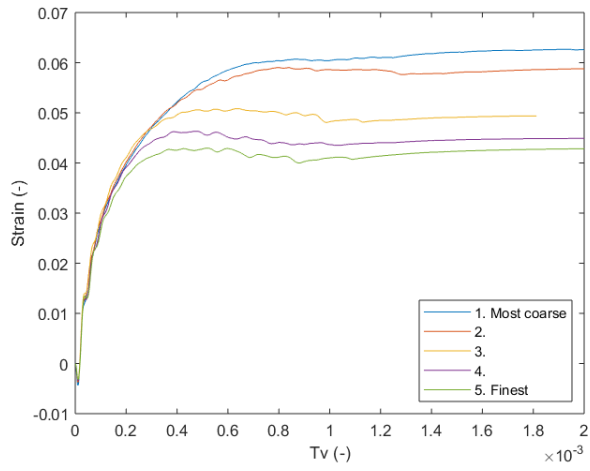


Figure 5.13: Total strain ( $\frac{\Delta H_{tot}}{H_{0 tot}}$ ) versus normalized time for five mesh refinements

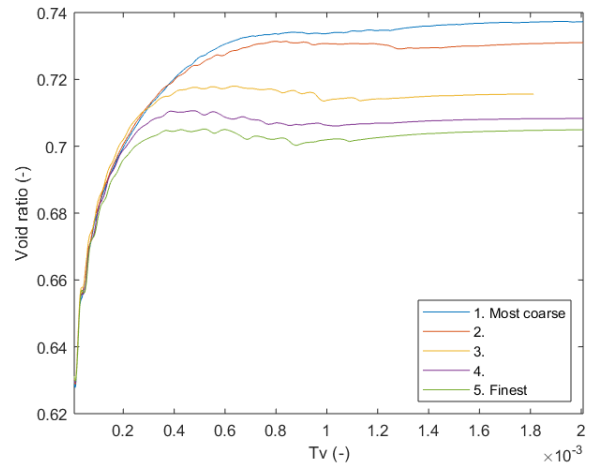


Figure 5.14: Total void space versus normalized time for five mesh refinements

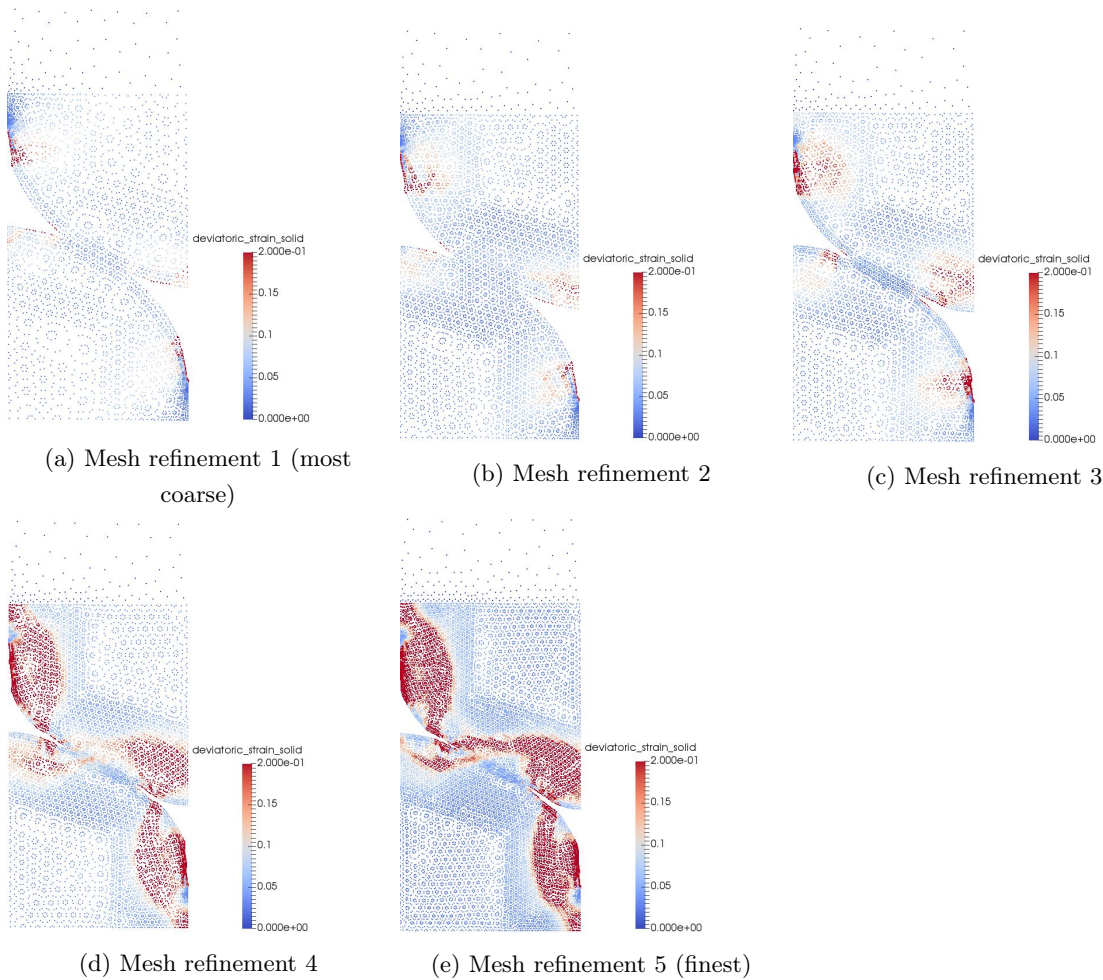


Figure 5.15: Deviatoric strains in the clay balls at timestep  $T_p = 5 * 10^{-4}$  for different mesh refinements. Larger deviatoric strains can be observed for the finer mesh refinements, this is a result of the more flexible mesh. Accordingly, the local strains can be followed better.

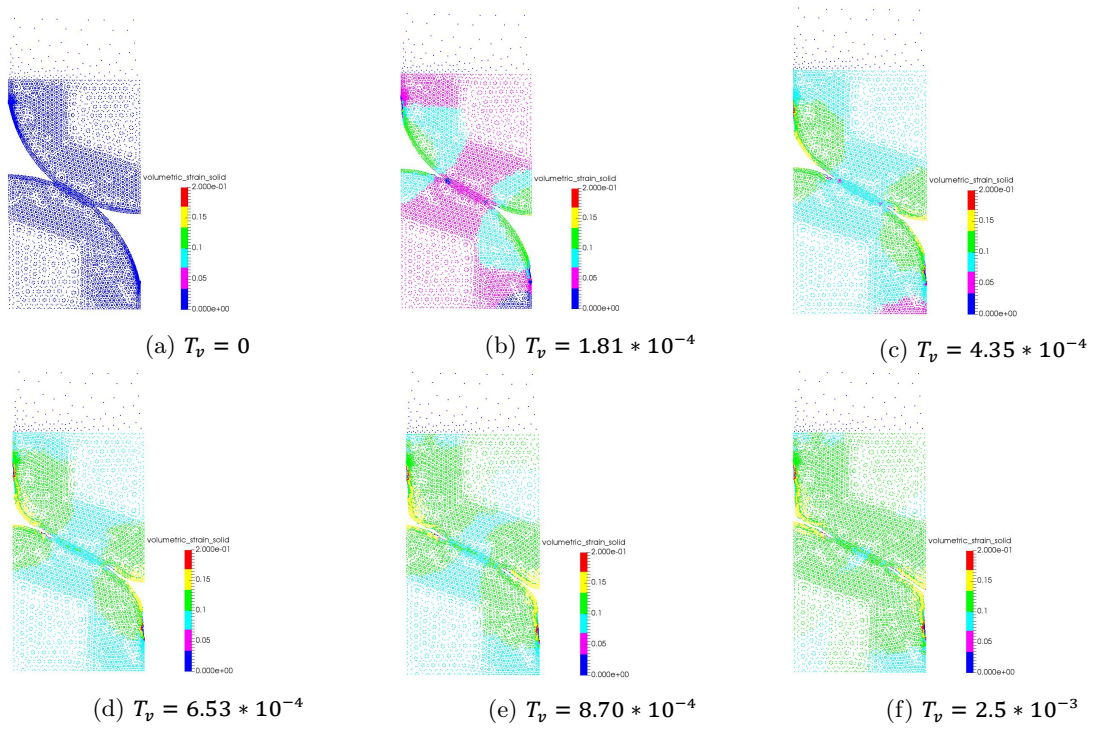


Figure 5.16: Volumetric strains in the clay balls at several timesteps for mesh refinement 4. Over time the interlump void diminishes because positive strains are present due to the softening process in the clay lumps.

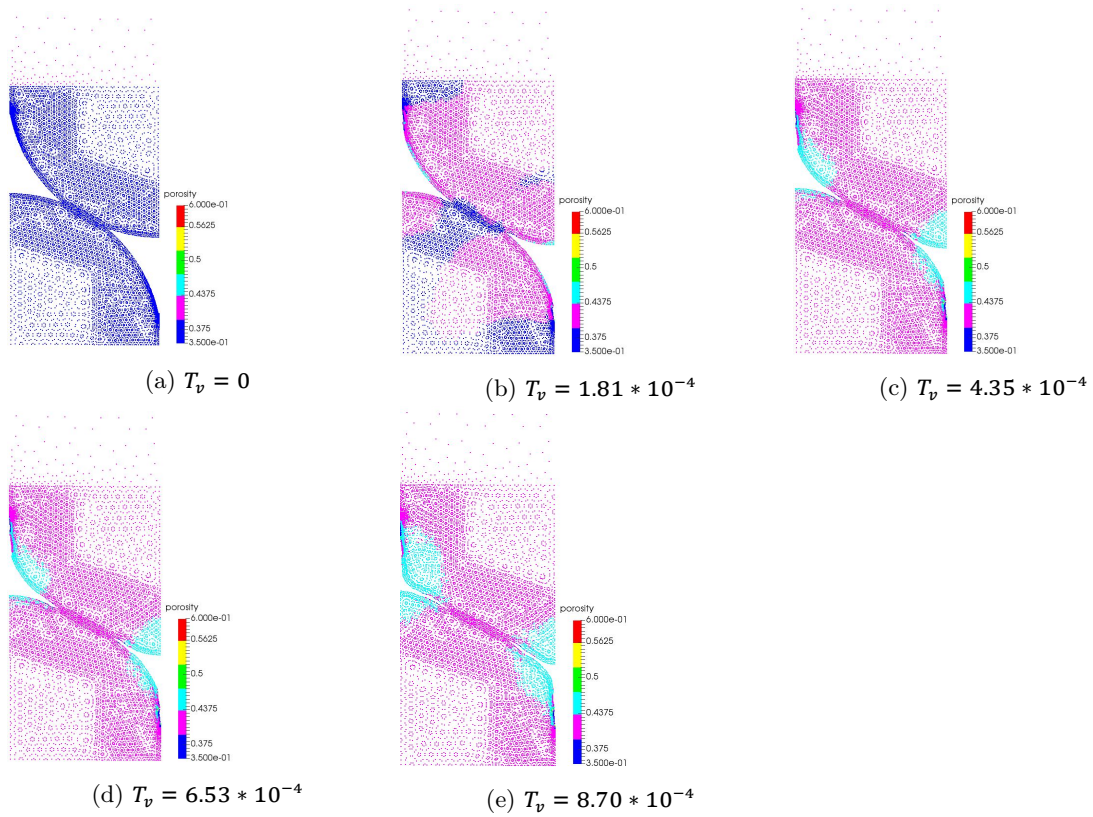


Figure 5.17: Porosity over time for mesh refinement 4. The porosity increases over time as a result of softening.

## 2. Hydraulic conductivity

The displacements of the clay ball structure for the three different hydraulic conductivities are plotted in figure 5.18. The time after which the final swelling condition is reached differs for the different hydraulic conductivities. The final swelling condition is reached in several seconds for hydraulic conductivity 3, while it takes substantially longer for the smaller hydraulic conductivity.

The normalized strain versus the normalized time is shown in figure 5.19. The final swelling condition (end of consolidation) is reached for all hydraulic conductivities at a normalized time of  $0.5 * 10^{-3}$ . The normalized results show the same trend for different hydraulic conductivities. According to the consolidation equation, the relation between hydraulic conductivity and time is linear. The normalized results show that the relation is indeed almost linear as the results show the same trend. But, the initial peak differs slightly because the model is not perfectly linear. The non-linearity originates from two processes: (i) The material behaviour: a Mohr-Coulomb model is used in this study and this model includes failure (ii) The geometry: for large displacements it is not possible to configure the results to the regional configuration. It is required to update the geometry and non-linearity results.

Large deviatoric strains indicate the failure zones inside the clay balls (fig: 5.20). The deviatoric strains are larger for the larger hydraulic conductivity ( $K_3$ ). Failure zones arise at locations where there is large stress (pressure) difference between the stress inside the clay ball as in (fig: 5.21c). The deviation in the peak strain and time is a result of the non-linearity of the model as the failure zones at the peak strain differ.

For stiff clays, such as the Boom clay, the hydraulic conductivity is several orders smaller than the hydraulic conductivity in the MPM model. Consequently, the time until the final swelling condition is reached will be exceedingly larger and can be estimated by scaling of the normalized results. The time until the final swelling condition is reached for the Boom clay for this model is determined in equation 5.4. The results can be scaled by the hydraulic conductivity of the Boom clay as the stiffness, unit weight of water and the radius of the clay lumps do not vary. The hydraulic conductivity of the fissured Boom clay is in the order of  $10^{-10}$  m/s as explained in section 5.1.1.

$$t(\text{end of consolidation}) = \frac{T_v * R^2}{c_v} = \frac{T_v * R^2 * \gamma_w}{K * E} = \frac{0.5 * 10^{-3}}{10^{-10}} = 5 * 10^6 s = 58 \text{ days} \quad (5.4)$$

For an unfissured Boom clay the hydraulic conductivity is in the order of  $10^{-12}$  m/s. This results in a final swelling time of 16 years, see equation 5.5. Scaling of the results give only correct results for linear problems. However, the problem is not perfectly linear and therefore scaling of the results give not completely correct values. But, the order of magnitude will be similar, and that is the main purpose of a modelling analysis in MPM as there will always be uncertainty due to the uncertainty in soil characteristic values. The time until the final swelling condition is reached, depends highly on the lump size and soil characteristics. So, these results cannot be generalized for other geometries and deposits.

$$t(\text{end of consolidation}) = \frac{T_v}{K} = \frac{0.5 * 10^{-3}}{10^{-12}} = 5 * 10^8 s = 15.9 \text{ yr} \quad (5.5)$$

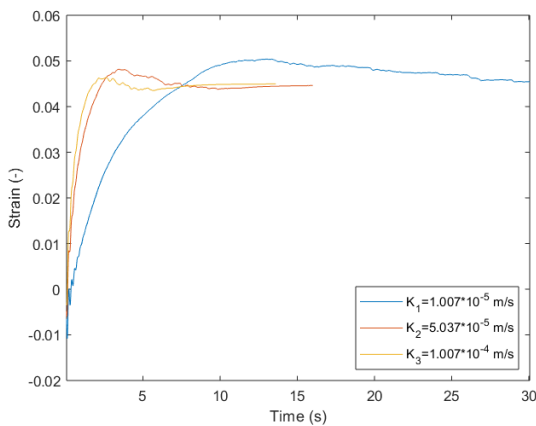


Figure 5.18: Result of sensitivity analysis for the hydraulic conductivity for mesh refinement 4: total strain ( $\frac{\Delta H_{tot}}{H_{0 tot}}$ ) versus time. The softening time is substantially longer for a smaller permeability.

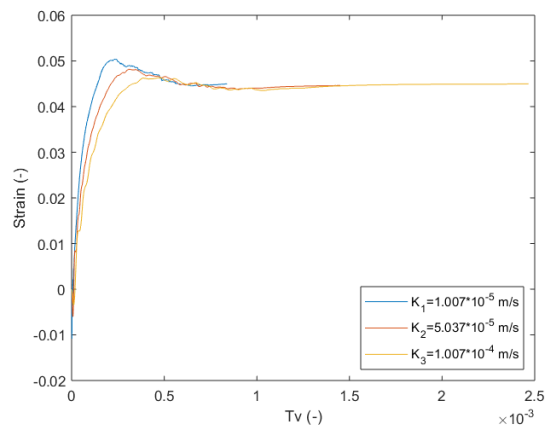


Figure 5.19: Result of sensitivity analysis hydraulic conductivity: total strain ( $\frac{\Delta H_{tot}}{H_{0 tot}}$ ) versus normalized time for mesh refinement 4. The Softening time is substantially longer for a smaller hydraulic conductivity.

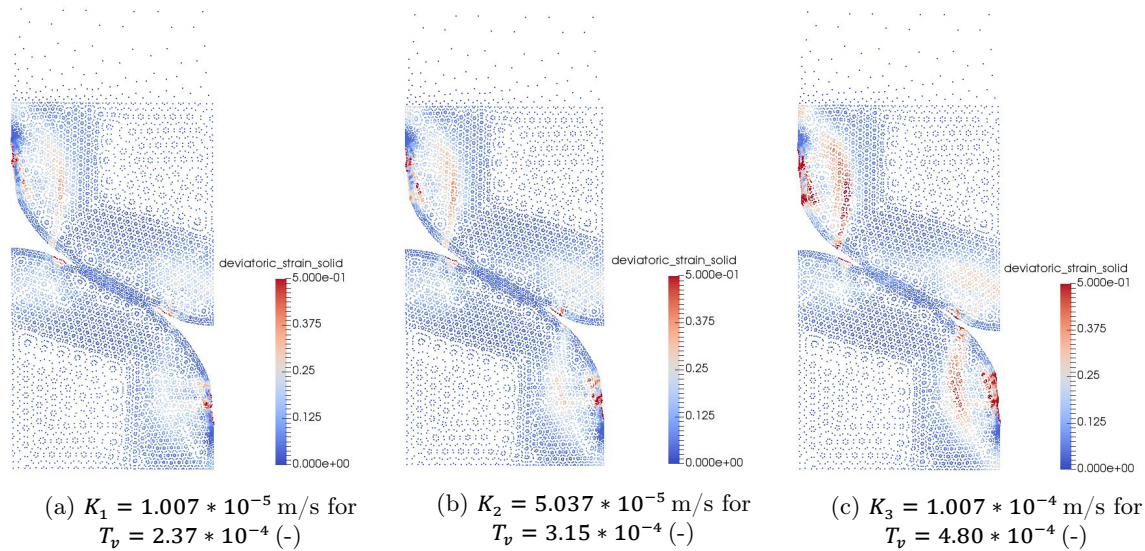


Figure 5.20: Visualization of the deviatoric strains in the clay balls at the peak strain for mesh refinement 4. Larger deviatoric strains are present in the clay ball with a larger hydraulic conductivity ( $K_3$ ) compared to the lower hydraulic conductivity ( $K_1$ ).

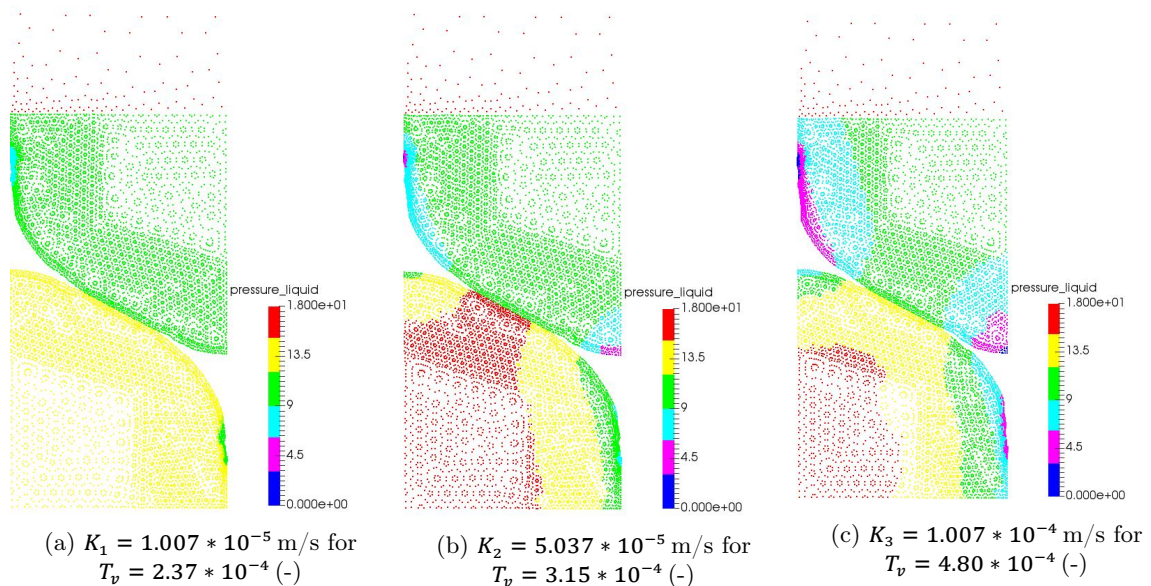


Figure 5.21: Visualization of the pore pressure in the clay balls at the peak strain for mesh refinement 4. Larger relative differences in pore pressure are present inside the clay ball with a larger permeability. This results in a failure zone as indicated in figure 5.20.

### 3. Stiffness

The results of the sensitivity analysis for different stiffness, i.e. young's modulus: 1.  $E_{min} = 1073$  kPa, 2.  $E_{average} = 1800$  kPa and 3.  $E_{max} = 2503$  kPa, are presented in figure 5.22. It is important to mention that the permeability and pre-consolidation stress are kept constant in this sensitivity analysis. While in reality, a softer clay will be more permeable and be governed by a smaller pre-consolidation stress. There are three clear differences visible in the results:

(i) Less stiff clays swell more and the relation between stiffness and strain is non-linear. The difference in the degree of softening for the different stiffness can be explained by the constant pre-consolidation stress in the model. Softer clays swell more than stiffer clays for a constant pre-consolidation stress. At first, this may sound counter-intuitive, as a softer clay is expected to swell less because the pre-consolidation stress is normally smaller in softer clays. But, in the theoretical case where the pre-consolidation stress is kept constant softer clays swell more than stiffer clays (fig:5.23).

(ii) The presence of negative strains (rebound) at  $T_v = 0.4 * 10^{-3}$  for stiffer clays, while this is not present for softer material. Rebound is not present for the softer material because a softer material swells more and the swelling process is slower. The maximum strains are reached at a later moment in time for the softer material compared to a stiffer material (fig: 5.22). That is because the pore pressure dissipation is slower for a softer material (fig: 5.24 and fig: 5.25). Pore pressure dissipation and thus swelling are slower for a softer material because the consolidation coefficient is smaller (eq: 5.6). Consequently, the interlump void space closes already during the swelling process for softer clays. While for stiffer clays a sudden drop in displacements occurs after most of the swelling took place due to the closure of the interlump void space.

(iii) A wiggly line can be observed for  $E = 1800$  kPa and  $E = 2503$  kPa, while it is almost not present for  $E = 1073$  kPa. The wiggly line is a result of the dynamic model. The same damping factor is applied for all three stiffnesses and that is why the dynamic influence differs.

$$c_v = \frac{k}{m_v * \gamma_w} = \frac{k * E_{oed}}{\gamma_w} \tag{5.6}$$

It can be concluded, that the results comply with the expectation of stiffness adjustment. So, the MPM model seems to work correctly for stiffness adjustments, because the results comply with the expectation based on theoretical soil mechanics theory.

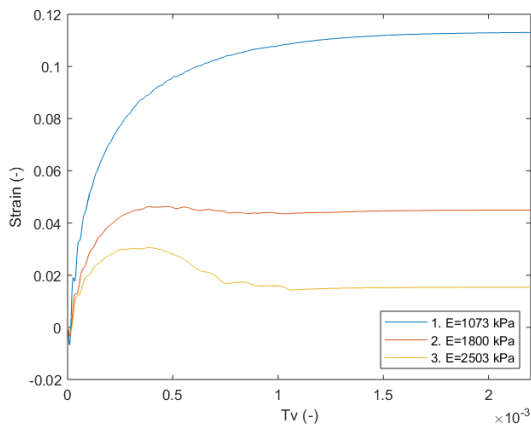


Figure 5.22: Result of sensitivity analysis for stiffness for mesh refinement 4:  
 $E_{min} = 1073kPa, E_{average} = 1800kPa, E_{max} = 2503kPa$ .  
 The total strains ( $\frac{\Delta H_{tot}}{H_{0 tot}}$ ) versus the normalized time are plotted.

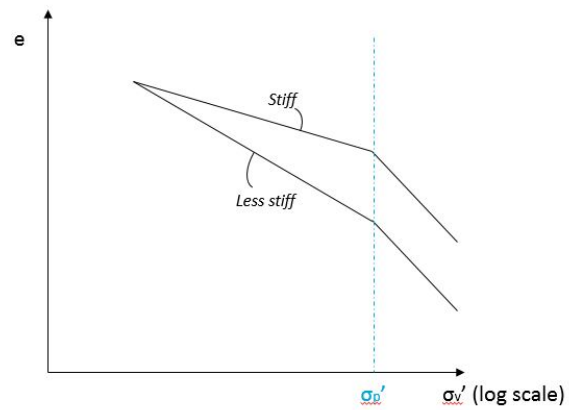


Figure 5.23: Sketch of the theoretical case: swelling for stiff and a less stiff material with a constant preconsolidation stress. A less stiff material will swell more under the same stress change.

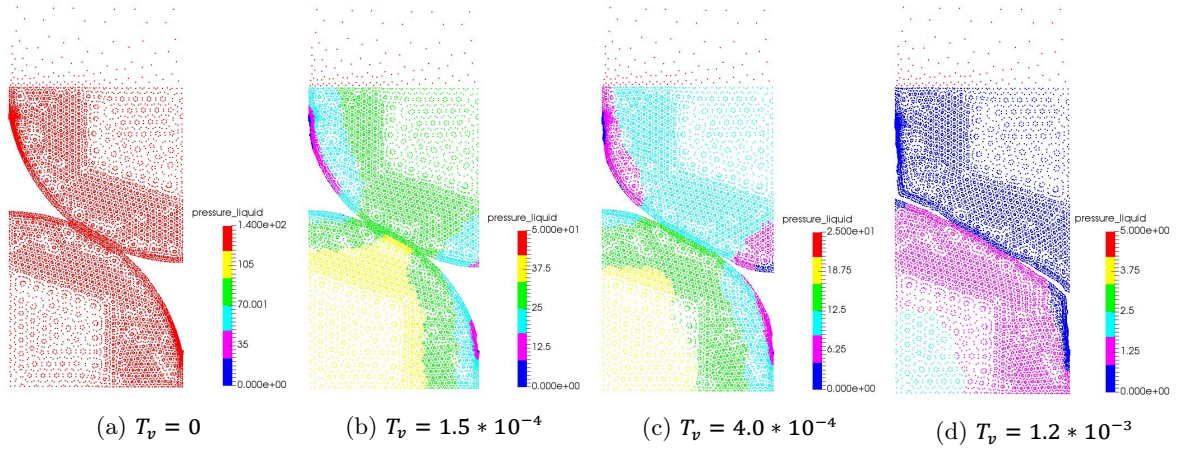


Figure 5.24: Stiffness = 2503 kpa. Pore pressure at certain timesteps inside the clay balls for mesh refinement 4. Please note the change of legend over time. The pore pressures are smaller compared to the pore pressures for the softer material (fig: 5.25) at the same normalized time.

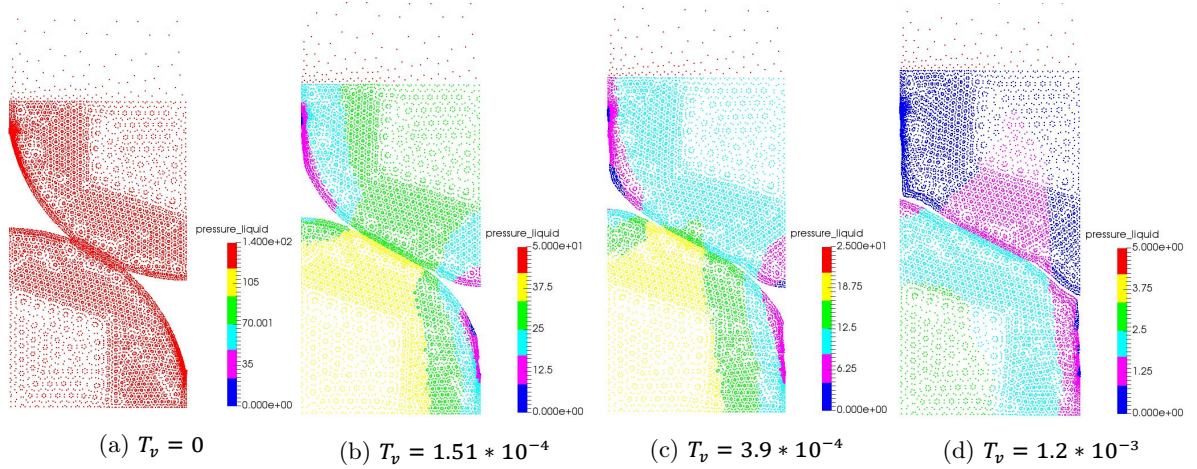


Figure 5.25: Stiffness = 1073 kpa. Pore pressure at certain timesteps inside the clay balls for mesh refinement 4. Please note the change of legend over time.

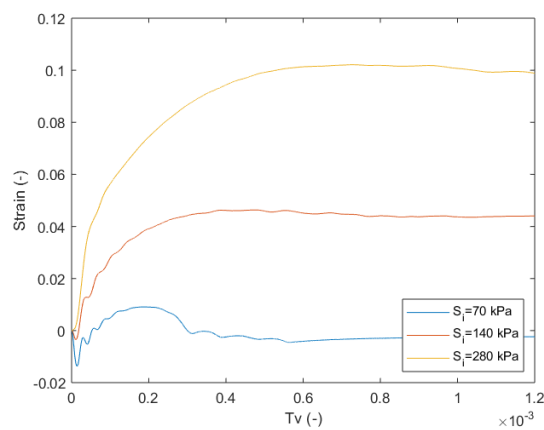


Figure 5.26: Result of sensitivity analysis for suction:  $S_1 = 70 \text{ kPa}$  and  $E_1 = 1180 \text{ kPa}$ ,  $S_2 = 140 \text{ kPa}$  and  $E_2 = 1800 \text{ kPa}$ ,  $S_3 = 280 \text{ kPa}$  and  $E_3 = 2843 \text{ kPa}$ . The total strains ( $\frac{\Delta H_{tot}}{H_0}$ ) versus the normalized time are plotted for mesh refinement 4.

#### 4. Suction

The results of the sensitivity analysis for initial suction are shown in figure 5.26. Positive strains are present for an initial suction of 140 and 280 kPa, while small final negative strains result for an initial suction of 70 kPa. In the literature study, it was described that a larger initial suction would result in more mechanical swell. This effect is clearly visible in the results. A final negative displacement only results when the volume increase due to mechanical swell is smaller than the initial interlump porosity.

Larger initial negative strains, just after application of the preload, can be observed for smaller initial suctions. The reasons lies in the relation between the initial suction and strength in the model. The initial suction influences the initial strength of the material, see section 4.2.2. A larger initial suction will result in a material with a higher initial strength. The initial negative displacement just after load application is larger for materials with a smaller strength. This is the case because clay balls with a higher initial strength will deform less under the small preload.

#### 5. Preload and 6. Moment of application

The results of the preload sensitivity analysis are shown in figure 5.27. The degree of swelling decreases for a larger preload, which is confirmed by equation: 5.7 and equation: 5.8. A larger load results in a smaller change in effective stress and thus smaller strains. Furthermore, it can be observed that initial negative strains are present and that the magnitude increases with the preload. This means that the instantaneous application of the preload results in a decrease of the void space inside the lump.

Final negative strains result for a preload of 75 kPa or more. Accordingly, the theoretical swelling pressure for the current geometry is larger than 50 kPa and smaller than 75 kPa. It is important to mention that this theoretical swelling pressure is highly dependant on the geometry and its interlump void space, i.e. smaller positive strains are expected for a larger interlump void space.

$$\Delta \varepsilon_v = \frac{\Delta \sigma'_v}{E_{oed}} \quad (5.7)$$

$$\Delta \sigma'_v = \Delta \sigma_v - \Delta q \quad (5.8)$$

The load application scheme for the normalized time is presented in figure 5.28. The influence of the moment of load application can be found by the sensitivity analysis of the moment of load application. The final strains (fig: 5.29) are similar in all four cases, but their profile differs. Larger initial positive strains are present for case 1, 2 and 3 compared to case 4. The larger initial positive strains result because there is no downward force present at the start. The final strains similar for all loading schemes. This complies with the expectation as an elastic constitutive model is used. The true soil behaviour is not perfectly elastic. Therefore, the true soil response will likely differ from these MPM results.

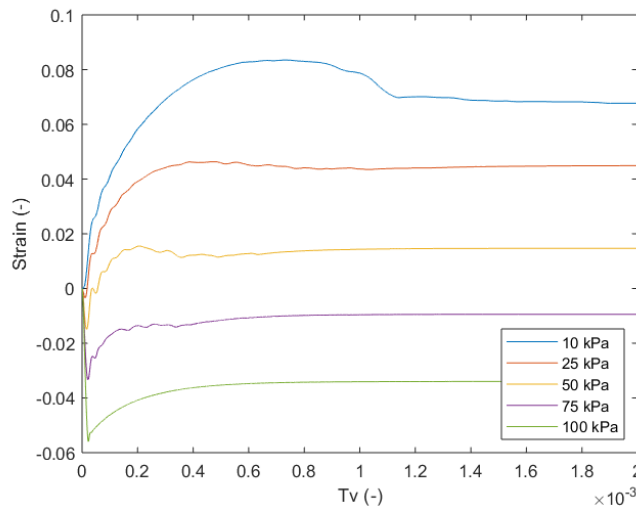


Figure 5.27: Result of sensitivity analysis for preload:  $L_1 = 10, L_2 = 25, L_3 = 50, L_4 = 75, L_5 = 100$ . The total strains ( $\frac{\Delta H_{tot}}{H_0_{tot}}$ ) versus the normalized time are plotted for mesh refinement 4.

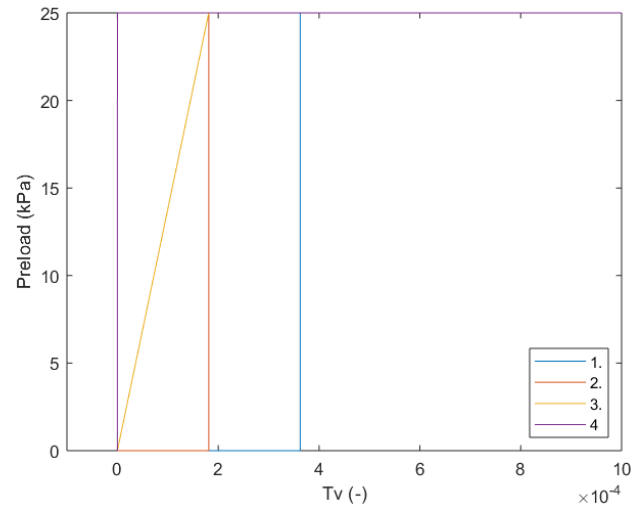


Figure 5.28: Moment of load application on the normalized time scale. Load application schemes: 1. Load applied at 33.3% 2. Load applied at 16.7% 3. Load is applied linearly during the first 16.7% 4. Instantaneous load from the start.

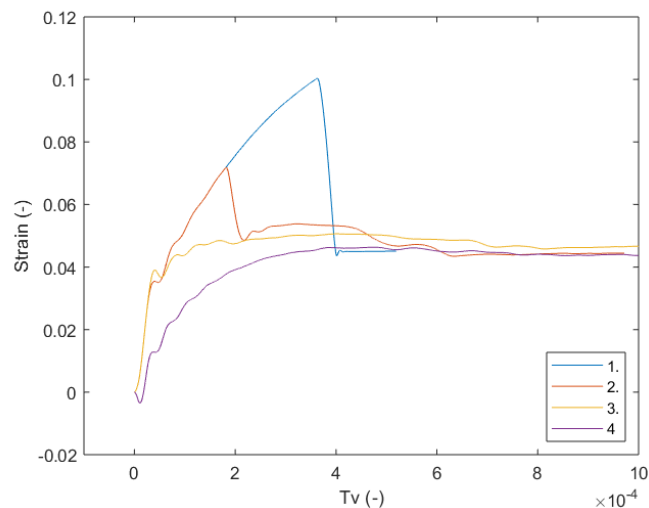


Figure 5.29: Result of sensitivity analysis for load application moments as stated in figure 5.28. The total strains  $\left(\frac{\Delta H_{tot}}{H_{0 tot}}\right)$  versus the normalized time are plotted for mesh refinement 4.

## 7. Cohesion

Small failure surfaces can be identified inside the non-cohesive clay balls (fig: 5.30). The black ovals indicate breakage of the clay ball. As an overconsolidated material is initially cohesive, the influence of cohesion is tested by a model that includes cohesion as described in section 4.2.3. The cohesive clay balls do not show internal failure surfaces (fig: 5.31) because the cohesion term prevents failure to occur.

The interlump void space does not close for the cohesive model. Even after 30 s closure of the clay balls does not occur, while for non-cohesive clay balls closure took place after 4 s. Figure 5.33 shows the mean effective stress after 30 s for the cohesive model. At the contact in between the clay balls the mean effective stress remains high while this did not occur for the non-cohesive clay balls (fig: 5.32). Consequently, the clay balls do not deform towards each other in the cohesive model as the applied preload is smaller than the mean effective stress. There are two possible explanations for the high mean effective stress at the contact: (i) An outer non-cohesive layer is present in the cohesive model because of the boundary contact issues. Two different material properties are present next to each other. It might be possible that modelling issues arise at the contact between the clay balls. Material points with different material properties end up in the same elements and thereby cause unrealistic results. (ii) The load is applied by a rigid plate, thus resulting in a non-uniform load application in the material. The unequal load application results

in failure inside the non-cohesive clay balls, while failure can not occur in the cohesive clay balls. The stresses in the cohesive model can not spread evenly, and a large mean effective stress at the contact results. Accordingly, the clay balls will not merge as the mean effective stress at the contact remains high. It is expected that the applied preload spreads more for a model that consists of several cohesive clay balls. Therefore, it is recommended to perform a model analysis for a 2D or 3D model that consists of several clay balls.

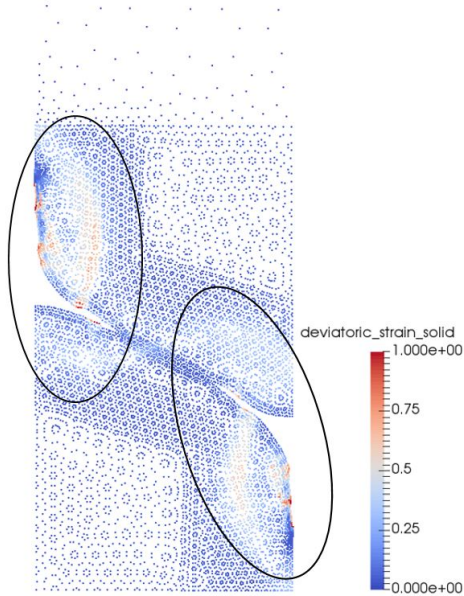


Figure 5.30: Mesh refinement 4 for the non-cohesive model. The large deviatoric strains (in black ovals) indicate the failure surfaces inside the clay balls.

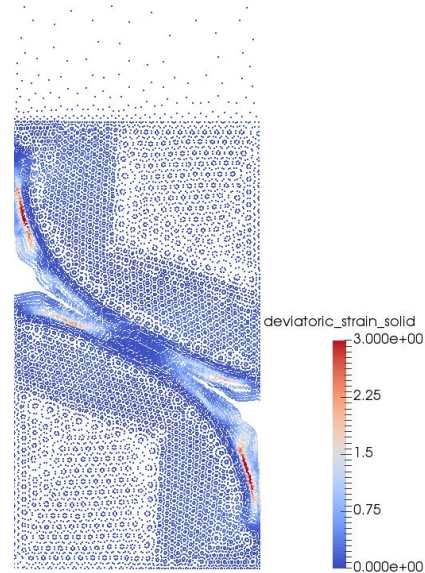


Figure 5.31: Mesh refinement 4: deviatoric strains in the cohesive model. No failure zones are present inside the cohesive clay balls. Small failure zones are present in the outer non-cohesive layer of the clay ball.

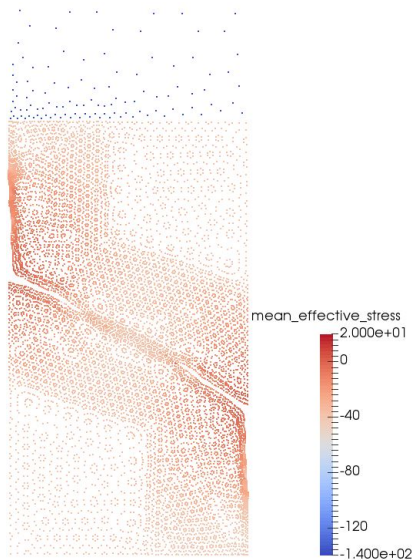


Figure 5.32: Mesh refinement 4: mean effective stress for the non-cohesive model. The clay balls merge because the mean effective stress is small and equally distributed in the clay ball.

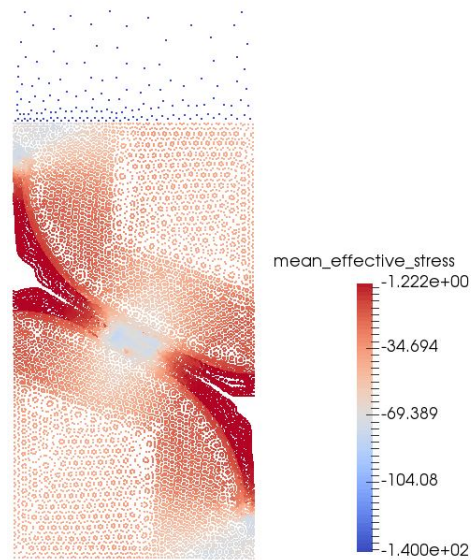


Figure 5.33: Mesh refinement 4: clay balls do not merge due to the high mean effective stress (70 kPa) at the contact in between the clay balls.

## 8. Geometry

The mean effective stresses for the two different geometries are plotted in figure 5.34. The results in figure 5.34 show that the MPM model realistically show the distribution of the mean effective stress for several geometries. It can be concluded that alteration of only the inner geometry is possible and give realistic results. This is interesting to know for further studies, as this means that only small model adjustments are required to study the influence of clay ball size, shape and geometry.

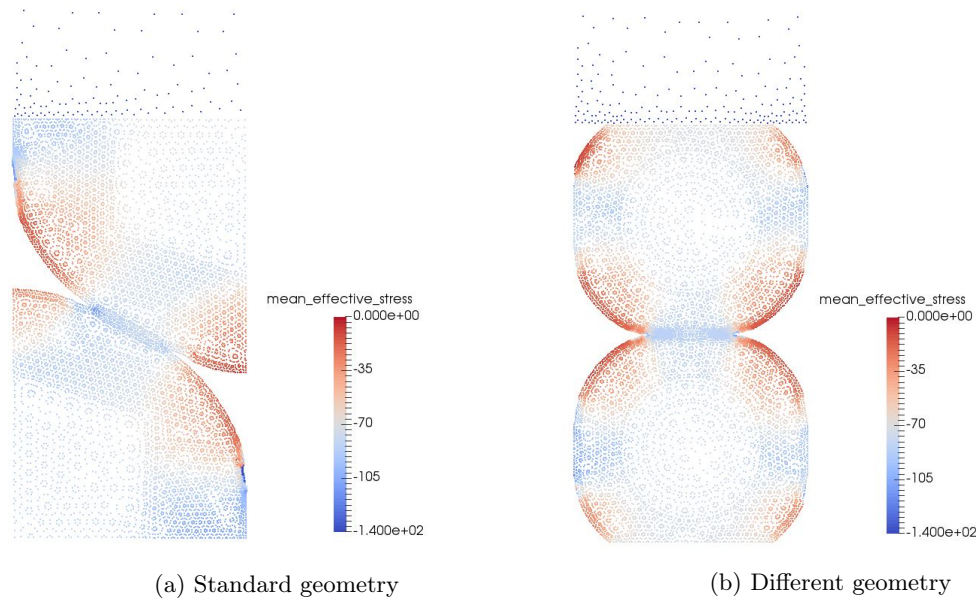


Figure 5.34: Mean effective stress during softening for different geometries

### 5.2.2. Summary numerical results

The results of this study are very promising and show the opportunities of MPM. A broad sensitivity analysis was conducted and it was shown that MPM can model the softening behaviour over time for several input properties. Modelling issues were only present for the cohesive case and can probably be solved by a more advanced constitutive model and a more advanced geometry. The results of the sensitivity analysis showed:

- Small deviations in the peak strain and time for different hydraulic conductivities are a result of the non-linear model.
- The material softens more for a smaller stiffness.
- Expansive total strains result for an initial suction larger than 70 kPa.
- Final negative strains result for a preload of 75 kPa or more. Accordingly, the theoretical swelling pressure for the current geometry is larger than 50 kPa and smaller than 75 kPa.
- The moment of load application in time has no influence on the final strains, because the model is elastic.

The initial interlump void space and lump size largely influence the final strains. It must be kept in mind that the outcome of this sensitivity analysis only shows the potential of the MPM model and can not be generalized because the results are highly dependant on the initial geometry.

### 5.2.3. Model issues in MPM

The material point method has several limitations and disadvantages that influence the results. Besides, the method is fairly new and therefore not all features are implemented yet in the *Dynamic MPM 2D DP* model of Deltares.

The first disadvantage of MPM is the fairly large numerical error that originates from integration on the MPs. Besides, error accumulation can take place due to mapping forwards and backwards (Vardon, 2019). Secondly,

MPM has an explicit time-stepping scheme which results in a very large calculation time for small permeabilities and small elements. To overcome this, a larger permeability can be used and the results should be scaled. Scaling of the results give no perfect results as the problem is non-linear. Another limitation in the *Dynamic MPM 2D DP* model, is the missing implementation of the generalized boundary contact. This boundary condition is implemented for the more standard problems but not generalized yet. Boundary condition issues arise as a result of MPs that end up in adjacent elements, i.e. in the adjacent element across the boundary with different material properties. Thirdly, it is only possible to apply a load by a rigid body force and thus a non-uniform load is applied. Lastly, it is only possible to model the clay balls as a homogeneous medium. Consequently, the influence of discontinuities, the rearrangement effect and the aggravation of the outer shell is not included. But the influence of discontinuities can be indirectly included by the hydraulic conductivity.

### 5.3. Comparison experimental, numerical and theoretical strains

The MPM results can be checked by the theoretical strains via a simplified calculation. Furthermore, the experimental strains can be compared to the strains numerical strains for a model with comparable input properties.

#### Comparison theoretical strains to strains MPM

The strains in the MPM model can be checked by the theoretical expected strain. The theoretical small-strain can be calculated by the change in effective stress and the oedometer loading stiffness as described in equation 5.9.

$$\Delta\varepsilon_v = \frac{\Delta\sigma'_v}{E_{oed}} \quad (5.9)$$

The stiffness could be derived from the experimental swell-load test results. But, in the experimental swell-load test (section: 5.1.5) the material was first able to swell completely and afterwards loaded. While, in the MPM model the load was applied instantaneously from the start. Therefore, it would be incorrect to use the unloading or loading stiffness from the experimental tests as the stiffness in the MPM model is likely to differ. Therefore, the oedometer modulus is determined by the input stiffness and Poisson's ratio of the MPM model.

$$E_{oed} = \frac{1 - \nu}{(1 + \nu)(1 - 2\nu)} * E \approx 1.11 * E \quad (5.10)$$

The change in effective stress is governed by the change in suction, i.e. the initial suction minus the final suction. It is assumed that the soil stays fully saturated such that the initial suction of the lump is equal to the mean effective stress. The set-up is laterally constraint, so the suction can only dissipate in the vertical direction. Therefore, the dissipation of the initial suction is translated into a vertical stress change ( $\Delta\sigma_v$ ), and the final suction is equal to the applied load ( $q$ ). This results in a change in effective stress:

$$\Delta\sigma'_v = \Delta\sigma_v - \Delta q = 140 - 25 = 115 \text{ kPa} \quad (5.11)$$

Such that the theoretical strain is:

$$\Delta\varepsilon_v = \frac{115}{1.11 * 1800} = 0.0575 \text{ (-)} \quad (5.12)$$

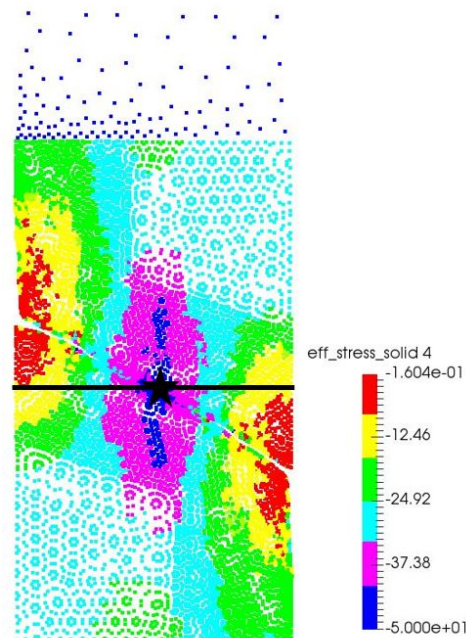


Figure 5.35: Mesh refinement 4: vertical effective stresses after dissipation of suction. At the contact in between the clay balls a mean effective stress of -50 kPa is present, while an average value of -25 kPa is present over the black horizontal line.

The theoretical strains are larger than the strains for the finest model in MPM. This is logical as the MPM model is not completely filled by the material, i.e. interlump voids are present. Consequently, the clay balls can expand and shear. Horizontal straining will take place and fill the gap in between the balls. This results in smaller strains than as if the whole model was completely filled with the material and therefore only vertical straining could take place. The reasoning above can be checked by the resulting vertical effective stresses in the MPM model (fig: 5.35). The highest effective stress, -50 kPa, occurs at the location where the clay balls initially touch each other. But if the effective stresses are averaged over the horizontal black line, a value of approximately -25 kPa results. The location where the clay balls initially touch each other, the star in figure 5.35, governs the vertical strains of the model. The theoretical strains can be recalculated based on this effective stress of -50 kPa (eq: 5.13) and a vertical strain of 0.045 results. That is in fact, almost similar to the vertical strain for mesh refinement 4 as shown in figure 5.13.

$$\Delta\varepsilon_v = \frac{\Delta\sigma'_v}{E_{oed}} = \frac{140 - 50}{1.11 * 1800} = 0.045 \text{ (-)} \quad (5.13)$$

### 9. Comparison experimental softening strains and strains determined by MPM

The results of MPM are very similar to the theoretical strains, but may not be comparable to the true soil behaviour. Therefore, the result of the swell test is compared to the strain in the MPM model. The permeability is several orders larger in the MPM model than for the Boom clay material. Consequently, the swelling time can not be compared directly.

The final strain for the MPM model is approximately 0.064 (-), as shown in figure 5.36. The strain is larger compared to the strains that result from the experimental swell test (fig: 5.8) and (fig: 5.10). While it was expected that the strains in the MPM model were smaller than in the experimental swell test if the material softens equally. This was expected because the MPM geometry consists of clay balls and interlump void space. The clay balls soften and fill the interlump voids, thereby resulting in smaller total strains than if the material was completely filled by clay. It can be concluded that the material modelled in MPM softens more than the true material behaviour. The input properties of the MPM model were based on literature values and may not be similar to the true sample material. Correspondingly, differences in the resulting strains arise.

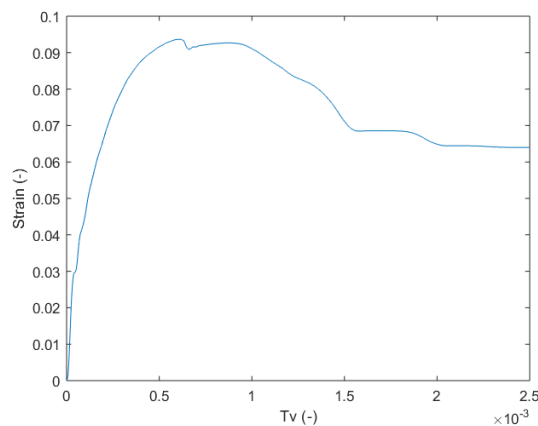


Figure 5.36: Results of MPM model 9. (comparable model to swell test). Total strains ( $\frac{\Delta H_{tot}}{H_{0 tot}}$ ) versus normalized time plotted for mesh refinement 4.



# IV

## Conclusions and recommendations



# 6

## Conclusions

Dredged materials can be reused for land reclamation projects, hereby generating economic and environmental benefits. Mechanical dredging of stiff clay results in large lumps of which, a reclamation fill can be established. Directly after placement, the fill consists of a matrix of stiff clay lumps and interlump voids. Preloading is a suitable method for interlump void closure, but it is uncertain if the interlump voids close under a reduced preload of 25 kPa within 1 - 2 years. It was found in the literature study that the initial soil characteristics, softening, and the presence of discontinuities largely influence interlump void closure. Softening as a result of swelling is the dominant process in the interlump void closure problem. Closure of the interlump voids was studied by an experimental and numerical approach in this research. The sample material used in this study is the stiff overconsolidated Boom clay.

Overconsolidated clay softens due to unloading and the dissipation of suction over time. In the experimental swell test, it was found that expansive strains up to 5% can occur for Boom clay samples originating from an in situ depth of 6 m. Furthermore, it was shown that a decrease in pore water salinity results in an increase of expansive strains. The microstructure was likely to be altered from a flocculated to a dispersed state, by the decrease in pore water salinity. The smaller compressibility compared to the saline tested sample underwrites this statement. It seems that the unloading and loading stiffness differ, which might imply that the pre-consolidation stress was lost during the softening process. But, it is uncertain if they truly differ because the results can not be compared to a virgin compression line as this is not available.

The unloading consolidation coefficient was determined by a small scale test. From the consolidation equation of a sphere and the softening time a value of  $c_v = 2.80 * 10^{-8} \text{ m}^2/\text{s}$  resulted. While the unloading coefficients that resulted by the swell test were an order smaller. The consolidation coefficient upon loading that was obtained in the load test is comparable to the theoretical value based on literature.

The presence of fissures in the Boom clay samples were identified on the CT and micro CT scans. Their presence increases around the pyrite inclusions. The smallest micro-fissures could not be identified due to the resolution of the images. Consequently, it is impossible to estimate the effect of fissures on the hydraulic conductivity. (Prof. N. Vandenberghe (personal communication, March 25, 2019)) estimated the hydraulic conductivity of the fissured Boom clay as two orders larger than the intact Boom clay, and this was used in the numerical model.

The initial soil characteristics have a large influence on interlump void closure. Accordingly, a sensitivity analysis was performed for several soil characteristics: hydraulic conductivity, stiffness, initial suction and cohesion. Besides, the influence of several preloads and load applications schemes were tested. It was found that the stiffness and initial suction largely influence the final strains. A smaller stiffness results in a larger expansive strain for a constant pre-consolidation stress. It was found in the literature review that a larger initial suction will result in more mechanical swell. The results of the MPM model comply to the expectation and show that a larger initial suction results in more expansion. The hydraulic conductivity does not influence the final strains but the time final softening time is largely influenced by the hydraulic conductivity. Furthermore, it was found that preloads larger than 75 kPa result in final compressive strains while expansive strains arise for preloads of 50 kPa and smaller. Besides, the moment of load application in time has no influence on the final strains because the model is elastic. While true soil behaviour is not elastic and the moment of load application in time will influence the final strains.

The prestudy into the feasibility of modelling interlump void closure by MPM showed that it is a suitable method to study softening. The sensitivity analysis showed that MPM gives plausible results for parameter adjustments. So that, MPM can be used as a investigation tool to increase the understanding of the influence of parameter variability

on the final interlump void closure problem. Modelling issues were only present for the cohesive case and can probably be solved by a more advanced constitutive model and a more advanced geometry.

The results of the sensitivity analysis showed that the resulting strains by MPM correspond to the theoretically calculated strains of 4.5%. Furthermore, the experimental strains of the swell test were compared to the numerical strain. In MPM a model was created with similar input and loading properties as for the swell test. A final expansive strain of 6.4% results from this numerical model. Due to the presence of interlump voids in the numerical model, it was expected that the numerical strains were smaller than the experimentally determined strains up to 5%. But, the numerical strains are larger compared to the experimental strains. In the sensitivity analysis, it was found that the final strains depend highly on the input soil parameters. It is likely that the input of the MPM model differs compared to the true sample material and thus different strains result.

MPM is a promising method to increase the understanding in the closure of the interlump voids. The influence of design parameter variability and interlump void closure time can be modelled. Although, the order of time for interlump void closure is conservative as several processes can not be incorporated in the model. The processes that can not be included directly in MPM are: the rearrangement effect of clay lumps, discontinuities and uniform loading. In this study, it was shown that a first conservative estimate of the interlump void closure time could be obtained by MPM for a simplified geometry. Accordingly, the formulated research question can be answered for this set-up.

*Will the interlump void space of a stiff lumpy clay fill close under a preload of 25 kPa within 1 - 2 years?*

The time until the interlump void space closes was determined by a simplified geometry in MPM under a preload of 25 kPa. For an unfissured Boom clay interlump closure takes place after approximately 16 years. While for a fissured Boom clay it only takes two months. So, interlump void closure will take place for a fissured Boom clay within 1 - 2 years for this simplified geometry used in this study. It is important to keep in mind that these results are highly dependent on the initial geometry, lump size and soil characteristics. Therefore, these results can not be generalized into an estimate of the interlump void closure time for any lumpy, stiff clay fill.

In conclusion, in this study the processes that influence interlump closure were identified. The dominant process is softening due to swelling and this was studied in more detail by the experimental and numerical approach. The feasibility of MPM to model the problem was explored, and it turned out to be a promising method. Further studies are required to check if the model gives plausible results for more advanced constitutive soil models and geometries. If the results are positive, MPM can be used as an investigation tool to increase the understanding of the interlump void closure time for more refined geometries.

Without further research, it is advised to place sand layers in between the lumpy clay layers. The sand settles in between the clay lumps. Consequently, sudden settlements due to interlump closure will not occur. An additional advantage is a major increase in the consolidation coefficient (Hartlen and Ingers, 1981). The required thickness of the sand layer depends on the initial interlump void space between the clay lumps. A volume of sand that is slightly larger than the interlump void space is required. However, the economic and environmental benefit of a lumpy clay fill reduces due to the required volumes of sand.

# 7

## Recommendations

The recommendations are subdivided into two sections. First, the recommendations on the experimental methodology are discussed. Secondly, the recommendations on the methodology of the MPM model are provided.

### 7.1. Recommendations on experimental methodology

#### Fissure identification test

The influence of fissures and other discontinuities on the hydraulic conductivity was studied by the fissure identification test.

- The smallest fissures ( $< 4 \mu m$ ) could not be identified in this study because the sample was relatively large and thus the resolution was not high enough. It is recommended to prepare smaller samples by a sampling tube, such that the smallest micro-fissures can be identified by the micro CT scanner.
- Fissures can be induced by the preparation of the sample. The fissure density in CT images might be higher compared to a natural sample as a result of the cutting process. Some large cracks can be identified at the outer shell of the sample block (fig: 5.2), those are likely induced cracks as they are substantially larger than the fissures inside the block. It is recommended to study the influence of the induced fissures as a result of sample preparation.

#### Miniature clay fill test

The goal of the miniature clay fill test was to study the influence of softening time and the rearrangement effect.

- The outflow velocity of the Rowe cell turned out to be too slow to obtain meaningful results. It is recommended to perform a similar test in a larger set-up with larger clay balls such that the rearrangement effect and softening time in a miniature set-up can be studied. Larger clay balls result in an increase in time until the cubes are fully softened. Consequently, the results for larger clay cubes are less sensitive to the time for water outflow.

#### Swell-load test

The influence of chemical and hydro-mechanical softening was studied by the swell-load test.

- The degree of chemical and mechanical swell can be determined by swell tests. So that, before the commencement of a project, the degree of swell is known. It is recommended to always perform those tests on an intact sample retrieved from an in situ depth conform to the proposed dredging depth. The test should be performed as quickly as possible after sampling because the suction might dissipate during storage.
- The results differ substantially per sample block, as was seen in section 5.1.5, due to soil variability. More accurate and reliable results can be obtained if the test is repeated several times on samples that originate from different sample blocks.
- The results of the swell-load test depend on the exact way the sample is prepared and this can differ slightly per test: (i) if the sample is cut carefully, most of the fissures at the top and bottom stay open which increases the permeability of the sample, (ii) the influence of wall friction can be decreased by a lubricate and the amount

of lubricate that is applied is likely to influence the results. Therefore, it is recommended to perform several tests on samples that originate from the same sample block such that the influence of sample preparation is included.

- It is recommended to perform a virgin compression test on the sample material such that the stiffness of the unloading and loading curves (fig: 5.12) can be compared to the virgin compression line.

## 7.2. Recommendations on numerical methodology

In this study, the opportunities of the MPM model for the lumpy clay fill problem were researched. Considering that this study is a prestudy, a highly simplified model was used. The limitations and consequences of this simplified model are described in this paragraph.

- The first simplifying solution lies in the constitutive soil model used. The clay balls are modelled by the Mohr-Coulomb constitutive soil model. This is a linear-elastic perfectly-plastic model. The model is relatively fast as it does not include stress-dependency nor stress-path dependency nor strain dependency of stiffness (Plaxis, 2014). However, this is a simplifying assumption of soil behaviour. Softening due to the dissipation of suction results in a large change in stiffness. Hence, the Mohr-Coulomb model can not model the soil behaviour correctly, and it is recommended to perform this analysis with a more advanced constitutive model.
- A highly simplified 2D geometry is used to model a clay fill. It is recommended to use a more advanced 2D geometry such that size, shape and packing effect can be studied.
- The geometry of the round clay balls was slightly adjusted towards a more hexagonal shape to decrease the size of the smallest element and thereby the calculation time. It is recommended to study the influence, if any, of the shape of the clay ball on the final results.
- The 'update porosity flag' was not set at 1 in the model. As a consequence, the porosity was not updated in the results file. A few models were re-run to show the effect on the porosity. It is recommended for further studies to always set the flag at 1.

# Bibliography

- Abels, H. A., Van Simaey, S., Hilgen, F. J., De Man, E., and Vandenberghe, N. (2007). "Obliquity-dominated glacio-eustatic sea level change in the early Oligocene: Evidence from the shallow marine siliciclastic Rupelian stratotype (Boom Formation, Belgium)." In: *Terra Nova* 19.1, pp. 65–73. ISSN: 09544879. DOI: 10.1111/j.1365-3121.2006.00716.x.
- Alapakam, V. (2006). "Characterization of lup fill in land reclamation." In: *Thesis* 30.3, pp. 243–250.
- Alonso, E. E., Vaunat, J., and Gens, A. (1999). "Modelling the mechanical behaviour of expansive clays." In: *Engineering Geology* 54.1-2, pp. 173–183. ISSN: 00137952. DOI: 10.1016/S0013-7952(99)00079-4.
- Andersland, O. and Landanyi, B. (2004). *Frozen ground engineering*. 2nd ed. John Wiley and Sons, pp. 1–357.
- Armstrong, C. P. (2014). "Effect of fabric on the swelling of highly plastic clays." Doctoral dissertation. University of Texas.
- Attewell, P. and Farmer, I. (1976). *Principles of engineering geology*. New York: John Wiley and sons, pp. 1–1044.
- Aylmore, L. and Quirk, J. (1967). "The micropore size distributions of clay mineral systems." In: *Journal of soil science* 18.1.
- Bader, S. (2005). "Osmosis in groundwater." Doctoral dissertation. University of Technology Delft, pp. 1–198. ISBN: 9090199004.
- Barden, L. (1974). "Consolidation of clays compacted 'dry' and 'wet' of optimum water content." In: *Géotechnique* 24.4, pp. 605–625. ISSN: 0016-8505. DOI: 10.1680/geot.1974.24.4.605. URL: <http://www.icevirtuallibrary.com/content/article/10.1680/geot.1974.24.4.605>.
- Bernier, F., Volckaert, G., Alonso, E., and Villar, M. (1997). "Suction-controlled experiments on Boom clay." In: *Engineering Geology* 47.96, pp. 325–338.
- Biot, M. (1941). "General theory of three dimensional consolidation." In: *Applied Physics* 12, pp. 155–164.
- Bjornshave, A., Hansen I, S., Magar, V., and Savioli, J. (2018). "Fehmarnbelt - A new link between Germany and Denmark." In: *PIANC-World Congress Panama city*, pp. 1–15.
- Blum, P. (1997). "Chapter 9: strength." In: *Physical properties handbook: a guide to the shipboard measurement of physical properties of deep sea cores*. 3, pp. 1–10.
- Bochner, B. Y. S. (1949). "Diffusion equation and stochastic processes."
- Bolt, G. H. (1956). "Physico-Chemical Analysis of the Compressibility of Pure Clays." In: *Géotechnique* 6.2, pp. 86–93. DOI: 10.1680/geot.1956.6.2.86. URL: <http://www.icevirtuallibrary.com/content/article/10.1680/geot.1956.6.2.86>.
- Boskalis (n.d.). "Engineering Geological Unit and deposit characterisation."
- British standards institution (1990). *BS 1377-2:1990 Soils for civil engineering purposes – part 2: Classification tests*. BS1377 (1990). "Part 6: Rowe cell." In:
- Burmister, D. M. (1949). "Principles and Techniques of Soil Identification." In: *Proceedings of Annual Highway Research Board Meeting* c, pp. 402–433.
- Cafaro, C. and Cotecchia, F. (2001). "Structure degradation and changes in the mechanical behaviour of a stiff clay due to weathering." In: *Geotechnique* 51.5, pp. 441–453. ISSN: 0016-8505. DOI: 10.1680/geot.2001.51.5.441.
- Calabresi, G. and Scarpelli, G. (1985). "Effects of swelling caused by unloading in overconsolidated calcs." In: *XI ICSMFE Conference*, pp. 411–414.
- Carman, P. C. (1953). "Properties of capillary-held liquids." In: *Journal of Physical Chemistry* 57.1, pp. 56–64. ISSN: 00223654. DOI: 10.1021/j150502a012.
- Chertkov, V. and Ravina, I. (2010). "Tortuosity of Crack Networks in Swelling Clay Soils." In: *Soil Science Society of America Journal* 63.6, p. 1523. DOI: 10.2136/sssaj1999.6361523x.
- Chiappone, A., Marelllo, S., Scavia, C., and Setti, M. (2005). "Clay mineral characterization through the methylene blue test: comparison with other experimental techniques and applications of the method." In: *Canadian Geotechnical Journal* 41.6, pp. 1168–1178. ISSN: 0008-3674. DOI: 10.1139/t04-060.
- Coduto, P., Yeung, R., and Kitch, A. (2011). *Geotechnical engineering: Principles and practices*. 2nd ed. Pearson. ISBN: 0131354256, 9780131354258.
- Cotecchia, F. (2018). "Composition, microstructure and state of consolidated clays." In: *ALERT Olek Zienkiewicz Winterschool 2018*. November.

- Cui, Y. J., Yahia-Aissa, M., and Delage, P. (2002). "A model for the volume change behaviour of heavily compacted swelling clays." In: *Engineering Geology* 64.2-3, pp. 233–250. issn: 00137952. doi: 10.1016/S0013-7952(01)00113-2.
- Dacus, B. (2009). "Facts about dredged material as a resource." In: *IADC* 1.
- De Beer, E. (1967). "Shear strength characteristics of the Boom clay." In: *Geotechnical conference Oslo*, pp. 83–88.
- De Craen, M., Swennen, R., and Keppens, E. (1998). "Petrography and geochemistry of septarian carbonate concretions from the Boom Clay Formation (Oligocene, Belgium)." In: *Geologie en Mijnbouw/Netherlands Journal of Geosciences* 77.1, pp. 63–76. issn: 00167746. doi: 10.1023/A:1003468328212.
- Dehandschutter, B., Vandycke, S., Sintubin, M., Vandenberghe, N., and Wouters, L. (2005). "Brittle fractures and ductile shear bands in argillaceous sediments: Inferences from Oligocene Boom Clay (Belgium)." In: *Journal of Structural Geology* 27.6, pp. 1095–1112. issn: 01918141. doi: 10.1016/j.jsg.2004.08.014.
- Delage, P. and Lefebvre, G. (1984). "Study of the structure of a sensitive Champlain clay and of its evolution during consolidation." In: *Canadian Geotechnical Journal* 21.1, pp. 21–35. doi: 10.1139/t84-003. URL: <http://www.nrcresearchpress.com/doi/10.1139/t84-003>.
- Della Vecchia, G., Jommi, C., Lima, A., and Romero, E. (2011). "Some remarks on the hydro-mechanical constitutive modelling of natural and compacted Boom clay." In: *Unsaturated Soils*, pp. 803–809. doi: 10.1201/b10526-124.
- Demoulin, A. (2018). *Landscapes and landforms of Belgium and Luxembourg*. 1st. Springer International Publishing AG, pp. 1–423.
- Department of the Army Washington (1999). "Field Manual No. 5-472: Material Testing."
- Dykstra, C. (2013). "Felixstowe Berth 9 Quay Extension – Use of Dredged Clay in Fill In-situ London Clay."
- Eastern Mediterranean University (2013). "Lec 9. Diffusive double layer." North Cyprus.
- EDEM (n.d.). *Webinar DEM*. URL: <https://register.gotowebinar.com/recording/recordingView?webinarKey=3862826633747878145&registrantEmail=amldortland%40gmail.com&recurrenceKey=2615735256756900609>.
- Editors of Freshwater inflows (n.d.). *Salinity*. URL: <https://www.freshwaterinflow.org/salinity>.
- Editors of Quantachrome (n.d.). *Features pycnometer*. URL: [http://www.quantachrome.com/density/autopycnometer\\_benefits.html](http://www.quantachrome.com/density/autopycnometer_benefits.html).
- Editors of Sandatlas (n.d.). *Conchoidal fracture*. URL: <https://www.sandatlas.org/conchoidal-fracture/>.
- Editors of the geological society (n.d.). *Compaction and Cementation*. URL: <https://www-geolsoc-org-uk.tudelft.idm.oclc.org/ks3/gsl/education/resources/rockcycle/page3559.html>.
- Elmashad, M. E. (2017). "Effect of chemical additives on consistency, infiltration rate and swelling characteristics of bentonite." In: *Water Science* 31.2, pp. 177–188. issn: 11104929. doi: 10.1016/j.wsj.2017.07.001. URL: <http://linkinghub.elsevier.com/retrieve/pii/S1110492916300558>.
- Encyclopaedia Britannica (2011). *Till*. URL: <https://www.britannica.com/science/till>.
- Fehmarn belt contractors (2017). "Fehmarn Ground investigations and GIS database."
- Fehmarn belt contractors (n.d.). *TDR Strategy for the use of dredged upper till*. Tech. rep.
- Foster, M. D. (1954). "The relation between composition and swelling in clays." In: *Clays and Clay Minerals* 3.1, pp. 205–220.
- Gimsing, J. and Iversen, C. (2001). *The Oresund technical publications - Dredging and Reclamation*. Tech. rep.
- Griffiths, D. V. and Fenton, G. A. (2001). "Bearing capacity of spatially random soil: the undrained clay Prandtl problem revisited." In: *Géotechnique* 51.4, pp. 351–359. issn: 0016-8505. doi: 10.1680/geot.51.4.351.39396. URL: <http://www.atypon-link.com/TELF/doi/abs/10.1680/geot.51.4.351.39396>.
- Groenendyk, D. G., Ferré, T. P., Thorp, K. R., and Rice, A. K. (2015). "Hydrologic-process-based soil texture classifications for improved visualization of landscape function." In: *PLOS ONE* 10.6. issn: 19326203. doi: 10.1371/journal.pone.0131299.
- Guggenheim, S. et al. (1995). "Definition of clay and clay mineral: Joint report of the AIPEA nomenclature and CMS nomenclature committees." In: *Clays and Clay Minerals* 43.2, pp. 255–256. issn: 15528367. doi: 10.1346/CCMN.1995.0430213.
- Haigh, S., Vardanega, P., and Bolton, M. (2013). "The plastic limit of clays." In: *Géotechnique* 63.6, pp. 435–440. doi: 10.1680/geot.11.P.123. URL: <http://www.icevirtuallibrary.com/doi/10.1680/geot.11.P.123>.

- Hartlen, J. and Ingers, C. (1981). "Land reclamation using fine-grained dredged material." In: *Proceedings of 10th International Conference on Soil Mechanics and Foundation Engineering, Stockholm 1*, pp. 145–148.
- Houmark-Nielsen, M. (1987). "Pleistocene Stratigraphy and Glacial History of the Central Part of Denmark." In: *Bull. geol. Soc. Denmark* 36, pp. 1–189. ISSN: 0362-2436. DOI: 10.1002/9781444317749.ch4.
- Huysmans, M. and Dassargues, A. (2006). "Hydrogeological modeling of radionuclide transport in low permeability media: A comparison between Boom Clay and Ypresian Clay." In: *Environmental Geology* 50.1, pp. 122–131. ISSN: 09430105. DOI: 10.1007/s00254-006-0191-7.
- IADC (2014a). "Facts about backhoe dredgers." In: 03. URL: <http://www.iadc-dredging.com/ul/cms/fck-uploaded/documents/PDF%20Facts%20About/facts-about-backhoe-dredgers.pdf>.
- IADC (2014b). "Facts about trailing suction hopper." In: 01. URL: <https://www2.iadc-dredging.com/wp-content/uploads/2016/07/facts-about-trailing-suction-hopper-dredgers.pdf>.
- IADC (n.d.). *Stiff clays*. URL: <https://www2.iadc-dredging.com/subject/dredging-terminology/stiff-clays>.
- Jessen, S. (2011). "Properties of Danish Clay Tills determined from laboratory testing." In: *Geotechnical Engineering: New Horizons*. URL: <http://www.kiviniirja.nl/eygec/papers/42%20DS%20Jessen.pdf>.
- Karthikeyan, M., Dasari, G. R., and Tan, T.-S. (2004). "In situ characterization of land reclaimed using big clay lumps." In: *Canadian Geotechnical Journal* 41.2, pp. 242–256. ISSN: 00083674. DOI: 10.1139/t03-087. URL: <http://www.nrcresearchpress.com/libproxy1.nus.edu.sg/doi/abs/10.1139/t03-087>.
- Ketterings, Q., Reid, S., and Rao, R. (2007). "Cation Exchange Capacity (CEC) Fact Sheet Series."
- Khattak, O. (n.d.). *What is a fracture?* URL: <http://geologylearn.blogspot.com/2015/08/types-of-fractures.html>.
- Kostkanová, V., Herle, I., and Bohác, J. (2014). "Transitions in Structure of Clay Fills due to Suction Oscillations." In: *Procedia Earth and Planetary Science* 9, pp. 153–162. ISSN: 18785220. DOI: 10.1016/j.proeps.2014.06.011. URL: <http://www.sciencedirect.com/science/article/pii/S187852201400040X>.
- Krogsbøll, A., Hededal, O., and Foged, N. (2012). "Deformation properties of highly plastic fissured Palaeogene clay – Lack of stress memory ?" In: *NGM Proceedings*, pp. 133–140.
- Kruse, G. (1985). *Kleigrond voor de bekleding van dijken: opmerkingen over het zwellen en krimpen en het ontwikkelen van structuur*. Tech. rep. COW, pp. 2–84.
- Lambe, T. (1958). "The structure of compacted clay." In: *ASCE* 84, pp. 1–35.
- Lambooy, A. M. (1984). "Relationship between cation exchange capacity, clay content and water retention of highveld soils." In: *South African Journal of Plant and Soil* 1.2, pp. 33–38. ISSN: 02571862. DOI: 10.1080/02571862.1984.10634106.
- Lancelotta, R. (2009). *Geotechnical Engineering*. Abingdon: Taylor & Francis, pp. 172–173.
- Leung, C. F., Wang, J. C., Manivanann, R., and Tan, S. A. (2001). "Experimental Evaluation of Consolidation Behavior of Stiff Clay Lumps in Reclamation Fill." In: *Geotechnical Testing Journal* 24.2, pp. 145–156. ISSN: 01496115. DOI: 10.1520/GTJ11334J.
- Li, X. (2013). "TIMODAZ: A successful international cooperation project to investigate the thermal impact on the EDZ around a radioactive waste disposal in clay host rocks." In: *Journal of Rock Mechanics and Geotechnical Engineering* 5.3, pp. 231–242. ISSN: 16747755. DOI: 10.1016/j.jrmge.2013.05.003. URL: <http://dx.doi.org/10.1016/j.jrmge.2013.05.003>.
- Lima, A. (2011). "Thermo-Hydro-Mechanical behaviour of two deep belgian clay formations: Boomand Ypresian clays." Doctoral dissertation. Politechnica de catalunya, pp. 1–253.
- Ltifi, M., Abichou, T., and Tisot, J. P. (2014). "Effects of Soil Aging on Mechanical and Hydraulic Properties of a Silty Soil." In: *Geotechnical and Geological Engineering* 32.4, pp. 1101–1108. ISSN: 09603182. DOI: 10.1007/s10706-014-9784-1.
- Manivanann, R., Leung, C., and Tan, S. (2000). "Analysis of lumpy fill." In: *Coastal Geotechnical Engineering in Practice*, p. 21.
- Manual of soil laboratory testing (1966). "Chapter 22: Hydraulic cell consolidation and permeability tests."
- Martinelli, M. (2016a). *Anura3D MPM software: scientific manual*. Tech. rep. May.
- Martinelli, M. (2016b). "Anura3D MPM software: tutorial manual." In: May.

- Mertens, J., Vandenberghe, N., Wouters, L., and Sintubin, M. (2003). "The origin and development of joints in the Boom Clay Formation (Rupelian) in Belgium." In: *Geological Society, London, Special Publications* 216.1, pp. 309–321. issn: 0305-8719. doi: 10.1144/GSL.SP.2003.216.01.20. URL: <http://sp.lyellcollection.org/lookup/doi/10.1144/GSL.SP.2003.216.01.20>.
- Mitchell, J. (2001). *Selected papers of James. K Mitchell (The fabric of natural clays and it's relation to engineering properties)*. ASCE, pp. 1–21.
- Moon, C. F. (1972). "The microstructure of clay sediments." In: *Earth Science Reviews* 8.3, pp. 303–321. issn: 00128252. doi: 10.1016/0012-8252(72)90112-2.
- Nelson, S. (2014). *Weathering and clay minerals*. URL: <https://www.tulane.edu/~sanelson/eens211/weathering&clayminerals.htm>.
- Nguyen, V. P. (2014). "Material point method: basics and applications." In: May, p. 207. issn: 0022-1899.
- Nishimura, S. (2005). "Laboratory study on anisotropy of natural London clay." Doctoral dissertation.
- Norbury, D. (n.d.). "Field description of soils in accordance with BS5930:2015." In: issn: 0028-0836. doi: 10.1038/155639c0.
- Ott, P. (2017). *Experimental Research of Consolidation Behavior of Stiff Clay Lumps and Hydraulic Mixture of sand and seawater in reclamation fill*. Tech. rep. URL: [https://lib.ugent.be/fulltxt/RUG01/002/367/311/RUG01-002367311\\_2017\\_0001\\_AC.pdf](https://lib.ugent.be/fulltxt/RUG01/002/367/311/RUG01-002367311_2017_0001_AC.pdf).
- Paassen, V., L.A., and Gareau, L. (2004). *Effect of pore fluid salinity on compressibility and shear strength development of clayey soils*. Berlin: Springer-Verlag, pp. 327–340. isbn: 9783540399186. doi: 10.1007/978-3-540-39918-6.
- PIANC (2014). *Classification of Soils and Rocks for the Maritime Dredging Process N144*. Tech. rep.
- Picarelli, L., Urciuoli, G., Mandolini, A., and Ramondini, M. (2006). "Softening and instability of natural slopes in highly fissured plastic clay shales." In: *Natural Hazards and Earth System Sciences* 6.4, pp. 529–539. issn: 15618633. doi: 10.5194/nhess-6-529-2006.
- Piriyakul, K. and Haegeman, W. (2009). "Stiffness anisotropy of Boom clay Rigidité anisotrope de l' argile de Boom." In: *Geotechnical Engineering*, pp. 167–170. doi: 10.3233/978-1-60750-031-5-167.
- Plaxis (2014). "Material Models Manual - Plaxis." In:
- Plaxis (n.d.). *Barcelona Basic model*. URL: <https://www.plaxis.com/support/models/udsm-barcelona-basic-model/>.
- Pluijn, B. van der and Marshak, S. (n.d.). *Macroscopic Aspects of Rheology*. URL: [http://www.geosci.usyd.edu.au/users/prey/ACSGT/EReports/eR.2003/GroupE/Report1/joint\\_morphology.html](http://www.geosci.usyd.edu.au/users/prey/ACSGT/EReports/eR.2003/GroupE/Report1/joint_morphology.html).
- Quantachrome (2016). "Gas Pycnometers." In:
- Ramboll (2013). *GDR 01.3-002 Summary of geological conditions*. Tech. rep. July. Femern Sand Baelt, pp. 1–91.
- Rambøll Arup Joint Venture (2011). "Geotechnical properties for Glacial deposits." In: May.
- Rao, S. e. a. (2013). "Crystalline and Osmotic Swelling of an Expansive Clay Inundated with Sodium Chloride Solutions." In: pp. 1399–1404. doi: 10.1007/s10706-013-9629-3.
- Reddy, K. (n.d.). "Specific gravity determination."
- Rijkers, R., Klaver, G., Lang, F. de, and Lange, G. de (1998). "Het effect van een vries-dooi cyclus op het mechanisch gedrag van de Klei van Boom bij de Westerscheldetunnel." URL: <http://cob.teamspace.nl/Gedeelde%20documenten/GKO-035.CT.09.A.pdf>.
- Robinson, R. G., Dasari, G. R., and Tan, T. S. (2004). "Three-dimensional swelling of clay lumps." In: *Géotechnique* 54.1, pp. 29–39. issn: 00168505. doi: 10.1680/geot.2004.54.1.29.
- Rogers, D. (n.d.). "Some engineering aspects of expansive soils."
- Santamarina, J. and Shin, H. (2009). "Discontinuities in granular materials: Particle-level mechanisms." In: *Mechanics of Natural solids*, pp. 223–238. doi: 10.1007/978-3-642-03578-4\_{\\_}10..
- Savage, P. F. (2007). "Evaluation of Possible Swelling Potential of Soil." In: *26th Southern African Transport Conference*. July, pp. 277–283. isbn: 192001702X.
- Schittekat, J. (2001). "Engineering geology of the Boom clay in the Antwerp area." In: *Screw Piles - Installation and design in stiff clay*. Lisse: ZEITLINGER, SWETS &, pp. 11–16. isbn: 9058091929.
- Shaw, R. (2010). "Review of Boom Clay and Opalinus Clay parameters. FORGE Report D4.6 - Ver 1.0." In: August.
- Skempton, A. W. and Northey, R. D. (1952). "The Sensitivity of Clays." In: *Géotechnique* 3.1, pp. 30–53. issn: 0016-8505. doi: 10.1680/geot.1952.3.1.30. URL: <http://www.icevirtuallibrary.com/doi/10.1680/geot.1952.3.1.30>.

- Skempton, A. W. (1977). "Slope Stability of Cuttings in Brown London Clay." In: *Proceeding of the 9th International Conference on Soil Mechanics and Foundation Engineering* 3, pp. 261–270. ISSN: 00130117. doi: 10.1680/sposm.02050.0021.
- Skempton, A. W., Schuster, R., and Petley, D. (1969). "Joints and Fissures in The London Clay at Wraysbury and Edgware." In: *Géotechnique* 20.2, pp. 208–209. ISSN: 0016-8505. doi: 10.1680/geot.1970.20.2.208. URL: <http://www.icevirtuallibrary.com/doi/10.1680/geot.1970.20.2.208>.
- Sorensen, K. K. and Okkels, N. (2013). "Correlation between drained shear strength and plasticity index of undisturbed overconsolidated clays." In: *Proceedings of the 18th International Conference on Soil Mechanics and Geotechnical Engineering*, pp. 423–428.
- Standing, J. R. (2018). "Identification and implications of the London Clay Formation divisions from an engineering perspective." In: *Proceedings of the Geologists' Association*. ISSN: 00167878. doi: 10.1016/j.pgeola.2018.08.007. URL: <https://doi.org/10.1016/j.pgeola.2018.08.007>.
- Strozyk, J. and Tankiewicz, M. (2013). "Undrained shear strength of the heavily consolidated clay." In: *Land reclamation* 45.45, pp. 207–216.
- Tate Boyce D; Larew, H. (n.d.). "Effect of Structure on Resilient Rebound Characteristic of Soils in The Piedmont Province of Virginia." In: *Stress distribution in Earth Masses*, pp. 97–111.
- Taylor, R. K. and Smith, T. J. (1986). "The engineering geology of clay minerals: swelling, shrinking and midrock breakdown." In: *Clay minerals in Engineering Geology - The geotechnical properties of clays*. 21, pp. 235–260.
- Terzaghi, K. (1936). "Stability of slopes of natural clay." In: *Proc. 1st. Int. Conf. Soil Mech. Found. Eng.* Cambridge, pp. 156–161.
- The Editors of Encyclopaedia Britannica (n.d.[a]). *Joint*. URL: <https://www.britannica.com/science/joint-geology>.
- The Editors of Encyclopaedia Britannica (n.d.[b]). *Weathering*. URL: <https://www.britannica.com/science/weathering-geology>.
- The editors of Encyclopaedia Britannica (n.d.[a]). *Cementation*. URL: <https://www.britannica.com/science/cementation-sedimentary-rock>.
- The editors of Encyclopaedia Britannica (n.d.[b]). *Fault*. URL: <https://www.britannica.com/science/fault-geology#ref93077>.
- Toth, D. J. (1975). "Movement and Time Limits of Existence1." In: 20.September.
- Totten, M. W., Hanan, M. A., Knight, D., and Borges, J. (2002). "Characteristics of mixed-layer smectite/illite density separates during burial diagenesis." In: *American Mineralogist* 87.11-12, pp. 1571–1579. ISSN: 0003004X. doi: 10.2138/am-2002-11-1207.
- Van Impe, W. and Flores, R. (2007). *Underwater embankments on soft soils*. London: Taylor and Francis, p. 78.
- Vandenbergh, N., De Craen, M., and Wouters, L. (2014). "The Boom Clay Geology from sedimentation to present-day occurrence - a review." In: *Memoirs of the Geological Survey of Belgium* 60, p. 76.
- Vandenbergh, N., Laenen, B., Van Echelpoel, E., and Lagrou, D. (1997). "Cyclostratigraphy and climatic eustasy. Example of the Rupelian stratotype." In: *Comptes Rendus de l'Academie de Sciences - Serie IIa: Sciences de la Terre et des Planetes* 325.5, pp. 305–315. ISSN: 12518050. doi: 10.1016/S1251-8050(97)81377-8.
- Vanicek, I. and Vanicek, M. (2008). *Earth structures in transport, water and environmental engineering*. Springer. ISBN: 9781402039638.
- Vardon, P. (2019). *CIE4366: The material point method (MPM)*. Tech. rep. University of Technology Delft, pp. 1–53.
- Verhoef, P. N. W. (1992). "The Methylene Blue adsorption test applied to geomaterials." In: 101, p. 83. URL: <http://publicaties.minienm.nl/documenten/the-methylene-blue-adsorption-test-applied-to-geomaterials>.
- Verruijt, A. (2013). "Theory and problems of poroelasticity." In: *Delft University of Technology, The Netherlands ISBN: 0071430997*.
- VOUB (2010). "Advanced training hydraulic engineering works: Dredging works."
- Waltham, A. (2002). *Foundations of engineering geology*. 2nd. CRC Press, p. 52. ISBN: 0415254493.
- Wang, G. and Wei, X. (2015). "Modeling swelling–shrinkage behavior of compacted expansive soils during wetting–drying cycles." In: *Canadian Geotechnical Journal* 52.6, pp. 783–794. ISSN: 0008-3674. doi: 10.1139/cgj-2014-0059. URL: <http://www.nrcresearchpress.com/doi/10.1139/cgj-2014-0059>.
- Whitman, R. V. (1970). "Hydraulic fills to support structural loads." In: *Journal of the soil mechanics and foundations division SM 1*, pp. 23–47.
- Wikipedia, E. o. (n.d.). *Dilatancy*. URL: [https://en.wikipedia.org/wiki/Dilatancy\\_\(granular\\_material\)](https://en.wikipedia.org/wiki/Dilatancy_(granular_material)).

- Yang, L. A. and Tan, T. S. (2005). "One-dimensional consolidation of lumpy clay with non-linear properties.pdf." In: *Geotechnique* 55.3, pp. 227–235.
- Yang, L. A., Tan, T. S., Tan, S. A., and Leung, C. F. (2002). "One-dimensional self-weight consolidation of a lumpy clay fill." In: *Géotechnique* 52.10, pp. 713–725. issn: 0016-8505. doi: 10.1680/geot.2002.52.10.713. URL: <http://eprints.soton.ac.uk/75799/>.
- Yong, R., Pusch, R., and Nakano, M. (2010). *Containment of High-level radioactive and hazardous solid wastes with clay barriers*. Spon Press, p. 169.
- Zimbone, S. M., Vickers, A., Morgan, R. P., and Vella, P. (1996). "Field investigations of different techniques for measuring surface soil shear strength." In: *Soil Technology* 9.1-2, pp. 101–111. issn: 09333630. doi: 10.1016/0933-3630(96)00002-5.

# V

## Appendices



# A

## Geotechnical vocabulary

### Overconsolidation

Stiff clays are often overconsolidated, which means that the material has experienced higher stresses in the past than its current overburden stress.

### Atterberg's limits

Atterberg described the behaviour of cohesive soils qualitatively at varying water contents by the liquid limit and plastic limit. The liquid limit relates to soil strength, and the plastic limit relates to the capillary suction at which the soil starts to form cracks. The liquid limit is based on the number of blows which are required to cause a groove in a clay bed. The plastic limit is found by rolling the clay into wires; the clay is at its plastic limit when it begins to crumble or when it is rolled to a diameter of 3mm. The plastic and liquid limit both need to be determined from a remoulded soil. The observation of an approximately hundredfold increase in strength between the liquid limit and plastic limit is often used but incorrect. For this reason, the assumption of fixed shear strength at the plastic limit is invalid (Haigh et al., 2013). Burmister (1949) made a classification of the plasticity index as presented in table A.1. The plasticity index  $I_p$  or  $PI$  is defined by equation A.1, in which  $W_l$  is the liquid limit and  $W_p$  is the plastic limit.

$$I_p = W_l - W_p \quad (\text{A.1})$$

The liquidity index is defined by:

$$LI = \frac{w - W_p}{W_l - W_p} \quad (\text{A.2})$$

| PI    | Description          |
|-------|----------------------|
| 0     | Nonplastic           |
| 1-5   | Slightly plastic     |
| 5-10  | Low plasticity       |
| 10-20 | Medium plasticity    |
| 20-40 | High plasticity      |
| >40   | Very high plasticity |

Figure A.1: Classification of PI (Burmister, 1949).

### Undrained shear strength

The undrained shear strength ( $S_u$ ) is one of the most important parameters to characterize clayey soils. It is usually determined by triaxial compression tests or unconfined compression tests. In heavily overconsolidated clays there is no correlation present between  $S_u$  and Atterbergs limits while this is present for normally consolidated clays. Strozyk and Tankiewicz (2013) performed several tests on overconsolidated clays and observed that some soil samples with a plasticity index smaller than 30 lost their intact structure and original undrained shear strength due to decompression. This is probably caused by mechanical swell, see section 2.1.6.

### Activity

The activity of clay can be expressed by the plasticity index and the % clay content (Waltham, 2002). A material with an activity  $< 0.75$  is considered as in-active, between 0.75 and 1.25 is neutral and an activity  $> 1.25$  is active material. High activity index signifies high volume changes.

$$A = \frac{PI}{\%claysizeparticles} \quad (A.3)$$

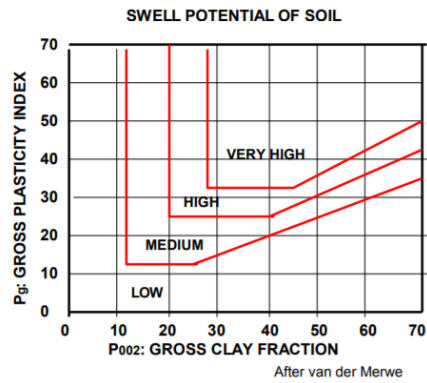


Figure A.2: Swell potential based on gross clay fraction and plasticity index (Savage, 2007).

# B

## Index tests

### Water content

The water content of the sample is determined by the oven drying method according to the BS 1377-2:1990 standard. In situ material is dried overnight in an oven of 107°C. Afterwards the water content of the specimen as a percentage of its dry mass can be calculated (British standards institution, 1990).

| Water content     |        |        |
|-------------------|--------|--------|
|                   | Test 1 | Test 2 |
| Water content (%) | 28.2   | 28.6   |

Table B.1: In situ water content of a Boom clay sample determined by the oven drying method

### Liquid limit test

The liquid limit is the moisture content at which soil passes from the liquid state to the plastic state and can be established empirically (British standards institution, 1990). The test is performed with the Casagrande apparatus as described in the BS-1377-2:1990 standard.

The measurements of the Casagrande test are shown in table B.2. The liquid limit is the water content at 25 drops of the Casagrande. The measurements are plotted in figure B.1. A trendline is plotted through the measurements from which a liquid limit of 79.0 results. The results of the liquid limit test can be checked by the correlation of the number of blows and the water content, as shown in figure B.2. The liquid limit test is performed correctly provided that  $R^2 > 0.95$  as presented in figure B.2. Lars Rook also performed a liquid limit test by the falling cone apparatus, which resulted in a liquid limit of 81.8%.

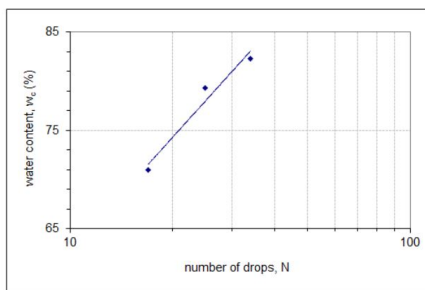


Figure B.1: Plot of the Casagrande test results on a Boom clay sample. The liquid limit is the water content at 25 blows. The water content at 25 blows on the trendline is 79.0

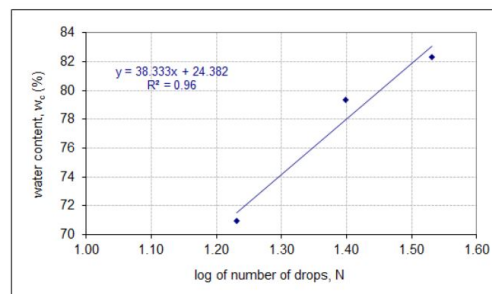


Figure B.2: Check of Casagrande test data on a Boom clay sample. The test is performed correct in case a strong correlation between the measurements is present, shown by  $R^2 > 0.95$

| Liquid limit test |        |        |        |
|-------------------|--------|--------|--------|
|                   | Test 1 | Test 2 | Test 3 |
| Number of drops   | 17     | 25     | 34     |
| Log (N)           | 1.23   | 1.40   | 1.53   |
| Water content (%) | 71.0   | 79.3   | 82.3   |

Table B.2: Measurements of the liquid limit test obtained by the Casagrande method on a Boom clay sample

#### Plastic limit test

The empirically established moisture content at which the soil becomes to dry is the plastic limit. The plastic rolling method is performed according to the BS 1377-2:1990 standard, after which the water content can be determined. The clay material used in this test is prepared following the RAW standard.

| Plastic limit test |        |        |        |
|--------------------|--------|--------|--------|
|                    | Test 1 | Test 2 | Test 3 |
| Plastic limit (-)  | 27.1   | 28.1   | 27.8*  |

Table B.3: Results of the plastic limit test determined by the rolling method on a Boom clay sample. \*Test result of plastic limit test of a Boom clay sample performed by Lars Rook

The boom clay sample can be described as a very highly plastic clay as its plasticity index is larger than 40 (Burmister, 1949), but it is important to keep in mind that the results of the Atterberg tests are subject to the judgement of the operator. The plastic limit results correspond with the literature as presented in table 2.1. Therefore, it can be concluded that the test is performed correctly. De Beer (1967) stated that the natural water content is nearly equal to the plastic limit, this corresponds well to the measurements on the sample.

#### Undrained shear strength

The in situ undrained shear strength is determined by the pocket penetrometer and the torvane. The pocket penetrometer measures the vertical strain. Subsequently, the undrained shear strength can be determined by dividing the reading value by two (Blum, 1997). The torvane is a testing instrument for the determination of shear strength in cohesive soils. For stiff soils the smallest size (CL102) should be used after which the shear strength is determined by a correlation method. The correlation method relates the torsional applied force to one complete revolution, which corresponds to a shear strength of 273.4 kPa.

The undrained shear strength is generally overestimated by the pocket penetrometer as it generates both compressive and shear type failure simultaneously (Zimbone et al., 1996). Contrarily the torvane generally underestimates the shear strength as it applies a shear strength to a thin layer (Zimbone et al., 1996). Consequently, the most realistic undrained shear strength based on the tests is the average of the two tests, i.e. a value of 110 kPa. The undrained shear strength of 110 kPa is conform to the results of De Beer (1967), as presented in figure 2.18.

| Pocket penetrometer |            | Torvane |            |
|---------------------|------------|---------|------------|
| Reading             | $S_u(kPa)$ | Reading | $S_u(kPa)$ |
| 2.8                 | 137.3      | 3.0     | 82.1       |
| 2.5                 | 122.6      | 2.5     | 68.4       |
| 3.55                | 174.1      | 3.1     | 84.8       |
| 2.1                 | 103.0      | 2.8     | 76.5       |
| 3                   | 147.1      | 3.6     | 98.4       |
| 3                   | 147.1      | 3.2     | 87.5       |
| 2.7                 | 132.4      | 3.9     | 106.6      |
| 3.25                | 159.4      | 2.9     | 79.3       |

Table B.4: Undrained shear strength data of Boom clay sample.

| Pycnometer test      |                  |                |
|----------------------|------------------|----------------|
|                      | Basic pycnometer | Gas pycnometer |
| Specific gravity (-) | 2.642            | 2.741          |
|                      | 2.645            | 2.724          |

Table B.5: Specific gravity test results by a basic pycnometer and gas pycnometer on a Boom clay sample

### Specific gravity

The specific gravity describes the unit mass of a material compared to the unit mass of water and can be determined by a basic pycnometer or by a gas pycnometer. The specific gravity can be determined by the specific density of the material and water as expressed in equation B.1.

$$G_s = \frac{\rho_s}{\rho_w} \quad (\text{B.1})$$

- The specific gravity determined by a basic pycnometer is the ratio of mass per unit volume to the mass of the same volume of gas-free distilled water both at a stated temperature (Reddy, n.d.). It is determined by a basic pycnometer according to the ASTM D 854-00 standard. The entrapped air is removed by applying a partial vacuum. According to the standard, applying a partial vacuum for 10 minutes should be sufficient. During the test it was observed that air was still present after 15 minutes. Therefore, a partial vacuum was applied for 4 hours to remove the entrapped air.
- More accurate and reproducible results can be obtained by a gas pycnometer. The principle of operation is based on gas displacement to measure volume. Helium is pressurized to a target pressure in a sealed sample chamber of known volume. Once the pressure is stabilized its value is recorded and a valve is opened. Afterwards, the gas is transferred to a reference chamber. The gas expands in the reference chamber and its pressure is recorded after stabilization. The pressure drop between the chambers is compared to the behaviour of the system when a known volume underwent the same process. Accordingly, the specific density can be determined (Quantachrome, 2016). It can be chosen to operate by a continuous flow or by pulse flow (Editors of Quantachrome, n.d.). The gas pycnometer provides the specific density in (g/cc), so that after division by the specific density of water the specific gravity results.

The specific gravity of quartz particles range between 2.65 – 2.67 (Department of the Army Washington, 1999) and clay minerals span a wide range from 2.0 for smectites to 3.3 for chlorites (Totten et al., 2002). The specific gravity of inorganic clay generally ranges between 2.7 – 2.8 (Department of the Army Washington, 1999), and depend on the clay mineralogy and clay content.

The value of 2.64 determined by the basic pycnometer is not realistic for a clayey material. Errors probably result from the presence of air due to an uncomplete vacuum whereas, the result of the gas pycnometer,  $G_s = 2.724$  is more in accordance with the literature values. The literature value of the Boom clay ranges from 2.7 – 2.73 (Andersland and Landanyi, 2004), and can differ per location. The result of the gas pycnometer corresponds well to the literature value.

### Grain size distribution

The grain size distribution is determined by a hydrometer test in accordance with BS 1377: Part 2: 1990 at a room temperature of 23°C. It is important that the dry material is as fine as possible before mixing with the dispersant solution. Grinding by a mortar is a time consuming but efficient method to obtain a clay powder. The permeability of the material is very low and therefore the dispersant solution will not reach all aggregates if the material is not well grinded. The standard dispersant solution is formed by a solution of 33 g sodium hexametaphosphate and 7 g sodium carbonate per liter distilled water.

Figure B.3 shows the result of the hydrometer and sieving test, the material can be identified as fine-grained soil with a high clay content of 61.4%.

A relative large offset between the grain size of 57  $\mu\text{m}$  and 63  $\mu\text{m}$  is present in figure B.3. The large offset can be described to measuring errors, small inevitable inaccuracies in the testing procedure, and temperature fluctuations. Small inaccuracies in the testing procedure can result in loss of material. For instance, a small amount of the material is lost during the mixing and sieving process.

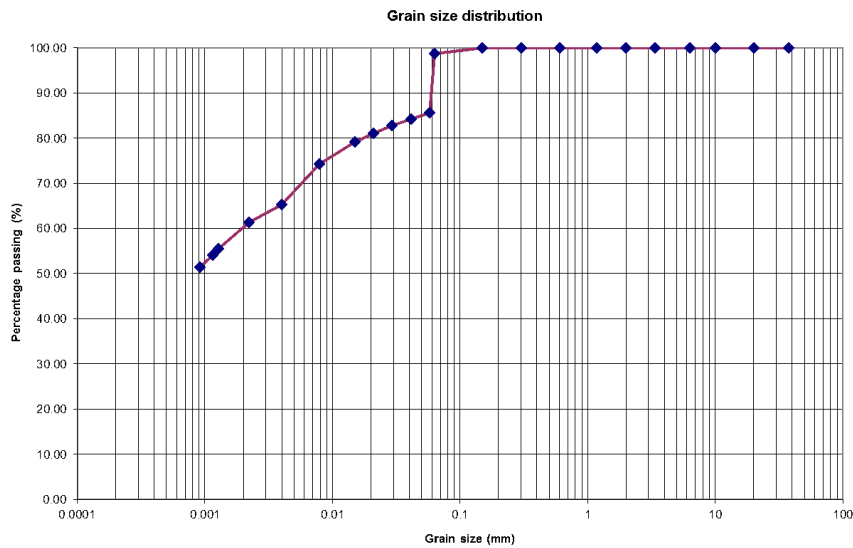


Figure B.3: Grain size distribution curve

### Methylene blue test

The methylene blue test is used to quantify the presence of swelling clay minerals. It gives a semi quantitative indication of the activity of a material (Chiappone et al., 2005). Some other substances may also absorb methylene blue, though this can be identified by a X-ray diffraction technique to identify the true nature of the absorbing substance (Verhoef, 1992).

Methylene blue ( $C_{16}H_{18}N_3ClS$ ) is an organic molecule built up of benzene rings. The structural formula is formed by a negatively charged  $Cl^-$  and a large positively charged ion. Addition of methylene blue to a watery clay mixture results in an exchange of the positive ions of the diffuse-ion-layer by the positive methylene blue ion. This process continues until all positive ions have been expelled and from then on methylene blue will stay in the solution. The absorbed methylene blue by the clay minerals corresponds to the total coverage of the surface areas of the clay minerals (Verhoef, 1992).

Titration of methylene blue by the 'spot method' is a titration technique to determine the methylene blue adsorption value (MBA). A methylene blue solution with a concentration of 3.20 g/L is added to the watery clay mixture in successive volumes of 0.5 ml. The flask is agitated for 1 minute after every addition. Afterwards, a drop of the dispersion is placed on filter paper by a glass rod. A light blue halo forms around the edge of the circle when the adsorption point is reached (Verhoef, 1992).

The test is performed in duplo in view of measuring uncertainties. The values used in the following calculation are based on the average of those two tests. The methylene blue adsorption value is determined by:

$$MBA = \frac{(X/Y) * p}{(A/100)} = \frac{(3.2/1000) * 5.75}{(0.50125/100)} = 3.67; \quad [g\%] \quad (B.2)$$

It is preferred to express the MBA in milliequivalents absorbed per 100 grams of sample material.

$$M_f = \frac{(100 * n * p)}{A} = \frac{(100 * 0.010027 * 5.75)}{0.50125} = 11.51; \quad [meq/100g] \quad (B.3)$$

In which X = weight of dried methylene blue crystals (g), Y = volume of diluted methylene blue solution (ml), p = volume of methylene blue solution added (ml), A = weight of dry soil powder (gr) and n = normality of the MB solution (meq/l).

The activity of the soil can be determined by an activity index based MBA and the clay fraction (61.4% < 2 $\mu$ m) (Verhoef, 1992):

$$A_{CB} = \frac{100 * MBA}{clayfraction} = \frac{100 * 3.67}{61.4} = 5.98; \quad [-] \quad (B.4)$$

The soil is identified as normal active based on the classification presented in figure B.5.

| Clay mineral    | range MBA [g/100g] | range $M_t$ (CEC) [meq/100g] |
|-----------------|--------------------|------------------------------|
| Kaolinite       | 2 - 5              | 5 - 15                       |
| Illite          | 5 - 15             | 20 - 40                      |
| Montmorillonite | 15 - 40            | 40 - 100                     |

Figure B.4: Typical range of adsorption values for the common clay minerals (Verhoef, 1992).

| CLASS                   | $A_{CB}$ |
|-------------------------|----------|
| 1. Non-clay soil        | < 1      |
| 2. Inactive soil        | 1 - 3    |
| 3. Slightly active soil | 3 - 5    |
| 4. Normal soil          | 5 - 8    |
| 5. Active soil          | 8 - 13   |
| 6. Very active soil     | 13 - 18  |
| 7. Noxious soil         | > 18     |

Figure B.5: Activity index classes (Verhoef, 1992).

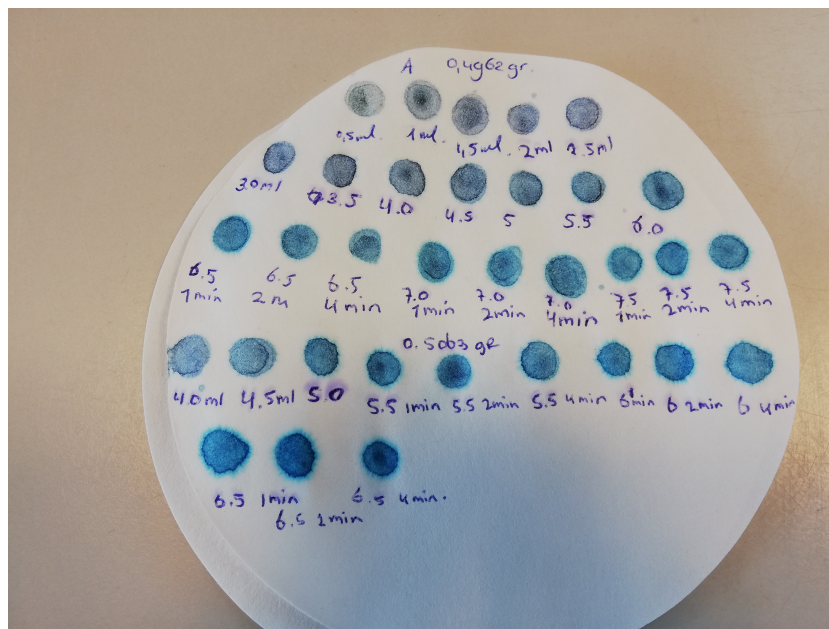


Figure B.6: Results of methylene blue tests on filter paper.



# C

## Diffusion script

Matlab script

```
%% Matlab diffusion code (based on heat equation)
% Anne-Martine Dortland
%% Input
L = 60; %length in m
n = 100; %number of simulation nodes
phi_0 = 0.5; % [kg/m^3], initial density of diffusing material
phi_1s = 35; % [kg/m^3], initial density of salt water at the top
phi_2s = 35; % [kg/m^3],

d=3*10^-9; % [m^2/s], diffusion coefficient of the species in fluid.
r = (30*10^-10)/2; % [m], size of water molecule + chloride
rp = (40*10^-10)/2; % [m], size of micropore
%tau_micro = (1-(r/rp)^2)*(1-2.10*(r/rp)+2.09*(r/rp)^3 -0.95*(r/rp)^5);
tau= 1.7 ; % [-], tortuosity
por= 0.33; % [-], porosity
%por_micro= 0.05;
Sw = 0.95; % [-], Degree of saturation of mesopores
%Sw_micro = 1;

D= d*(1/tau)*(por*Sw); % [m^2/s], Diffusion coefficient.
%% Numerical loop
dy = L/n; % m, node thickness
yr = 24*3600*365; % s, nr of seconds in 1 year
t_final = yr*80000; % s, simulation time
dt = 100000; % s, fixed time step

y = dy/2:dy:L-dy/2; % node centre locations
phi = ones(n,1)*phi_0; % make vector and fill with initial density
dphidt = zeros(n,1); % density derivative
t = 0:dt:t_final; % vector for time steps

for j = 1:length(t)
    for i = 2:n-1
        dphidt(i) = D * (-(phi(i)-phi(i-1))/dy^2 + (phi(i+1)-phi(i))/dy^2);
    end
    dphidt(1) = D * (-(phi(1)- phi_1s)/dy^2 + (phi(2)-phi(1))/dy^2);
    dphidt(end) = D * (-(phi(n)-phi(n-1))/dy^2 + (phi_2s-phi(n))/dy^2);
    phi = phi + dphidt*dt;
end
```

```
end
%% Plotting
figure(1) ;
plot(phi,y, 'Linewidth', 3)
axis([0.4 40 0 0.5*L])
xlabel('Salt density (kg/m^3)')
ylabel('Depth (m)')
set(gca, 'Ydir', 'reverse')
```

# D

## Fehmarn Project

### D.1. Project overview

The Fehmarnbelt fixed link is a planned tunnel to be built between Germany and Denmark and will connect the Fehmarn and Lolland-Falster lands. A combined road and railway tunnel of 18 km will be built, which will be the world longest immersed tunnel. Immersed tunnels avoid long-term disturbance of the aquatic environment. To place the immersed tunnel elements a trench needs to be dredged in the seabed. Consequently, 19 million  $m^3$  of sediments will be produced (Bjornshave et al., 2018). The reclamation landscapes will be built at the Danish side and a streamlined area along the existing coast will be shaped at the Danish side. Figure D.3 gives an impression of the design proposal at the Danish side (Bjornshave et al., 2018).

This dredged surplus material can be used for land reclamation which brings new natural, environmental and recreational values to the area. Care must be taken during the dredging and reclamation process to minimize the sediment spill. The Palaeogene clay and Upper glacial till are both stiff clays, which potentially could be re-used within a reclamation. For this reason, more in depth knowledge of those materials is required.



Figure D.1: Location of the Fehmarnbelt tunnel (Bjornshave et al., 2018).

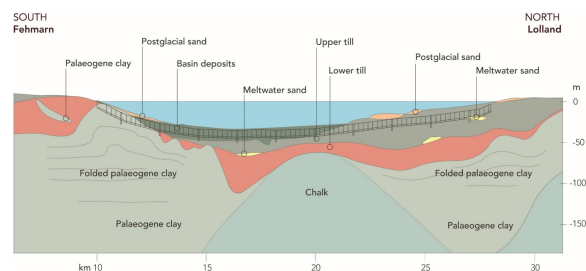


Figure D.2: Planned tunnel trajectory (Fehmarn belt contractors, 2017).



Figure D.3: Conceptual impression of the reclaimed land at the Danish side (Bjornshave et al., 2018).

## D.2. Geology

More insight in the geological history of the Palaeogene clay and Glacial clay till is necessary. Such that to their geotechnical properties and their mechanical behaviour after dredging is understood. A clear distinction between the term "deposit" and "unit" is made in this report. The term "deposit" is always used when a single geological body is described, while a "unit" describes multiple deposits with one name. As an example: A Palaeogene clay unit consists out of several deposits.

Local geology Fehmarnbelt Several geological groups were identified as in figure D.4 based on different testing technique such as classification testing, in situ testing, geotechnical testing and geophysical borehole (Rambøll Arup Joint Venture, 2011). Four different groups can be distinguished, listed from youngest (top) to oldest (bottom):

- Postglacial/Lateglacial deposits
  - Postglacial marine sand deposit
  - Postglacial marine gyttja deposit
  - Postglacial/Lateglacial marine and freshwater clay/silt deposits
  - Lateglacial meltwater and/or freshwater sand/gravel deposits
  - Transitional layer
- Glacial units
  - Upper till unit
  - Meltwater sand deposits
  - Lower till unit
- Palaeogene unit
  - Aebelo until Lillebaelt deposits present at Fehmarn belt ref Appendix XX
- Chalk deposit

The North European mid-latitude lowlands, figure D.5, endured several glaciations during the Pleistocene. Denmark is located within this area, glaciers originating from the Scandinavian highlands invaded the country from different directions (figure D.5). Mixing of sediments by the glacier led to the successive deposition of tills and outwash, occasionally interbedded with interglacial deposits (Houmark-Nielsen, 1987). The water broke through in the Holocene (8305 B.C), the Baltic Lake was connected to the sea, resulting in the Baltic Sea (Rambøll, 2013). All units deposited before the Holocene were deposited during freshwater conditions, hence glacial till and Palaeogene are deposited during a freshwater regime.

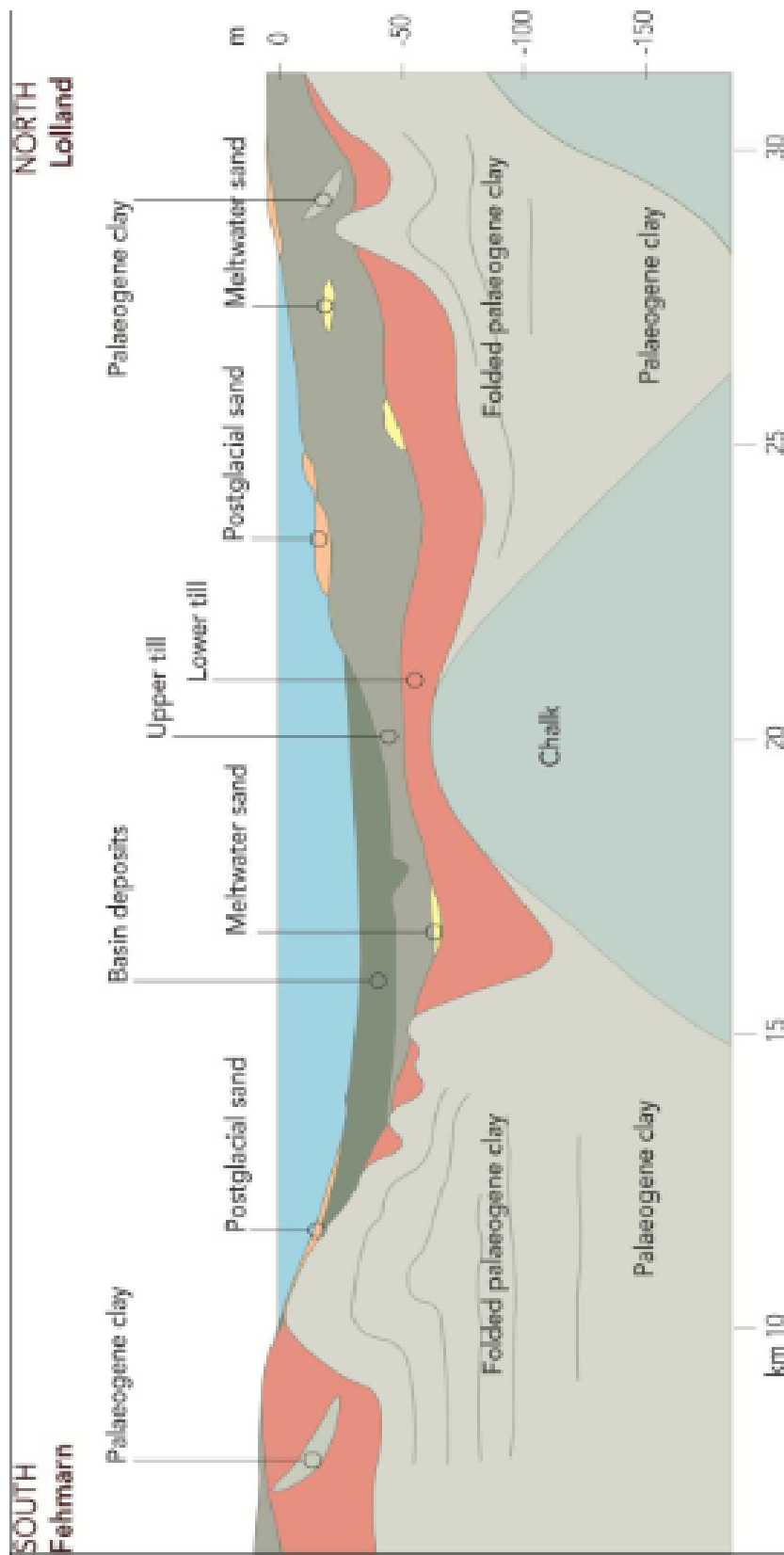


Figure D.4: Overview of the geology in the longitudinal direction (Ramboll, 2013).

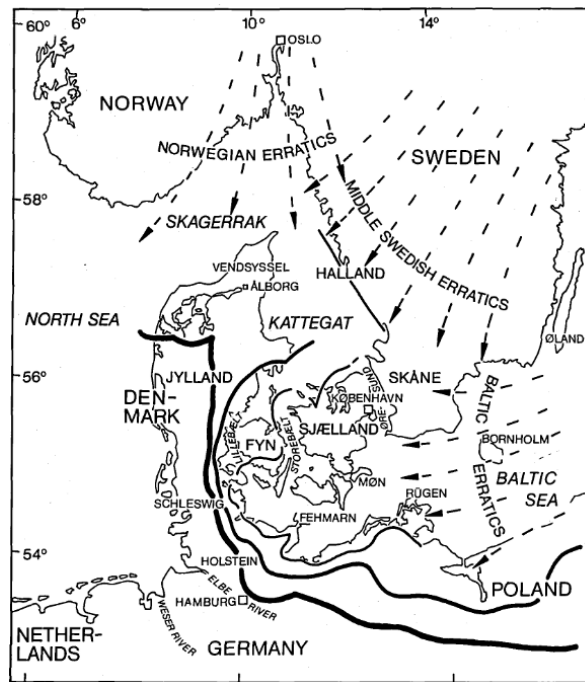


Figure D.5: Glacier movements during Pleistocene (Houmark-Nielsen, 1987).

**Glacial till** Encyclopaedia Britannica (2011) states that the definition of till is an unsorted material with no stratification deposited by glacial ice. Basal and ablation tills exist in which sediments carried in the base of a glacier are basal tills, while ablation till was carried on or near the surface and is deposited when the glacier melts (Encyclopaedia Britannica, 2011). The weight of the ice cover results in highly overconsolidated tills but different processes can disturb this resulting in a locally normally consolidated clay till. Mechanical and chemical processes like weathering and melting can disturb the overconsolidated clay till such that variations within a few meters are likely (Jessen, 2011).

#### Upper till unit

The upper till is called a unit because it is too thick to be a deposit from only one glacial event. The different deposits within this unit have similar technical properties and an almost continuous regional distribution. For this reason, it is not possible to make a clear distinction between the deposits.

Progressing glaciers often erode their basis and remove the till deposits from the previous glaciation. The lower till unit eroded a lot of material from the original area, it contains remnant of older deposits originally covering the area. Contrarily the upper till unit slipped over its base, almost without erosion of the older deposits. Resulting in a upper till dominated by foreign material with only a small portion of material from the local base.

The upper till can be described as a hard to very hard, silty-sandy clay till. Inclusions of thin meltwater silt/clay layers and sand layers may locally be present within the unit. A plasticity index of 6-10 is typical for the upper till unit, some local medium plasticity clay layers in the unit are interpreted as floes originating from the lower unit (Ramboll, 2013). The upper till unit is considered as inactive. It is highly variable and local variations within several m are likely to present. Most parts appear the be heavily over-consolidated due to weight of the glacier in the past, but some normally consolidated parts can also be experienced. The normally consolidated zones are disturbed parts formed by mechanical and chemical processes, e.g. high pore pressure beneath the sole of the glacier, weathering and melting of interbedded ice (Jessen, 2011). This unit includes a closely spaced net of of vertical fractures.

Experience of the Storebaelt and Øresund projects has shown that the glacial clay till may be prone to liquefaction, the liquefaction limit of the material is close to the in situ water content at Øresund. Re-handling of the material by excavators and dumpers increases the water content and may result in liquefaction (Fehmarn belt contractors, n.d.).



Figure D.6: Glacial till lumps on the barge at Oresund (Gimsing and Iversen, 2001).



Figure D.7: 'Porridge' glacial till after re-handling at Oresund (Gimsing and Iversen, 2001).

**Palaeogene unit** The Paleogene unit at the Fehmarnbelt contains all known deposits from Aebelø to the Lillebaelt formation. The Rosnaes clay is the most important and common formation within the range of project.

During the Quaternary the upper part has undergone folding by pressures of the overlying ice. As a result partial areas of the folded Palaeogene are destructured and later in time weakening occurred due to ice retreat followed by erosion and swelling (Krogsbøll et al., 2012). The folded Palaeogene contains a wide range of geotechnical properties ranging from intact to fully weakened. The folds are very steep with an almost vertical direction (Ramboll, 2013).

Except for the Aebelø deposit, all formations are formed by high plasticity to very high plasticity clays with a clay content > 75%, but the Aebelø deposit is a silty to very silty clay. Figure D.8 shows that the deposits differ quite highly in their clay mineralogy, the Røsnaes clay is more calcareous than the other deposits. Internal variation of clay mineral distribution within each of the Palaeogene deposits is also significant.

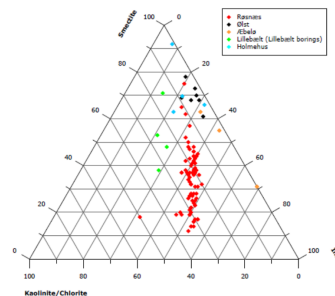


Figure D.8: Clay mineralogy of 120 samples from different Palaeogene deposits (Ramboll, 2013).

The Palaeogene clays were deposited during a period with high volcanic activity in the North Atlantic area. The volcanoes erupted more than 150 times and spread their ash over the area. Shiny, slickensided shear surfaces are present in the Palaeogene clay, formed by the deposited ash layers. Over 100 shear surfaces are present in the Olst formation, the Rosnes and Lillebilt formation also contain some shear surfaces (Boskalis, n.d.). The strength is dominated by the pre-existing shear planes, as explained in section 2.1.5, formed by tectonism and ash layers.